Massachusetts Bay Eutrophication Model: 2002-2004 Simulation

Massachusetts Water Resources Authority
Environmental Quality Department
Report ENQUAD 2006-13

Jiang M, Zhou M. 2006. Massachusetts Bay Eutrophication Model: 2002-2004 Simulation. Boston: Massachusetts Water Resources Authority. Report 2006-13. 126 p.

Massachusetts Water Resources Authority
Boston, Massachusetts

Massachusetts Bay Eutrophication Model: 2002-2004 Simulation

Prepared by:
Mingshun Jiang & Meng Zhou
Department of Environmental, Earth and Ocean Sciences
University of Massachusetts Boston
100 Morrissey Blvd
Boston, MA 02125

June 2006

EXECUTIVE SUMMARY

Under the cooperative agreement between the University of Massachusetts Boston (UMB) and Massachusetts Water Resources Authority (MWRA) in 2001, the UMB modeling team has been maintaining, enhancing and applying the existing hydrodynamic and water quality models for Boston Harbor, Massachusetts Bay and Cape Cod Bay system. Five years (2000-2004) simulations have been conducted since 2001. This report presents the validation of the Massachusetts Bay (MB) water quality model (also called Bay Eutrophication Model, BEM) for years 2002-2004 and results of sensitivity experiments.

This study concludes that the modeled water quality variables are well compared to the observed ones in the period 2002-2004 with similar qualities as the model results in 1998-2001 simulations. The model results also well represent physical, biological and chemical environment and processes in the water column and sediments:

1. Seasonal cycles of surface nutrient enrichment due to vertical mixing and nutrient depletion due to phytoplankton intake and onset of stratification, the diatom-dominated new production in spring and fall and the flagellate blooms due to onset of silica depletion, nutrient regeneration and dissolved oxygen (DO) fluctuation during the summer, and transport and retention of biota associated with seasonal circulation patterns.
2. Responses to short term forcing by producing upwelling, downwelling and mesoscale eddies along the coast and CCB, and episodic phytoplankton bloom events.
3. Inter-annual variability such as the strong spring bloom and weak fall bloom in 2004.

The analysis of model results also led to new understandings:

1. Rich mesoscale features such as eddies, filaments and coastal jets are found in Massachusetts Bay resulted from complex interactions between winds, GOM intruding currents, freshwater plumes and topography;
2. These mesoscale eddies, filaments and coastal jets are important to the biogeochemical processes in the MBS through transport, retention and isolation of nutrients and biota; and
3. These coupled physical and biogeochemical processes directly impact the pathway, dispersion and bio-removal of MWRA effluent.

The model certainly has limitations: it did not reproduce the early bloom in February 2002; the model over-estimated chlorophyll and bottom particular organic nitrogen (PON) concentrations; the model over-estimated primary production (PP) in BH during late summer and early fall; and the model did not reproduce high surface DO values associated with short-term events in summer. The causes for these mismatches between model and observed results are complicated by the natural complexity of an ecosystem, empirical formulations, limitation of model schemes and resolution, errors in measurements and not enough data for boundary conditions. All of these need to be further investigated.

Improving the BEM will first require improving the hydrodynamic model. For example, over-smoothed vertical distribution of chlorophyll may be caused by over-estimated vertical mixing. In summer during upwelling events, the hydrodynamic model tends to predict warmer temperature in western MB than the observed, which may lead to over-estimation of phytoplankton biomass (and chlorophyll). A higher horizontal resolution in both hydrodynamic and BEM models may improve horizontal gradients of temperature, salinity, currents and mixing from the hydrodynamic model and gradients of nutrients, production and biomass in the BEM model.

The next step is to improve our understandings of the biogeochemical processes. Two sensitivity experiments conducted suggest that results from the BEM are sensitive to empirical formulas of air-sea O_2 exchange and phytoplankton growth. Better empirical formulas for these biogeochemical processes require better understandings of these processes first, which have to be done by observations. The experiment with and without effluent nutrients indicates the possible impacts of the MWRA effluent on the chlorophyll and primary productivity near the outfall site with the specific impact areas depending on the strength and direction of the coastal current.

These new findings and understanding have indicated areas in both the model and field observations which need to be further improved:

1) Better understanding and quantitative estimate of volume transport of the intruding GOM coastal current off Cape Ann, which primarily determines the general circulation strength, patterns and salinity in the MBS;
2) Better understanding the mesoscale eddy formation and translation in the north shore area associated with northeasterly wind events, and the pathway and dispersion of effluent associated with these eddies;
3) Better understanding *Phaeocystis* and red tide blooms associated with physical processes and nutrient dynamics in the MBS;
4) Quantitative relationship between the model quality and the spatial and temporal coverage of observations at open boundaries; and
5) Impacts of zooplankton grazing (top-down controls) on algal blooms in the MBS.

TABLE OF CONTENTS

LIST OF FIGURES

LIST OF TABLES

1. INTRODUCTION

1.1 Project overview

The Boston Harbor (BH), Massachusetts Bay (MB) and Cape Cod Bay (CCB) system (MBS) is important to the regional economy by serving a busy commercial harbor, a productive fishing ground, a critical habitat of endangered North Atlantic Right whales and a prosperous tourism industry. A healthy marine environment is important to the more than three million people living in the surrounding area. Significant efforts have been made to clean up Boston Harbor in last decades. The construction of the Deer Island wastewater treatment plant and the relocation of the effluent outfall from Deer Island to 15 km offshore were among the biggest human efforts in the nation to restore an urbanized harbor.

To evaluate environmental and ecological impacts of the new treatment and outfall relocation on the MBS, the Massachusetts Bay Program, US Geological Survey and Massachusetts Water Resources Authority (MWRA) have funded a number of projects to study the physical-biological-chemical processes and monitor the marine environment changes in the MBS (Geyer et al., 1992; Werme and Hunt, 2002). Under these projects, numerical models have been developed to simulate and predict the physical and biological environment in the MBS (HydroQual, 2000; HydroQual, 2003; HydroQual and Signell, 2001; Jiang and Zhou, 2004a, 2004b, 2004c).

A long-term Cooperative Research Agreement made in 2001 between the University of Massachusetts Boston (UMB) and MWRA stated that the UMB and MWRA will maintain, enhance and apply the existing MB Hydrodynamic and Water Quality Models (MB model), and provide model run results to the MWRA for its obligations under its National Pollutant Discharge Elimination System (NDPES) permit. The hydrodynamic model for the MBS was constructed by the U.S. Geological Survey (USGS) in Woods Hole based on the ECOM-si developed by HydroQual Inc. (HydroQual) (Signell et al., 1996). The Water Quality Model was developed by HydroQual (HydroQual, 2000). HydroQual had maintained and conducted model runs up to 1999. Under the agreement between the MWRA and HydroQual, the MB Model was transferred to the UMB in 2001. To ensure successful model transfer and consistency between model results

produced by different computer systems, a comparison task between the UMB and HydroQual model runs has been completed at the UMB (Zhou, 2002; Jiang and Zhou, 2003). The UMB modeling team had successfully simulated and validated hydrodynamic and water quality simulations for 2000-2001. The results were presented in two MWRA reports (Jiang and Zhou, 2004b, 2004c), and several regional and national conferences. The performance of the MB model was reviewed at the Model Evaluation Group (MEG) meeting held on September 12, 2005.

1.2 Physical setting

The MBS is a semi-enclosed embayment located in the western Gulf of Maine (GOM) and surrounded by the Boston metropolitan region in the north and west, and Cape Cod in the south (Figure 1.1). The MBS is about 100 km long and 50 km wide, and has an average depth of 35 m. Stellwagen Basin is the only deep basin in the MBS with a maximum depth up to 90 m. It is bounded in the east by Stellwagen Bank with the shallowest depth of about 20 m. Thus the MBS is connected to the GOM mostly through the North Passage off Cape Ann and the South Passage off Race Point.

Previous studies have indicated that the circulation in the MBS varies in response to short- and long-term local and remote forcing including 1) wind stresses and heat fluxes at the sea surface, 2) tides and mean surface slopes at the open boundary, and 3) freshwater runoff including outfall effluent (Geyer et al., 1992; Signell et al., 1996; Jiang and Zhou, 2004b). The yearly-mean current in the MBS is characterized by a counterclockwise circulation, which is primarily driven by both the intruding current through the North Passage associated with mean sea surface slopes, and baroclinic pressure gradients associated with the horizontal salinity and temperature gradients produced by freshwater runoff and differential warming. Tides are dominated by the semi-diurnal M_2 constituent. Tidal currents vary from 10 cm s^{-1} in the Stellwagen Basin, to 50 cm s^{-1} in the South Passage. The water column stratification varies seasonally. Stratification occurs in spring due to both freshwater runoff and surface heating, which is intensified and reaches a maximum strength during summer. The water column is destratified during fall due to surface cooling and increasing wind mixing, and is well mixed in winter.

The seasonal surface slope off Cape Ann represents the southward flow of the Western Maine Coastal Current (WMCC). As early as 1927, Bigelow suggested that this current breaks into two branches at Cape Ann: one intrudes deeply into MB, and another follows the outer edge of the Stellwagen Bank (Bigelow, 1927; Lynch et al., 1996). This bifurcation is determined by the interactions between topography, coastal lines and freshwater plume of the Merrimack River though the specific mechanisms remain unclear. The volume transport of this intruding current primarily determines the general circulation in the MBS. It circulates counterclockwise along western Massachusetts Bay and frequently penetrates into CCB, especially in winter and spring seasons (Geyer et al., 1992; Jiang and Zhou, 2004b).

Our modeling study indicates pronounced seasonal variation in the circulation pattern (Jiang and Zhou, 2004b). In western MB, surface currents are strongly driven by winds. In winter and spring seasons, northerly winds drive a southward coastal current creating a counterclockwise circulation (Geyer et al., 1992). In summer and early fall, predominantly southwesterly winds produce offshore Ekman transport and coastal upwelling, which induce a northward coastal current along the upwelling front along the western coast. The coastal upwelling and downwelling have also been discussed in previous studies (e.g., Geyer et al., 1992; HydroQual and Signell, 2001; Signell et al., 1996; Butman, et al., 2002).

1.3 Biological environment

Phytoplankton growth in the MBS is primarily driven by nutrients, temperature and photosynthetic available radiation (PAR) (Libby et al., 2000; Libby et al., 2001). The spring bloom is triggered by the onset of stratification and strengthened with the increase in solar radiation. The available nitrogen and silica in a well-mixed water column during winter lead to the dominance of diatoms. In late spring and summer, stratification limits upward nutrient fluxes, which in turn limits the primary production in the MBS. The abundance of phytoplankton cells reaches a maximum at mid-summer with some exceptions. For example, the maximum abundance in 2000 was reached during a *Phaeocystis*-dominated spring bloom. The late summer assemblage is comprised of primarily dinoflagellates and mixed species of diatoms, mainly the genus *Chaetoceros*.

The fall bloom typically occurs in late September when strong mixing produced by wind and surface cooling destratifies the water column and brings nutrients from deep water to euphotic zones, and declines in November as solar radiation decreases and mixing further increases. The fall bloom is characterized by increases of nutrient concentrations in the surface water and a 2-4 fold increase in diatom abundances. One of the prominent features in the MBS ecosystem is occurrences of strong fall blooms in some years with the averaged chlorophyll in western MB higher than 6 $\mu g\ l^{-1}$. The timing of fall bloom is determined by the fall mixing and the strength of fall bloom is likely controlled by the strength of mixing, available nutrients and zooplankton grazing.

Abundant phytoplankton in the MBS supports abundant zooplankton, ranging from 10 to 50×10^3 individuals m^{-3} (Turner, 1994; Libby et al., 2001; Libby et al., 2002). In winter, zooplankton assemblages are dominated by copepod nauplii, *Oithona similis* females and copepodites, gastropod veligers, and *Acartia hudsonica* females and copepodites. In late winter and early spring, in addition to these dominant species, subdominant species are bivalve veligers, copepodites of *Calanus finmarchicus*, *Pseudocalanus* and *Temora longicornis*, and *Oikopleura dioica*. In summer and early fall, marine cladoceran *Evadne nordmanni*, *Microsetella norvegica* and copepodites of the genus *Centropages* are added to the species spectrum.

The sea floor in the MBS is complicated with a variety of bottom types. Soft-bottom occupies most areas in BH, CCB and Stellwagen Basin, while hard-bottom dominates the shallow nearshore areas. The annelid worms are most abundant in soft-bottom communities, accounting for more than 80% of the fauna at most MWRA monitoring stations, and crustaceans are second most abundant fauna (Kropp et al., 2001; Kropp et al., 2002; Maciolek et al., 2003). The most dominant taxa in hard-bottom communities are algae, including *Lithothamnion spp*., dulse, and red filamentous species. The dominant animal taxa include *Asterias vulgaris*, and the horse mussel *Modiolus modiolus*.

The benthic processes in BH are dominated by biological processes, while in MB and CCB they are generally influenced by region-wide physical and biological phenomena (Maciolek et al., 2003; Tucker et al., 2002). High sediment oxygen demand (SOD) and fluxes of dissolved inorganic nitrogen (DIN) have been observed in the harbor, both of which have been decreasing in the last decade due to the reduction in pollutant loadings

to the harbor. Intensive denitrification also occurs in the harbor, which increases since the outfall relocation. Sediments in the MBS are well oxygenated; and the denitrification dominates DIN fluxes, accounting for about 60-80% of the total flux. No obvious seasonal pattern in DIN fluxes has been observed. On the contrary, the SOD fluxes exhibit strong seasonal patterns, which are well correlated with the bottom temperature.

Most of these processes are simulated in the BEM, which focuses mostly on the nutrient cycling and related oxygen processes, including phytoplankton growth (primary productivity), transformation of phytoplankton biomass into various forms of organic matter and regeneration of inorganic nutrients occurring in both the water column and sediment. The physical processes are simulated by the hydrodynamic model. The bulk of phytoplankton species are represented as three functional groups that carry the overall physiological characteristics during winter-spring, summer and fall, respectively. Activities of both zooplankton and benthic community are only crudely parameterized, however, understanding of these processes is important to understand the strengths and limitations of the BEM. The model structure of the BEM and model implementation will be described in Section 2.

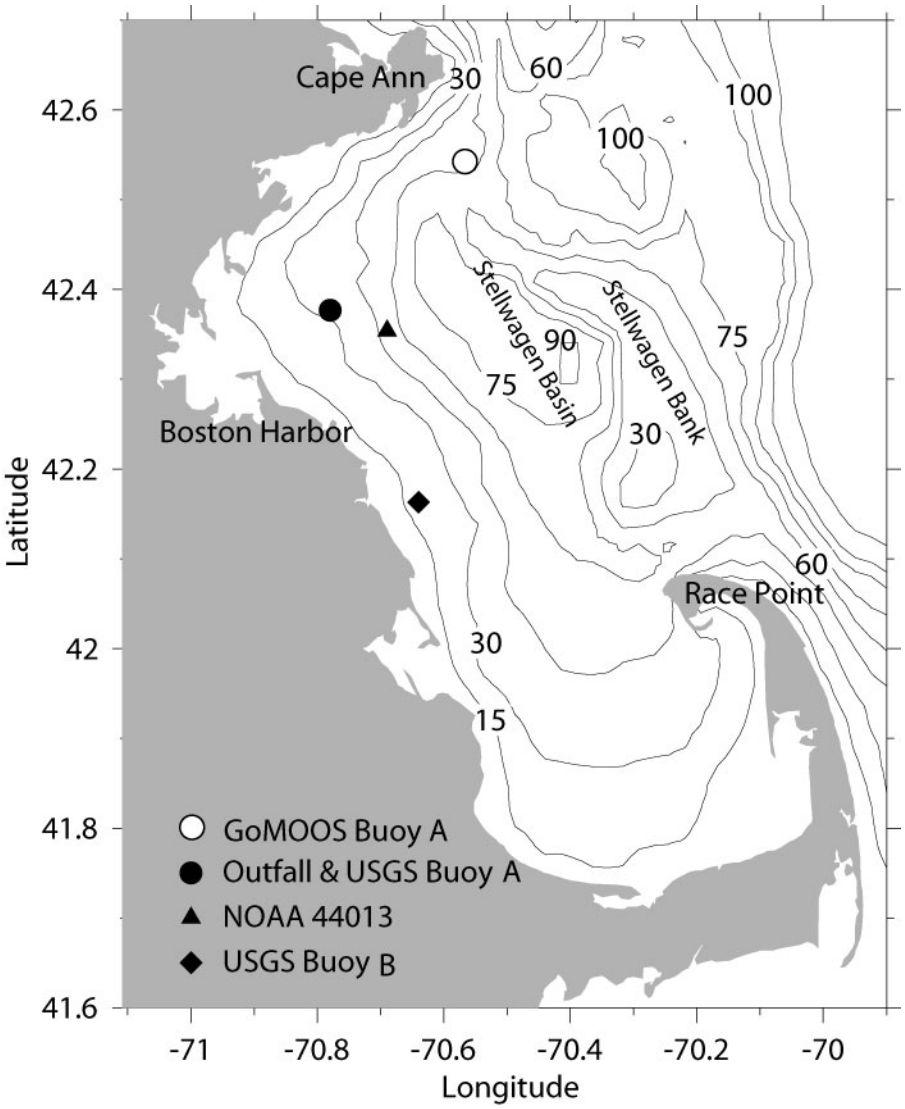

Figure 1.1. Bathymetry and existing buoy stations in the Boston Harbor (BH), Massachusetts Bay (MB) and Cape Cod Bay (CCB) system (MBS).

2. MODEL DESCRIPTION

2.1 Model domain and grids

The BEM grids are essentially the same as the grids used for the hydrodynamic model with two modifications: 1) the model domain covers the entire MBS with the open boundary starting from Cape Ann to the outer edge of Cape Cod (Figure 2.1), that is, those grids east of this boundary in the hydrodynamic model are eliminated in the BEM; and 2) the top 3 sigma layers in the hydrodynamic model are integrated to 1 sigma layer in the BEM. Therefore, the BEM has 54×68 horizontal grids and 10 vertical layers.

2.2 Nutrient dynamics

The water quality model describes the phytoplankton growth and nutrient cycling through a number of prognostic variables and a set of differential equations, which govern the temporal and spatial changes of these variables based on fluid motion, biogeochemical process rates and mass conservation. Key biological and chemical processes included in these equations are based on theoretical and empirical relationships and parameters. The current BEM has 26 prognostic variables, which include salinity, 3 phytoplankton groups, 4 type of nutrients (C, N, P, Si) and related organic components, dissolved oxygen, aqueous oxygen, and trace metal, and more than 100 model parameters (Tables 2.1 and 2.2). The three phytoplankton groups represent winter/spring, summer and fall algal assemblages, respectively, with different carbon-to-chlorophyll ratio, uptake ratios of nutrients and other physiological properties. The BEM also has a sediment sub-model to simulate the biogeochemical processes in the sediment and fluxes between the water column and sediment.

The model structure for the nitrogen cycle is shown in Figure 2.2. The central process is phytoplankton photosynthesis, which transforms dissolved inorganic nitrogen (DIN) to phytoplankton biomass. DIN includes ammonium (NH_4), nitrate (NO_3) and nitrite (NO_2). The latter two are combined and denoted as NO_3. NH_4 can be transformed into NO_3 through nitrification. The living cells of phytoplankton can be transformed into non-

living organic matter by respiration, mortality and zooplankton grazing. The zooplankton grazing is accounted for as instantaneous removal of phytoplankton standing stocks, which is subject to temperature modulation with a maximum of 10%. There are two non-living organic nitrogen types, dissolved organic nitrogen (DON) and particulate organic nitrogen (PON). They are further divided into refractory (RDON and RPON) and labile (LDON and LPON) forms. LDON and LPON are decomposed much faster than RDON and RPON. The regeneration process of organic matter involves two steps: 1) particles break down to DON, and 2) DON is further remineralized to ammonia. Particles settled down into sediments will be decomposed and feed back to water column through fluxes of NO_3 and NH_4. The sediment denitrification will produce N_2 gas, which is simply lost from the system. In addition to these internal cycling processes, water column receives inputs of nitrogen from land sources as runoff and effluent containing inorganic and organic nutrients, the atmosphere through gas exchange, and open boundaries (see Section 2.3.2 and 2.3.3). Mathematical equations for these processes can be found in HydroQual and Normandeau (1995). For the convenience of reading, we include them in the Appendix A.

The cycling processes of carbon and phosphorus have similar structures to that of nitrogen. However, each of them has only one dissolved inorganic form and dissolved organic carbon has two additional forms (see Table 2.1). The oxygen cycling generally follows the cycling of carbon in the water column while the exchange of oxygen with the air is driven by wind entrainment and solubility at the surface. Silicon has only one dissolved inorganic form (SiO_4) and one biogenic form (BSi). Detailed description can be found in earlier reports of this model (HydroQual, 2000; HydroQual, 2003; HydroQual and Normandeau, 1995; Jiang and Zhou, 2004c).

The sediment biogeochemical processes in the BEM are governed by a sediment sub-model (Di Toro, 2000). Particulate organic matters in water column settle down into the sediment, which are remineralized by sediment diagenesis processes. Fluxes of dissolved nutrients and sediment oxygen demand (SOD) through the water-sediment interface represent the interactions between biogeochemical processes in the water column and sediment. Nitrogen gas released by the denitrification process is removed from the

system through outgassing to the atmosphere. Re-suspension of sediments is simulated in the BEM by recycling 40% of the sinking fluxes back into the water column.

2.3 Forcing

2.3.1 Surface forcing

The surface forcing in the BEM includes solar radiation (provided by WHOI), day length and wind (measured at NDBC 44013) (Figure 2.3). The winter experiences shortest daylight and lowest solar radiation while the summer has the longest daylight and strongest radiation. Winds also exhibit a strong seasonal pattern with the strongest winds in winter and weakest in summer (Jiang and Zhou, 2004b). Wind forcing determines the air-sea gas exchanges as formulated by Hyer et al. (1971) (also see Section 4.1), and affects the biogeochemical processes indirectly through vertical mixing and horizontal transport. Solar radiation and day length determine the photosynthesis of phytoplankton. To account for the photo-adaptation of phytoplankton, the average solar radiation in previous three days is used as the current saturation solar radiation (see Appendix A).

2.3.2 Nutrient loadings

In addition to loadings from the GOM through the open boundary, the MBS receives large nutrient (including inorganic and organic matter) inputs from point sources including sewage effluents, river discharges, and combined sewage overflows (CSO) Other nutrient sources in the MBS include ground waters (NPS) and atmospheric inputs. The daily mean loadings of MWRA effluent and river discharges were calculated and updated every year based on nutrient concentrations and flows (carbon in river discharges used mutli-year mean) The ground waters loadings were calculated by HydroQual (HydroQual, 2003) based on the estimates of Menzie-Cura and Associates (1990). The non-MWRA effluent loadings used same values as in 2000-2001 simulation, which was partially updated by using latest CSO data provided by the MWRA (Jiang and Zhou, 2004c). The atmospheric loadings were the same as in previous simulations (HydroQual,

2003; Jiang and Zhou, 2004c).

Within these inputs, the MWRA effluent is the dominant source for nitrogen and phosphorus (Table 2.3, Figure 2.4). Among the other sources, non-MWRA wastewater treatment plant (WWTP) effluent is the largest for phosphorus, and the atmosphere provides most of the remaining nitrogen. Due to the secondary wastewater treatment, carbon and phosphorus loads in the MWRA effluent have been significantly reduced in the last several years. The total nitrogen loading in recent years is nearly unchanged compared to that of the period from 1992 to 2001 (see HydroQual, 2003, Jiang and Zhou, 2004c). We note that previous modeling and observational estimates indicate that the MWRA nutrient inputs are only 3~6% of the nutrients inputs from the GOM (Adams et al., 1992; Becker, 1992; HydroQual, 2000).

Because only total loading data of individual nutrients are available for MWRA effluents and other sources, they are converted to loadings of different components for each nutrient. For example, the total nitrogen flux is separated into fluxes of nitrate (including nitrite), ammonia, LPON, RPON, LDON and RDON. The partition coefficients for each nutrient in the previous simulations (1998-1999, 2000-2001) were used in the 2002-2004 model run (Table 2.4) (HydroQual, 2000; HydroQual, 2003; HydroQual and Normandeau, 1995; Jiang and Zhou, 2004c).

2.3.3 Open boundary conditions

The open boundary conditions for the 2002-2004 simulation were constructed based on the same objective interpolation procedures and software (OAX) used in the year 2000-2001 hydrodynamic model run, which was developed by Bedford Institute of Oceanography (Hendry and He, 1996). Because there are not enough data to compute the spatial and temporal de-correlation scales, the correlation function was specified as follows,

$$R(r) = \left(1 + r + \frac{r^3}{3}\right)\exp(-r) \tag{2.2}$$

where r is the pseudo-distance between the data point and the target point,

$$r = \sqrt{\left(\frac{x - x_0}{a}\right)^2 + \left(\frac{y - y_0}{a}\right)^2 + \left(\frac{z - z_0}{b}\right)^2 + \left(\frac{t - t_0}{T}\right)^2} \quad (2.3)$$

where *a*, *b*, and *T* are the horizontal, vertical and temporal correlation scales respectively. The pseudo-distance controls the selection of nearest points for interpolation. The RMS is a dimensionless parameter representing the relative estimation error, defined as the square-root of the error variance by interpolation, and is scaled from 0 to 1. The data used for constructing the open boundary for 2002-2004 were collected by the MWRA monitoring program and Stellwagen Bank National Marine Sanctuary (Figure 2.5). The data collected by Harbor Monitoring Program (Talyor, 2004) were not used in constructing the boundary conditions because these stations were far away from the open boundary. The horizontal, vertical and temporal correlation scales were 20 km, 15m and 15 day, respectively, which were chosen to ensure that the results rely mainly on the observations near the open boundary. During months when there were no data collected at stations near the open boundary (F26, F27, F28 and F29), the interpolation procedures would automatically select data collected (1) along the boundary in neighboring months and (2) those at the same months but inside the MBS, which might introduce significant uncertainties. Though the model prediction was determined by the combination of biogeochemical processes, local forcing, and open boundary conditions, a less accurate open boundary condition would lead to a less accurate prediction. The overall quality of data coverage is shown in Table 2.5. This objective interpolation incorporated all observed data in a statistical way, and provided detailed boundary values and spatial structures. Some interpolated results might not be very reliable due to the paucity of observations in some months.

The interpolated organic matter values were further separated into labile and refractory forms based on the partition coefficients used in previous simulations (Table 2.3). Data for phytoplankton biomass were insufficient to construct the open boundary conditions directly because the measurements were only taken at several selected monitoring stations. As an alternative, chlorophyll data were used and converted to phytoplankton biomass. A total chlorophyll value was divided based on empirical percentages of 3 individual groups (Table 2.6) and then the chlorophyll value for each

group was converted to the biomass using the ratio of carbon to chlorophyll (CChl). These ratios of carbon to chlorophyll were same as to those used in the BEM (HydroQual, 2000; HydroQual, 2003; Jiang and Zhou, 2004c).

These procedures were applied to construct the open boundary conditions for years 2002-2004. The objectively interpolated boundary conditions in April 2002 are shown in Figure 2.6. Most variables showed significant vertical and horizontal variations. For example, the subsurface chlorophyll maximum was present along the open boundary, and both nitrate and ammonia concentrations were low within the mixed layer. Nutrient concentrations decreased from north to south while concentrations of organic matters increased from north to south, which suggests that the MBS was importing nutrients from the GOM in the North Passage and producing organic matter exported to the GOM through the South Passage. Oxygen concentration showed a weak horizontal gradient and a strong vertical gradient with maximum concentration located in the north boundary.

In August, 2002, the surface nutrients were nearly depleted, and the horizontal nutrient gradients were much less than those in April (Figure 2.7). A weak surface maximum and a weak horizontal gradient of DO were found. However, the horizontal and vertical gradients of organic matters are similar to those in April. Overall, the objectively interpolated open boundary conditions reflect the observed spatial and temporal structures of biological and chemical variables.

The interpolated boundary conditions for 2003-2004 are shown in Figures 2.8-2.11. Similar features within the open boundary conditions as discussed in 2002 were found in 2003-2004 except a strong horizontal chlorophyll gradient found in April, 2003 (Figure 2.8a).

In summary, these procedures objectively interpolated observations and to a maximal extent preserved the spatial and temporal features of observations. Therefore we expect that these boundary conditions are better than the boundary conditions constructed manually (HydroQual, 2003).

2.4 Numerical scheme

The BEM is offline-coupled with the hydrodynamic model, which is the ECOM-si (HydroQual, 2000). The modeled hydrodynamic variables such as temperature, salinity, currents and turbulent mixing coefficients from the hydrodynamic model were averaged in every hour and stored. These data were input into the water quality model as the physical forcing. In the BEM, the top 3 layers in the ECOM-si were integrated into one top layer in the same way as used during previous runs. A collapse program was used to average hydrodynamic variables in the top 3 layers of the ECOM-si and assigned the resulted values to the top sigma layer in the BEM. The time dependent advection-diffusion-reaction equations in the BEM were integrated using the explicit upwind scheme and the Smolarkiewicz flux-correction algorithm (Smolarkiewicz, 1984). The variables at the open boundary were specified using the values derived from the objective interpolation and partitioning as discussed above.

2.5 Model parameters

All model parameters used in the 2002-2004 simulations were same as those of 1998-99, 2000-2001 simulations (HydroQual, 2003, Jiang and Zhou, 2004c). The value of light attenuation is spatially variable ranging from 0.6 m^{-1} in Boston Harbor to 0.16 m^{-1} offshore, which was calculated based on the light transmissivity data collected during the outfall monitoring program (HydroQual and Signell, 2001). These parameters and their values are shown in tables 2.1-2.3.

2.6 Initial conditions

The initial conditions for each year were derived from modeled results in the end of the previous year and no spin-up was used in the simulation.

2.7 Aggregation and filtering

Various aggregation and filtering have been used for above forcing data, and model output and validation data (section 3), which are listed in Table 2.7.

Table 2.1 Model variables

No.	Variables	Units
1	Salinity	ppt
2	Phytoplankton winter/spring group (diatoms)	mg C l^{-1}
3	Phytoplankton summer group	mg C l^{-1}
4	Phytoplankton fall group	mg C l^{-1}
5	Particulate organic phosphorous – refractory component	mg P l^{-1}
6	Particulate organic phosphorous – labile component	mg P l^{-1}
7	Dissolved organic phosphorous – refractory component	mg P l^{-1}
8	Dissolved organic phosphorous – labile component	mg P l^{-1}
9	Total dissolved inorganic phosphorous	mg P l^{-1}
10	Particulate organic nitrogen – refractory component	mg N l^{-1}
11	Particulate organic nitrogen – labile component	mg N l^{-1}
12	Dissolved organic nitrogen – refractory component	mg N l^{-1}
13	Dissolved organic nitrogen – labile component	mg N l^{-1}
14	Total ammonia (ammonia in water and phytoplankton cell)	mg N l^{-1}
15	Nitrite + nitrate	mg N l^{-1}
16	Biogenic silica	mg Si l^{-1}
17	Total silica – (silica in water and phytoplankton cell)	mg Si l^{-1}
18	Particulate organic carbon – refractory component	mg C l^{-1}
19	Particulate organic carbon – labile component	mg C l^{-1}
20	Dissolved organic carbon – refractory component	mg C l^{-1}
21	Dissolved organic carbon – labile component	mg C l^{-1}
22	Dissolved organic carbon – reactive component	mg C l^{-1}
23	Dissolved organic carbon – algal exudate	mg C l^{-1}
24	O_2* - aqueous oxygen	mg O_2 l^{-1}
25	Dissolved oxygen	mg O_2 l^{-1}
26	Total active metal (TAM)	mmol l^{-1}

Table 2.2. Model parameters for nitrogen cycle

Notation	Description	Values
Diatoms (winter/spring group) growth, carbon to nitrogen ratios and carbon to chlorophyll ratios		
T_{opt1}	Optimal growth temperature	8 ºC
β_{11}	Temperature correction coefficient on growth rate	0.004 $(ºC)^{-2}$
β_{21}	Temperature correction coefficient on growth rate	0.006 $(ºC)^{-2}$
G_{pre1}	Gross photosynthetic rate	2.5 day^{-1}
G_{pr01}	Nutrient-saturated gross photosynthetic rate per unit light intensity	0.28 m^2(mol quanta)$^{-1}$
k_{N1}	Half saturation constant for nitrogen uptake	0.01 mg N l^{-1}
k_{RB1}	Basal respiration rate	0.03 day^{-1}
k_{RG1}	Growth-rate-dependent respiration coefficient	0.28
k_{grz01}	Mortality rate due to grazing	0.1 day^{-1}
θ_{grz1}	Temperature dependent coefficient for grazing	1.1
f_{sc1}	Fraction of C allocated to structural purposes	0.1
W_{CChl1}	Nutrient-saturated carbon to chlorophyll ratio	40 mgC (mgChl a)$^{-1}$
QF_1	Quotient of nutrient-limited N:C ratio	0.85
W_{CN1}	Nutrient-saturated carbon to nitrogen ratio	5.0 mgC (mgN)$^{-1}$
Summer group growth, carbon to nitrogen ratios and carbon to chlorophyll ratios		
T_{opt2}	Optimal growth temperature	18 ºC
β_{12}	Temperature correction coefficient on growth rate	0.004 $(ºC)^{-2}$
β_{22}	Temperature correction coefficient on growth rate	0.006 $(ºC)^{-2}$
G_{pre2}	Gross photosynthetic rate	3.0 day^{-1}
G_{pr02}	Nutrient-saturated gross photosynthetic rate per unit light intensity	0.28 m^2(mol quanta)$^{-1}$
k_{N2}	Half saturation constant for nitrogen uptake	0.01 mg N l^{-1}
k_{RB2}	Basal respiration rate	0.036 day^{-1}
k_{RG2}	Growth-rate-dependent respiration coefficient	0.28
k_{grz02}	Mortality rate due to grazing	0.1 day^{-1}
θ_{grz2}	Temperature dependent coefficient for grazing	1.1
f_{sc2}	Fraction of C allocated to structural purposes	0.1
W_{CChl2}	Carbon to chlorophyll ratio	65 mgC (mgChl a)$^{-1}$
QF_2	Quotient of nutrient-limited N:C ratio	0.85
W_{CN2}	Nutrient-saturated carbon to nitrogen ratio	5.67 mgC (mgN)$^{-1}$
Fall group growth, carbon to nitrogen ratios and carbon to chlorophyll ratios		
T_{opt3}	Optimal growth temperature	14 ºC
β_{13}	Temperature correction coefficient on growth rate	0.004 $(ºC)^{-2}$
β_{23}	Temperature correction coefficient on growth rate	0.006 $(ºC)^{-2}$
G_{pre3}	Gross photosynthetic rate	2.5 day^{-1}
G_{pr03}	Nutrient-saturated gross photosynthetic rate per unit light intensity	0.28 m^2(mol quanta)$^{-1}$
k_{N3}	Half saturation constant for nitrogen uptake	0.005 mg N l^{-1}
k_{RB3}	Basal respiration rate	0.03 day^{-1}
k_{RG3}	Growth-rate-dependent respiration coefficient	0.28
k_{grz03}	Mortality rate due to grazing	0.1 day^{-1}
θ_{grz3}	Temperature dependent coefficient for grazing	1.1

f_{sc3}	Fraction of C allocated to structural purposes	0.1
W_{CChl3}	Carbon to chlorophyll ratio	15 mgC (mgChl a)$^{-1}$
QF_3	Quotient of nutrient-limited N:C ratio	0.85
W_{CN3}	Nutrient-saturated carbon to nitrogen ratio	5.67 mgC (mgN)$^{-1}$

Light attenuation

k_{base}	Background light attenuation coefficient (2-D parameter)	0.16~0.6 m^{-1}
k_c	Chlorophyll self-shading coefficient	0.017 m^2(mg chl)$^{-1}$

Nitrogen regeneration, nitrification and denitrification

k_{mp}	Half saturation constant for nitrogen regeneration	0.05 mgC l^{-1}
k_{RPON}	Hydrolysis rate of RPON to RDON at 20ºC	0.008 day^{-1}
θ_{RPON}	Temperature coefficient for RPON hydrolysis	1.08
k_{LPON}	Hydrolysis rate of LPON to LDON at 20ºC	0.05 day^{-1}
θ_{LPON}	Temperature coefficient for LPON hydrolysis	1.08
k_{RDON}	Mineralization rate for RDON at 20ºC	0.008 day^{-1}
θ_{RDON}	Temperature coefficient for RDON mineralization	1.08
k_{LDON}	Mineralization rate for LDON at 20ºC	0.05 day^{-1}
θ_{LDON}	Temperature coefficient for LDON mineralization	1.08
k_{Nit}	Nitrification rate at 20ºC	0.1 day^{-1}
θ_{Nit}	Temperature coefficient for nitrification	1.08
k_{Nit_DO}	Half saturation constant of oxygen for nitrification	1.0 mgO_2 l^{-1}
k_{Denit}	Denitrification rate at 20ºC	0.05 day^{-1}
θ_{Denit}	Temperature coefficient for denitrification	1.045
k_{Denit_DO}	Half saturation constant of oxygen for denitrification	0.1 mgO_2 l^{-1}

Fraction of respired and grazed phytoplankton into organic pool

f_{RPON}	Fraction of RPON from respiration and grazing	0.15
f_{LPON}	Fraction of LPON from respiration and grazing	0.325
f_{RDON}	Fraction of RDON from respiration and grazing	0.15
f_{LDON}	Fraction of LDON from respiration and grazing	0.175
f_{nh3}	Fraction of ammonia from respiration and grazing	0.2

Exudation of phytoplankton primary productivity into dissolved organic carbon

F_{ExDOC}	Exudation fraction of primary productivity to DOC	0.1

Phytoplankton settling

V_{b1}	Base algal settling rate for winter/spring group at 20ºC	0.5 m day^{-1}
V_{N1}	Nutrient stressed algal settling rate for winter/spring group at 20ºC	1.0 m day^{-1}
V_{b2}	Base algal settling rate for summer group at 20ºC	0.3 m day^{-1}
V_{N2}	Nutrient stressed algal settling rate for summer group at 20ºC	0.7 m day^{-1}
V_{b3}	Base algal settling rate for fall group at 20ºC	0.3 m day^{-1}
V_{N3}	Nutrient stressed algal settling rate for fall group at 20ºC	1.0 m day^{-1}
θ_{sp}	Temperature correction for phytoplankton settling	1.027

Settling of particulate organic nitrogen

V_{PON}	Settling rate for PON at 20ºC	1.0 m day^{-1}
θ_{PON}	Temperature correction for PON settling	1.027

Table 2.3 Mean Daily Nutrients (inorganic and organic) Loadings (kg/day)

		2002	2003	2004
Carbon	MWRA	30576	32550	31085
	Non-MWRA	41352	41351	41351
	NPS	20402	20402	20402
	River	16600	16600	16600
	Atmos.	18000	18000	18000
Nitrogen	MWRA	31176	30686	29160
	Non-MWRA	9149	9149	9149
	NPS	5278	5278	5278
	River	3211	3826	3501
	Atmos.	17600	17600	17600
Phosphorus	MWRA	3667	3268	3556
	Non-MWRA	1539	1539	1539
	NPS	834	834	834
	River	325	361	335
	Atmos.	100	100	100

Table 2.4 Partition coefficients for organic matter in the effluent and boundary inputs

Nitrogen	***PON***	***DON***
Labile	0.5	0.5
Refractory	0.5	0.5
Phosphorus	***POP***	***DOP***
Labile	0.647	0.66
Refractory	0.353	0.33
Carbon	***POC***	***DOC***
Labile	0.1	0.15
Refractory	0.9	0.8
Reactive	-	0.025
Exudate	-	0.025

Table 2.5 Quality of data coverage for objective interpolation in 2002-2004

Month	Rating*		
	2002	2003	2004
January			
February	+	+	+
March	-	0	-
April	+	+	+
May	-	-	-
June	+	+	+
July	-	-	-
August	+	+	+
September	-	-	-
October	+	+	-
November	-	-	+
December	-	-	-

* Definitions of symbols: + (good), 0 (fair), - (poor).

Table 2.6 Partition coefficients of chlorophyll at the open boundary

	Winter-spring diatoms	Summer assemblages	Fall diatoms
January-April	1.0	0	0
May	0.5	0.5	0
June-July	0	1.0	0
August	0	0.5	0.5
September-November	0	0	1.0
December	0.5	0	0.5

Table 2.7 Frequencies and filtering of forcing data, validation data, and model output.

Parameters	Frequencies in the model and for validation	Frequencies of original data	Filtering	Sources
Winds	daily	hourly	no	NDBC 44013
Solar radiation	daily	hourly	no	WHOI
Boundary conditions	bi-weekly	monthly	objective interpolation	MWRA, SBNMS
River loadings	weekly	daily flow and monthly for nutrients	no	USGS
Effluent	weekly	Weekly	no	MWRA
Non-MWRA effluent, CSO, Ground waters	monthly	various	"climatological" mean	Menzie-Cura, MWRA
Outfall Monitoring: Chlorphyll, nutrients and DO	17 cruises per year for nearfield 6 cruises per year for farfield	17 cruises per year for nearfield 6 cruises per year for farfield	no	MWRA
Outfall Monitoring: Primary productivity	17 samples at N04 & N18, 6 samples at F23	17 samples at N04 & N18, 6 samples at F23	no (monthly mean in Figure 3.26 & Table 3.2)	MWRA
Outfall Monitoring: Sediment fluxes	4 samples per year	4 samples per year	no	MWRA
Harbor Monitoring Program (chl, PON, DO)	weekly	weekly	no	MWRA
Model output: time series (nutrients, chlorophyll, DO)	3-day average	4 min.	no	UMB
Model output time series (primary productivity)	3-day average	4 min.	no (monthly mean in Figure 3.26 & Table 3.2)	UMB
Model output sediment fluxes	1-day average	4 min.	no	UMB

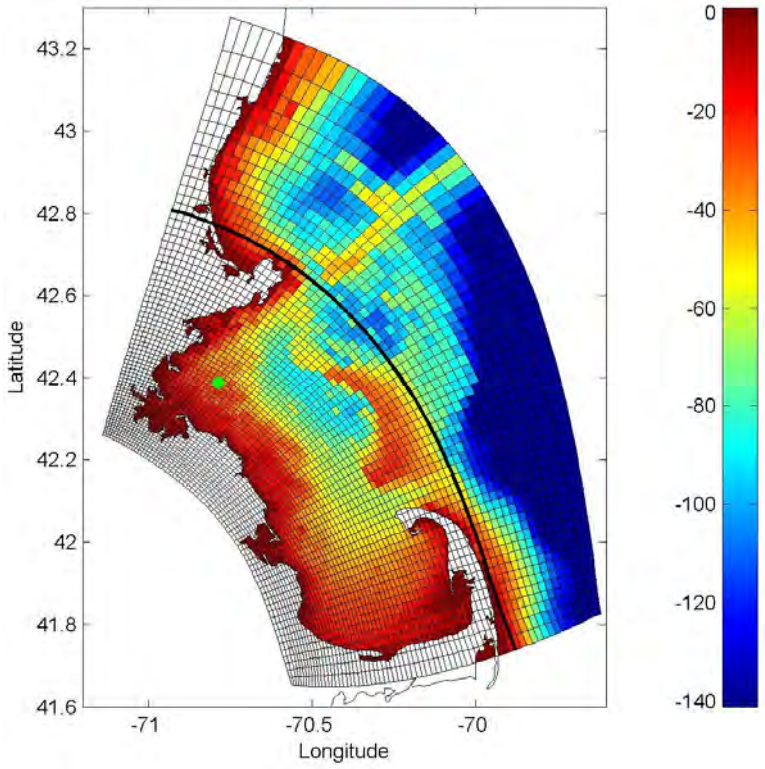

Figure 2.1. Model domain and grids in the MBS. Green dot indicates the MWRA outfall and the thick line indicates the boundary of the BEM.

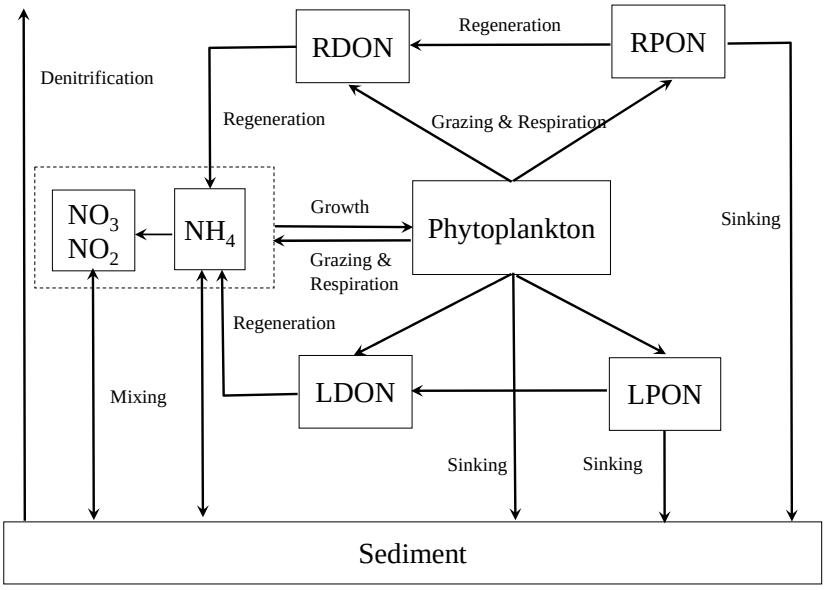

Figure 2.2. A schematic diagram for the nitrogen cycle in the BEM.

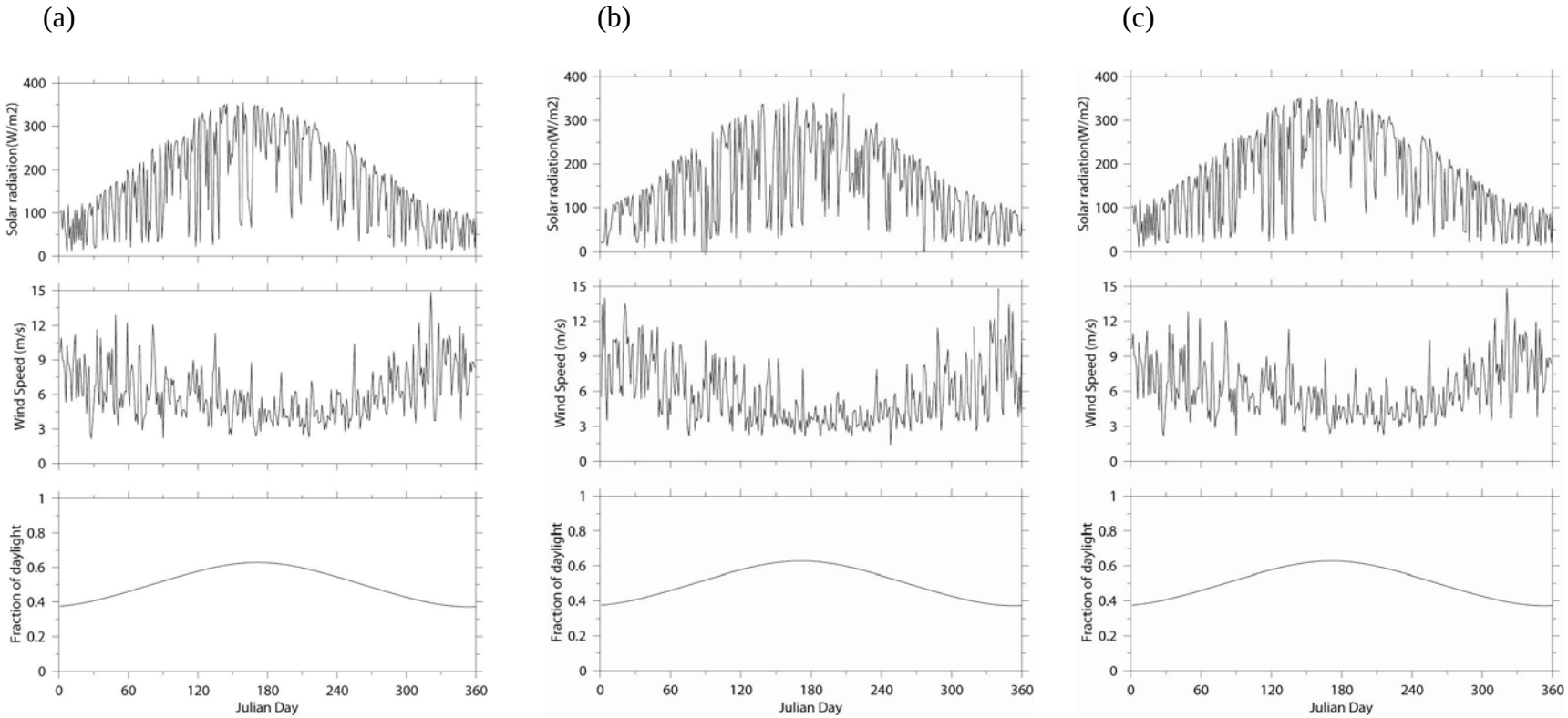

Figure 2.3. Solar radiation, wind speed, and fraction of daylight in (a) 2002, (b) 2003, and (c) 2004.

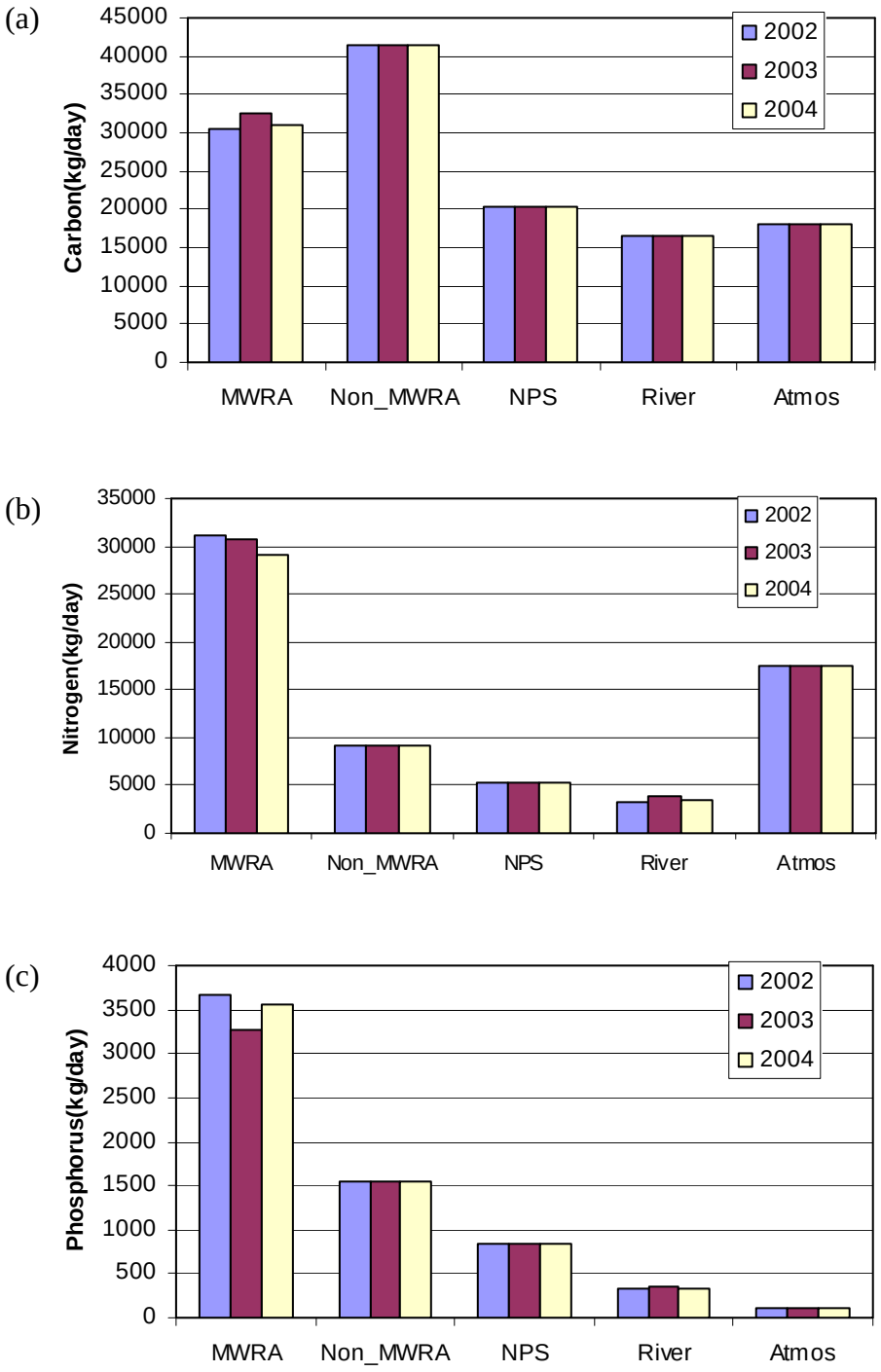

Figure 2.4. Mean daily nutrient loads: (a) carbon, (b) nitrogen, and (c) phosphorus.

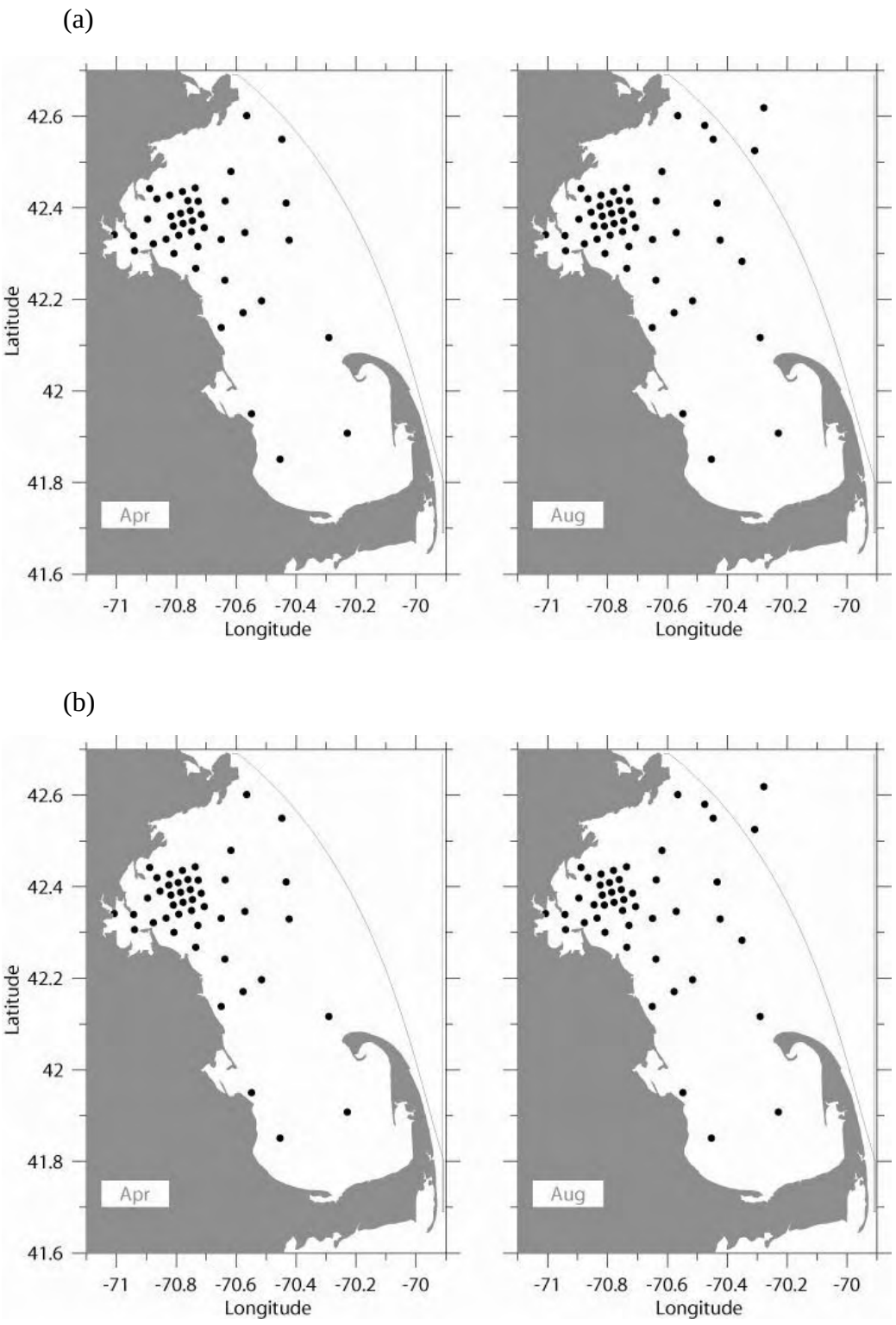

Figure 2.5. Station maps of available data in April and August: (a) 2002, (b) 2003, and (c) 2004 (to be continued on the next page).

(c)

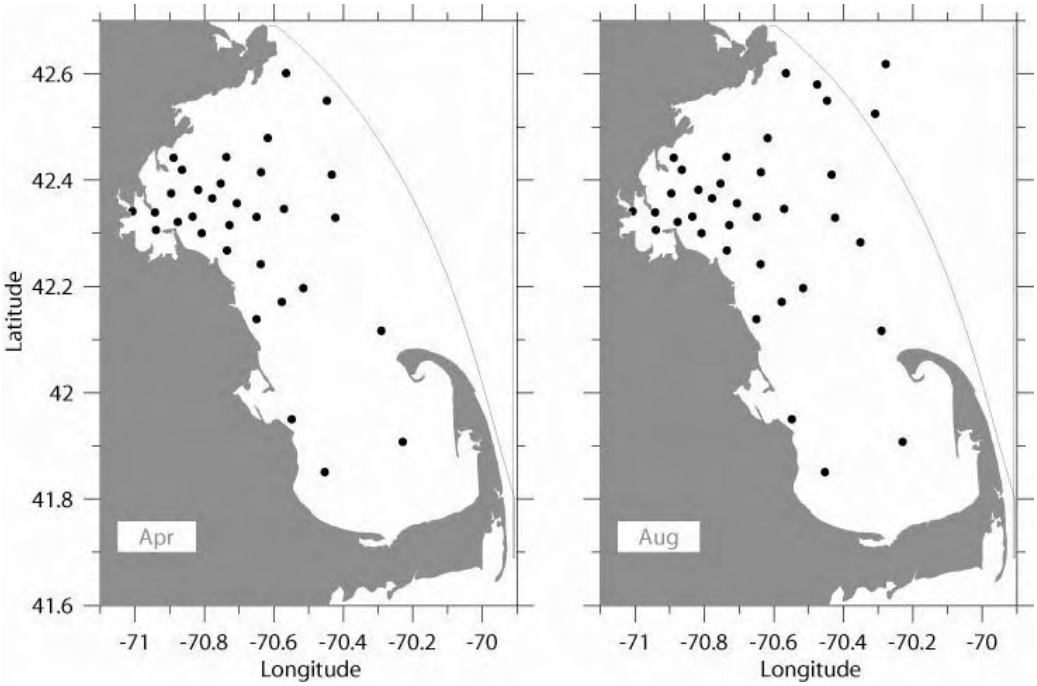

Figure 2.5. Continued.

(a)

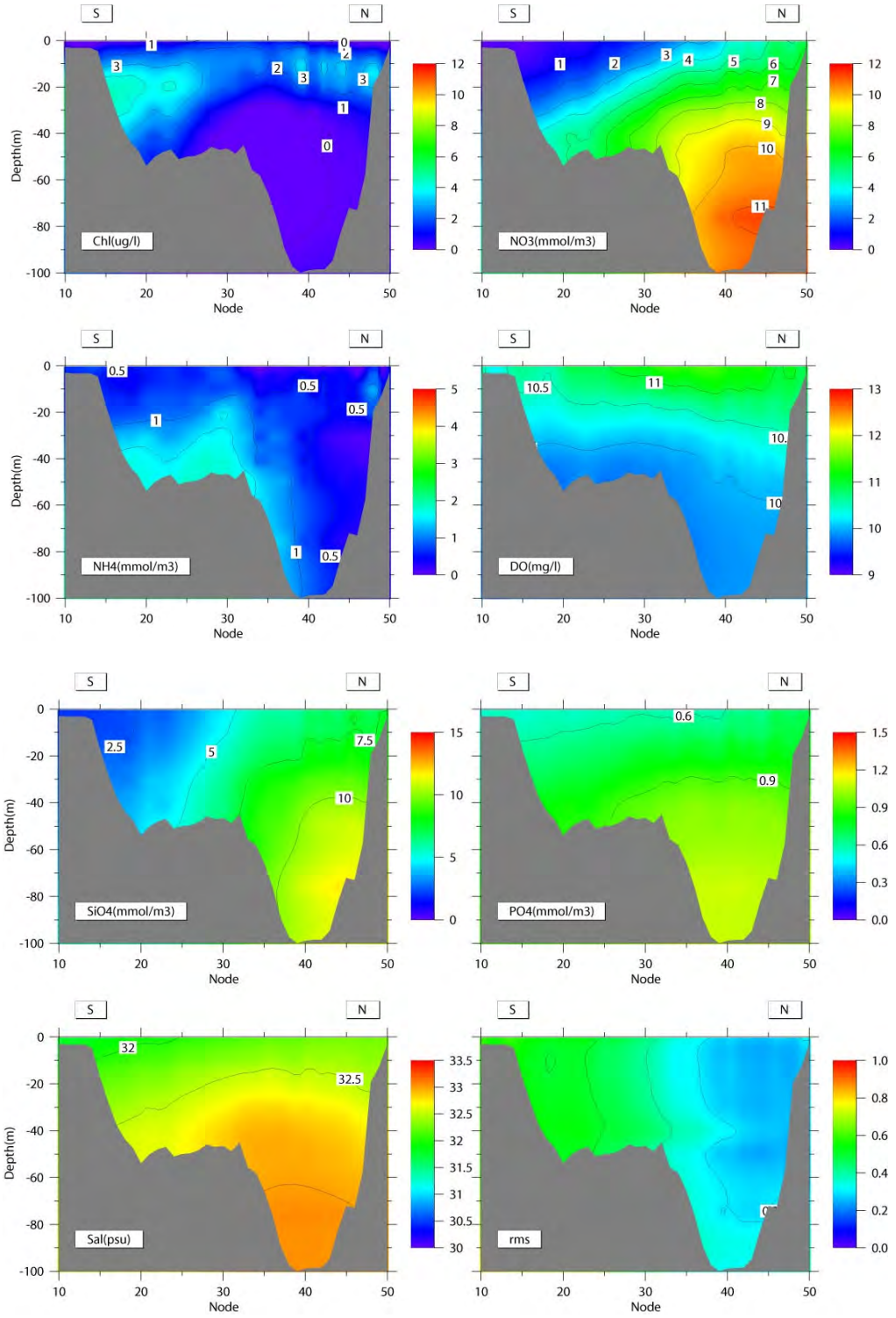

Figure 2.6. Open boundary conditions of (a) salinity, chlorophyll, nutrients, and DO, and (b) organic matter in April, 2002. The rms are also shown in the lower right panels, which apply to all of the seven parameters in (a) and (b), respectively. The node 10 indicates Cape Cod and node 50 Cape Ann. (to be continued on the next page).

(b)

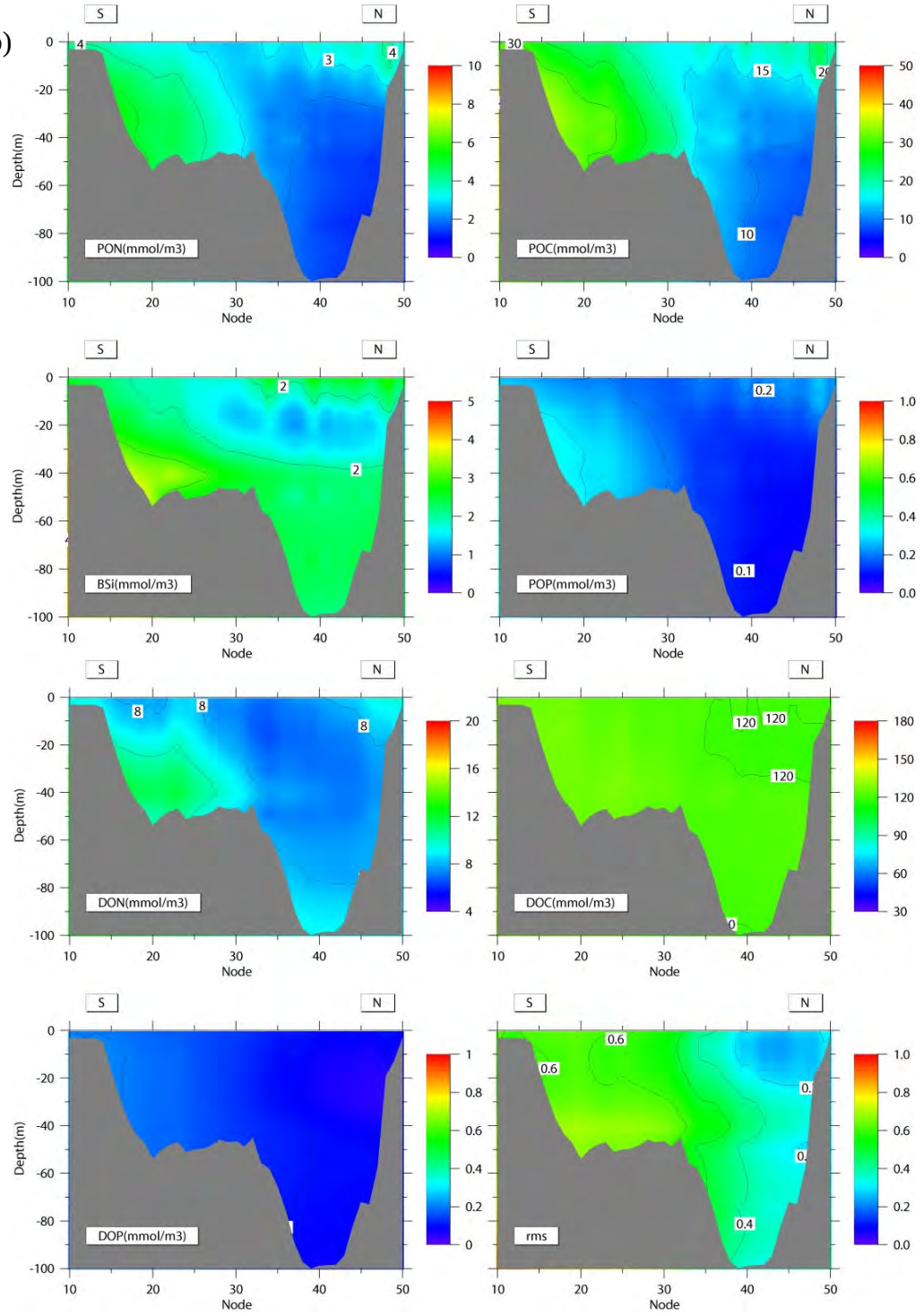

Figure 2.6. Continued.

(a)

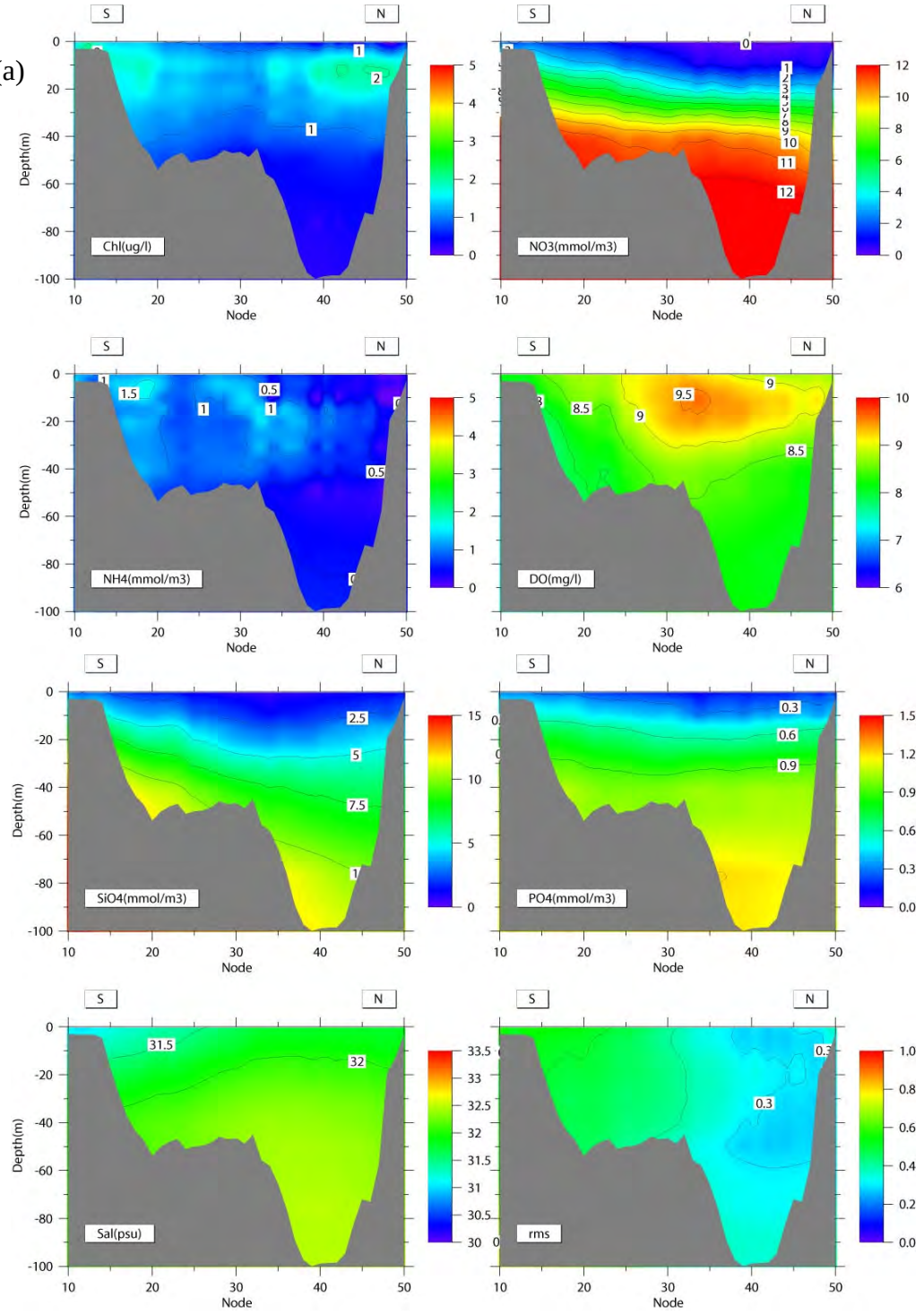

Figure 2.7. Open boundary conditions of (a) salinity, chlorophyll, nutrients, and DO, and (b) organic matter in August, 2002. The rms' are also shown in the lower right panels, which apply to all of the seven parameters in (a) and (b), respectively. The node 10 indicates Cape Cod and node 50 Cape Ann. (to be continued on the next page).

(b)

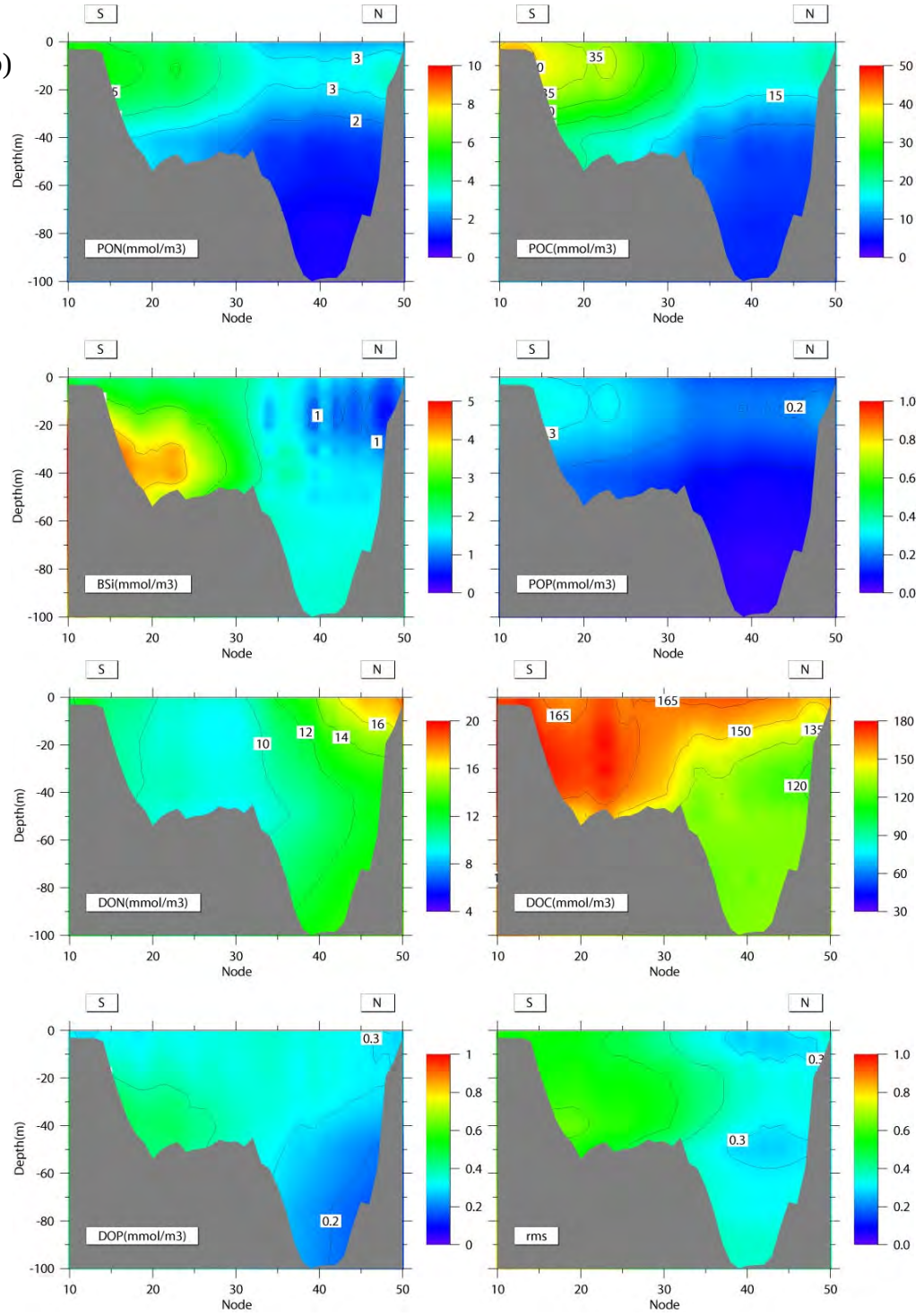

Figure 2.7. Continued.

(a)

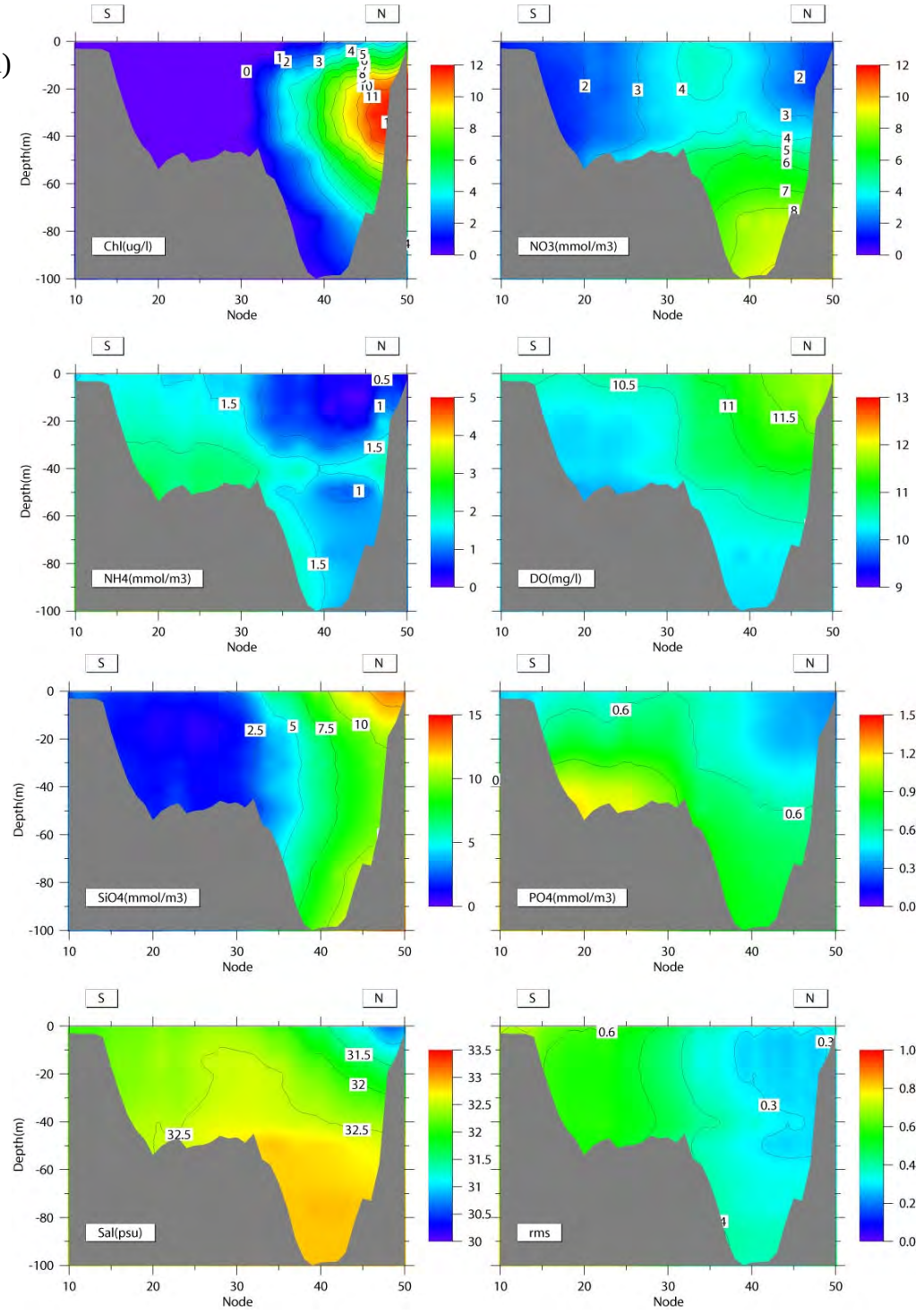

Figure 2.8. Open boundary conditions of (a) salinity, chlorophyll, nutrients, and DO, and (b) organic matter in April, 2003. The rms' are also shown in the lower right panels, which apply to all of the seven parameters in (a) and (b), respectively. The node 10 indicates Cape Cod and node 50 Cape Ann. (to be continued on the next page).

(b)

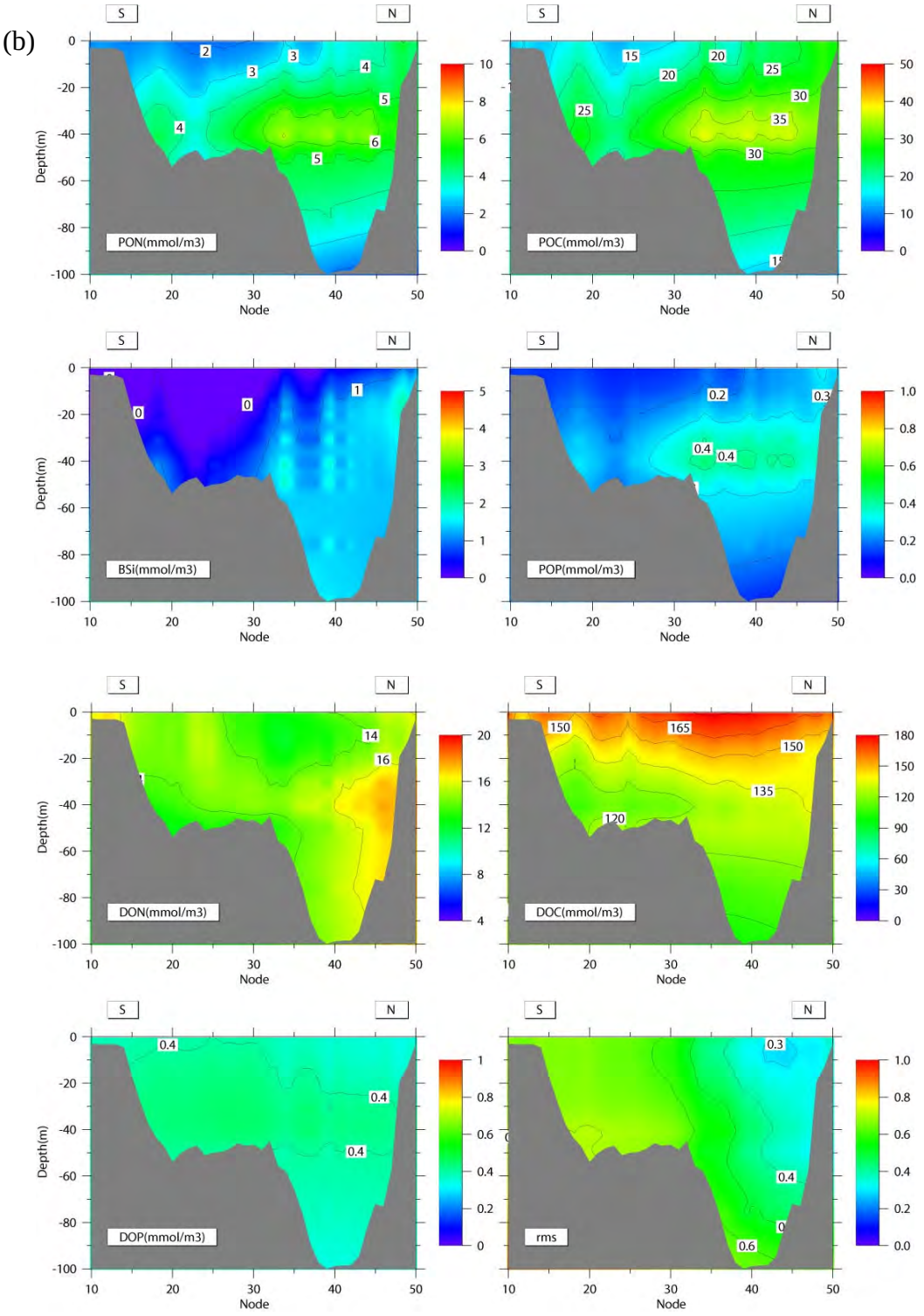

Figure 2.8. Continued.

(a)

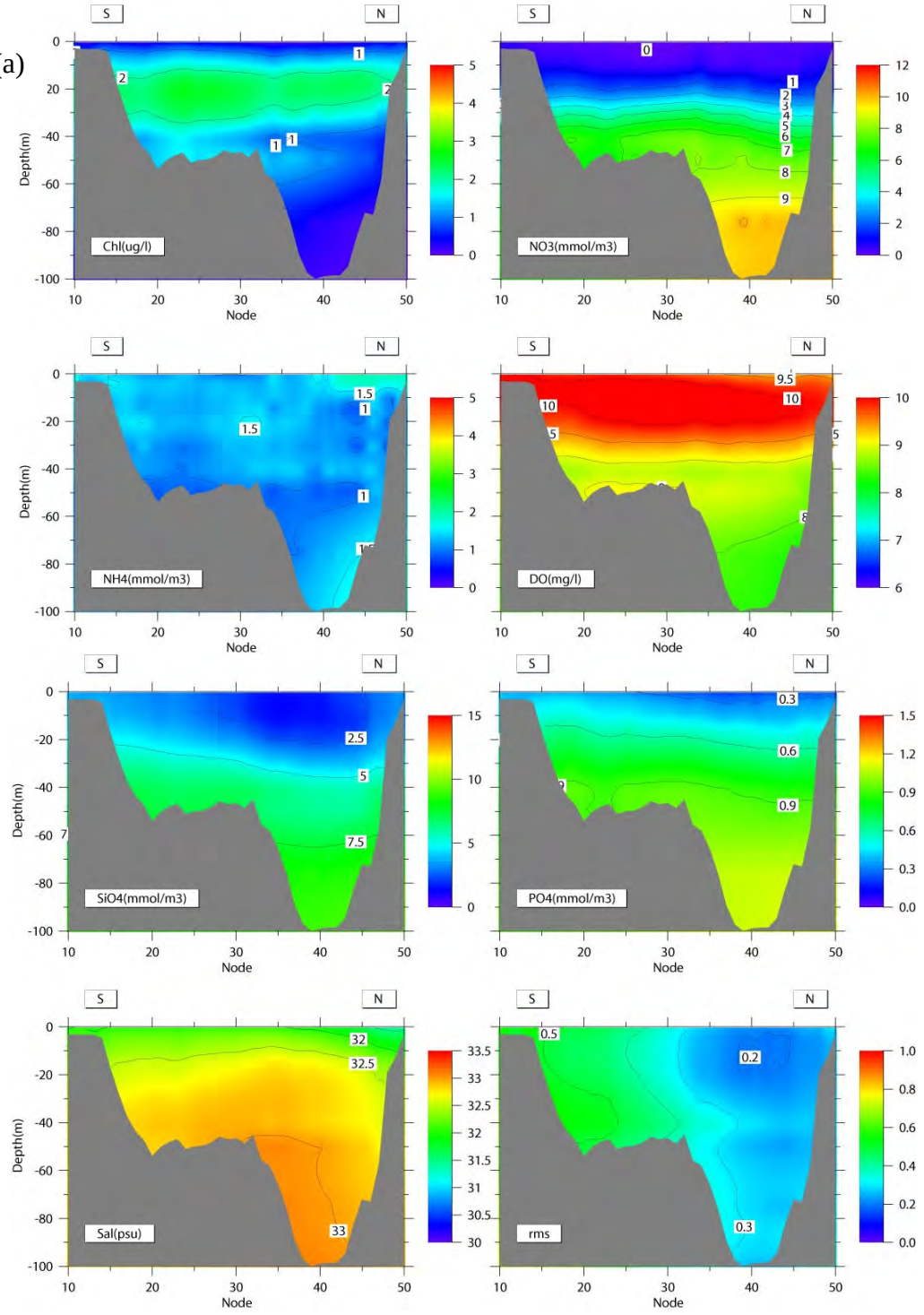

Figure 2.9. Open boundary conditions of (a) salinity, chlorophyll, nutrients, and DO, and (b) organic matter in August, 2003. The rms' are also shown in the lower right panels, which apply to all of the seven parameters in (a) and (b), respectively. The node 10 indicates Cape Cod and node 50 Cape Ann. (to be continued on the next page).

(b)

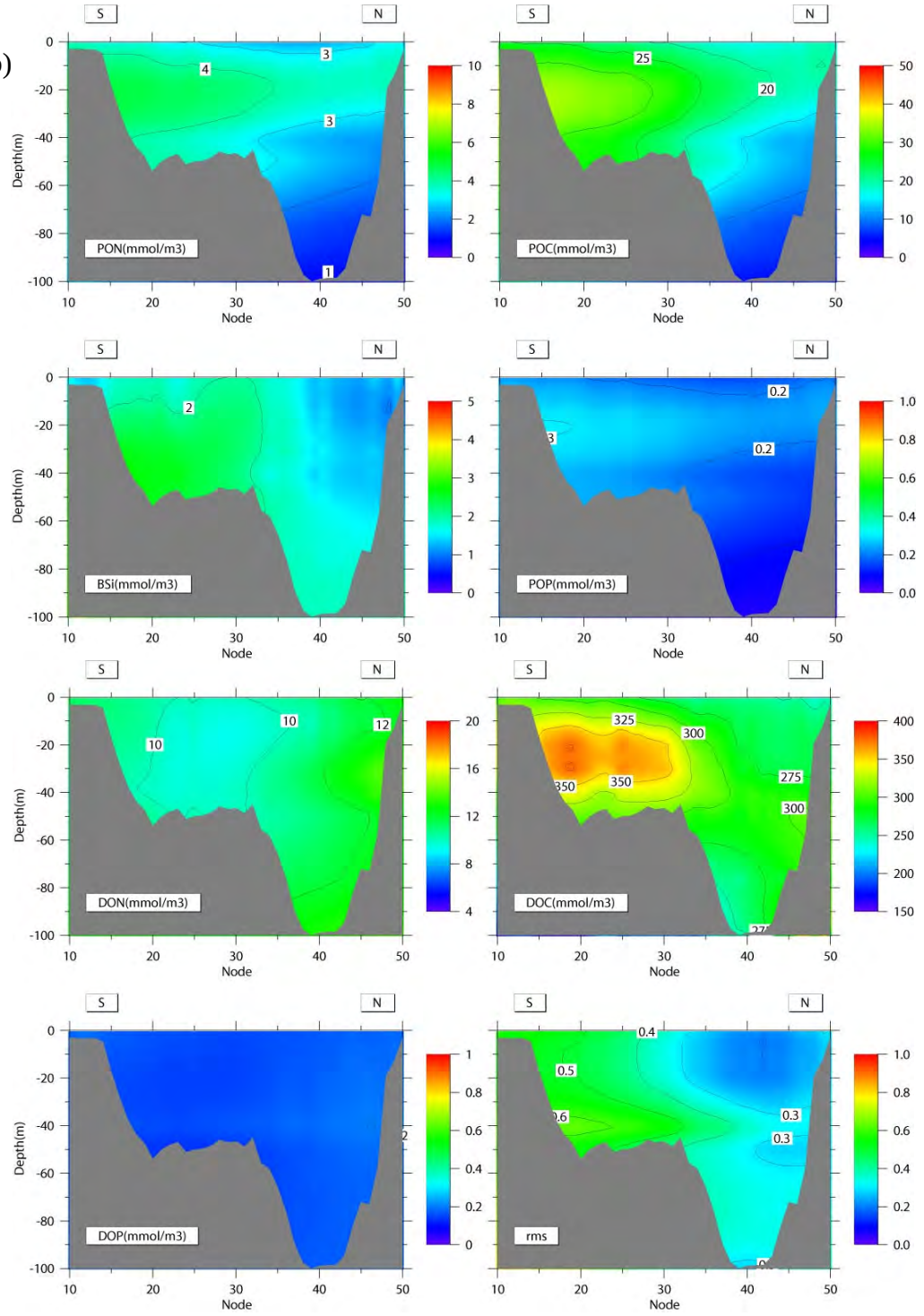

Figure 2.9. Continued.

(a)

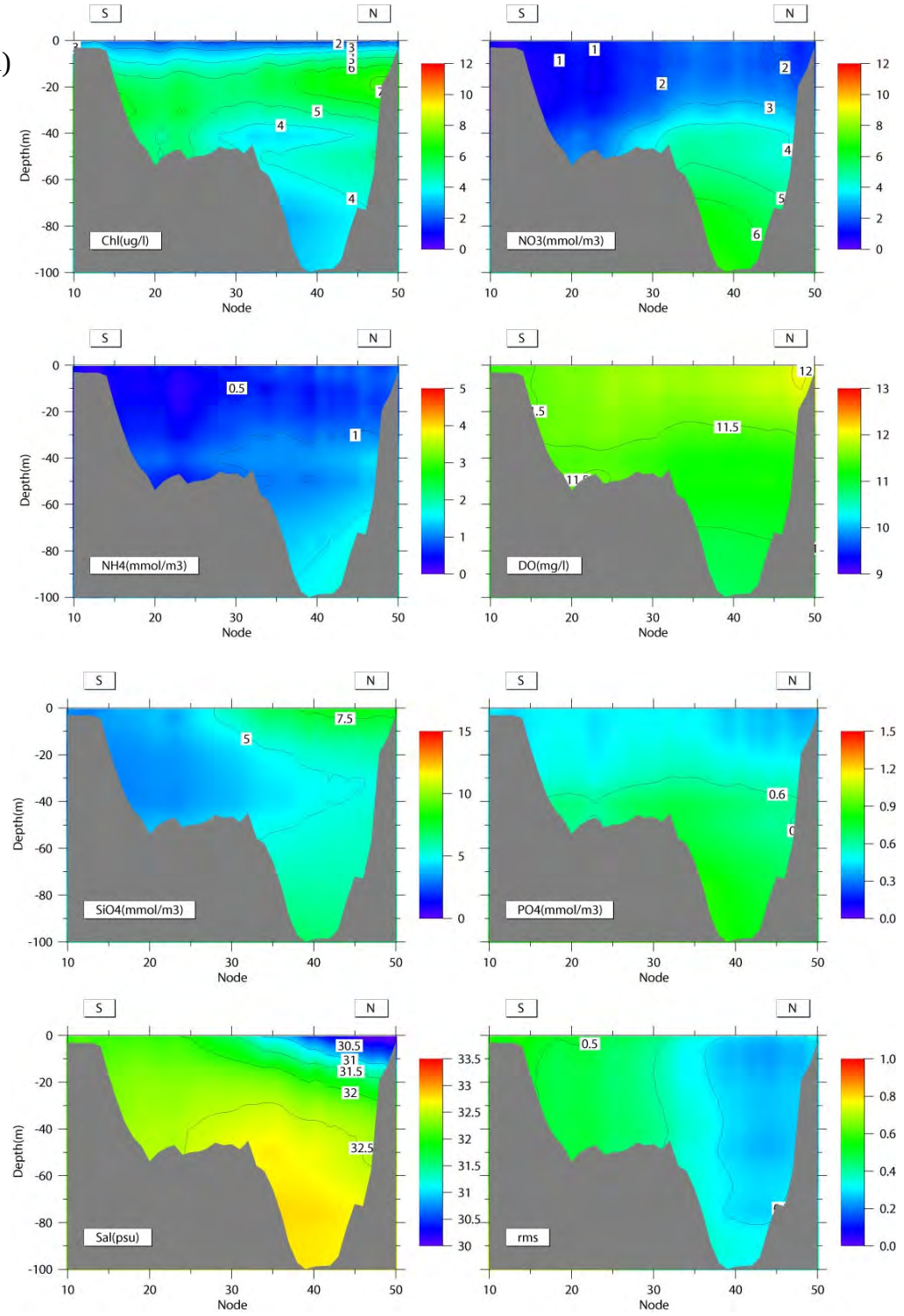

Figure 2.10. Open boundary conditions of (a) salinity, chlorophyll, nutrients, and DO, and (b) organic matter in April, 2004. The rms' are also shown in the lower right panels, which apply to all of the seven parameters in (a) and (b), respectively. The node 10 indicates Cape Cod and node 50 Cape Ann. (to be continued on the next page).

(b)

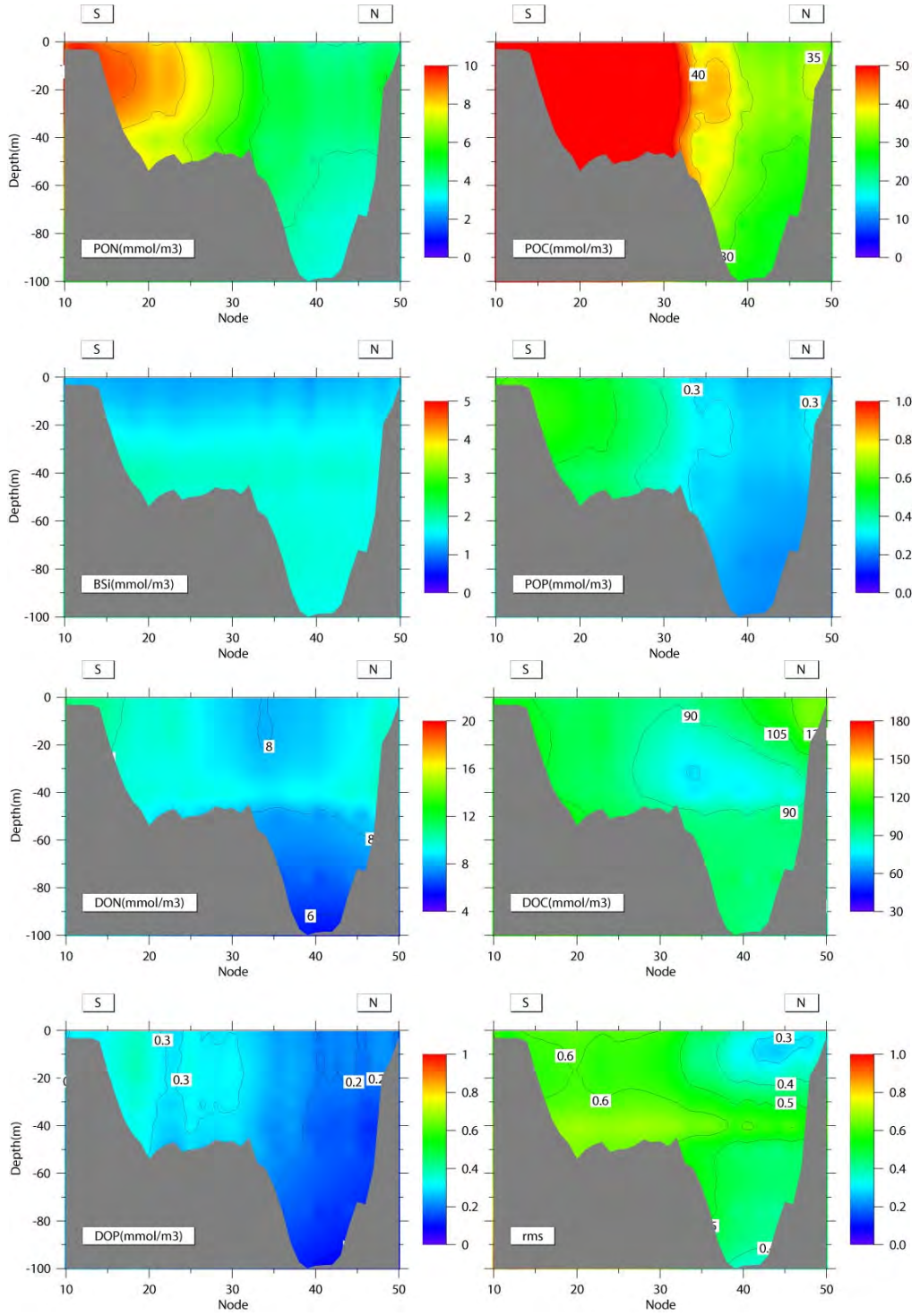

Figure 2.10. Continued.

(a)

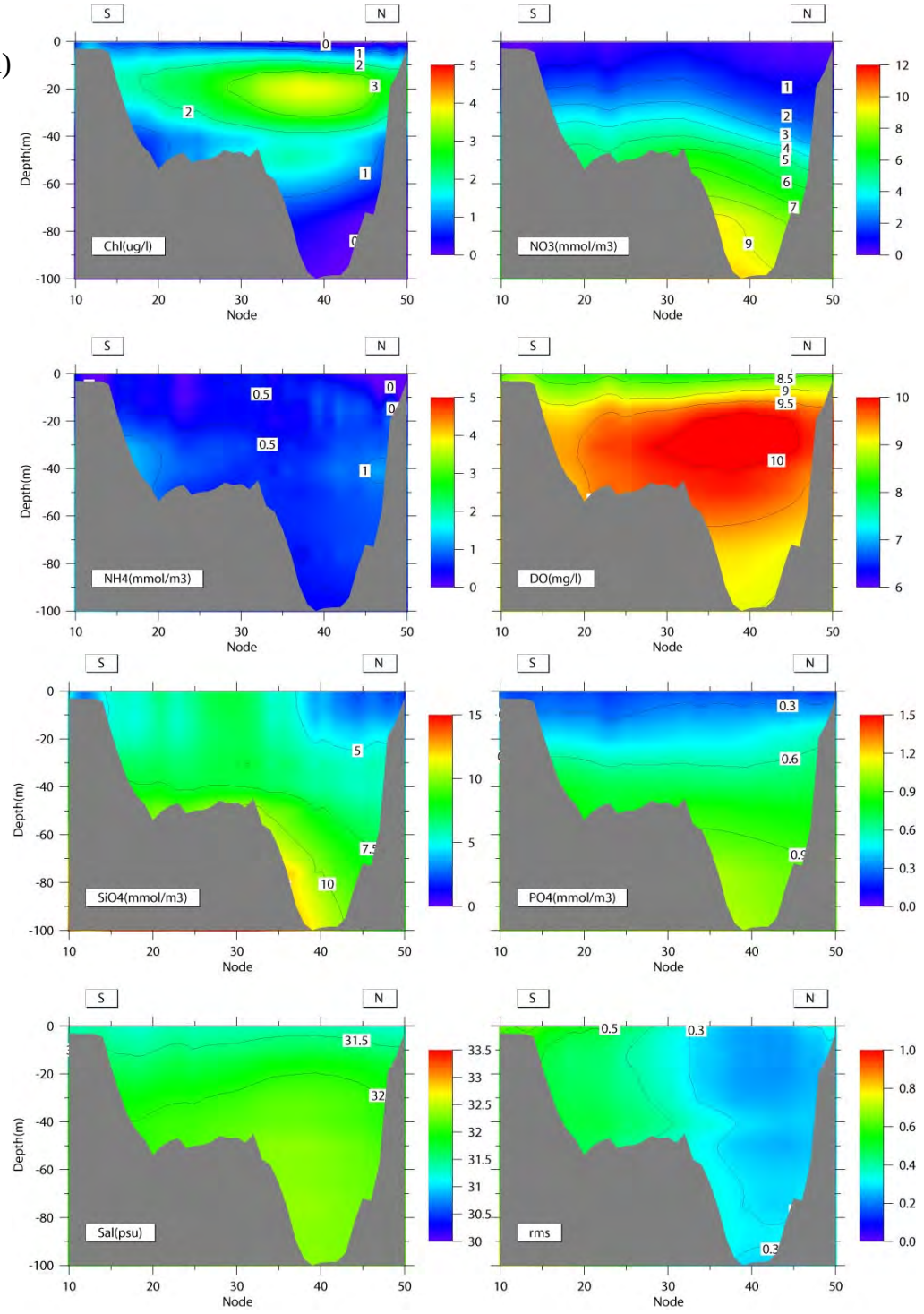

Figure 2.11. Open boundary conditions of (a) salinity, chlorophyll, nutrients, and DO, and (b) organic matter in August, 2002. The rms' are also shown in the lower right panels, which apply to all of the seven parameters in (a) and (b), respectively. The node 10 indicates Cape Cod and node 50 Cape Ann. (to be continued on the next page).

(b)

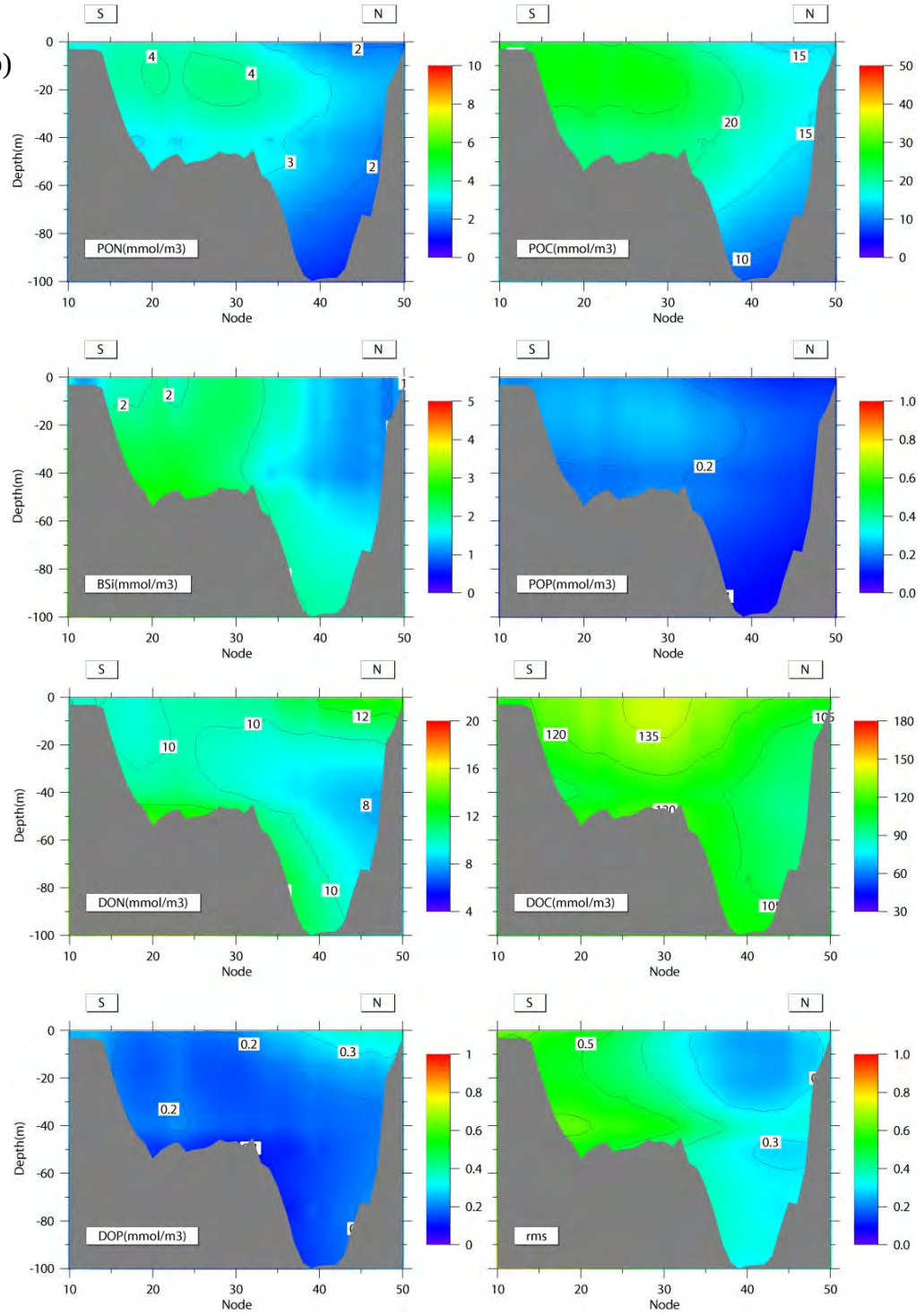

Figure 2.11. Continued.

3. VALIDATION

3.1 Survey and data description

The hydrography and water quality in the MBS were monitored with 17 one-day cruises per year at 21 nearfield (defined as an area within 5 km of the outfall) stations in 2002-2003; in 2004 this was reduced to 7 stations and 12 cruises per year. Each year, 6 of those nearfield cruises were paired with a 3-4 day bay-wide cruises, which covered the entire bay with an extra 20 farfield (beyond the nearfield) stations. In addition to hydrographic measurements (CTD, DO, chlorophyll fluorescene, light transmittance, and light intensity), water samples were collected at 5 pycnoline-bracketing depths to measure dissolved inorganic nutrients. A subset of those samples was analyzed for organic matter (17 stations), phytoplankton abundances (12 stations), chlorophyll, suspended solids, and DO. The 12 phytoplankton stations also had net tows for zooplankton abundance. The Primary productivity was measured at 3 stations: F23 close to Deer Island and N04 and N18 offshore in the nearfield. Detailed information about samples and data can be found in the MWRA reports (e.g., Libby et al., 2003; Libby et al., 2004). In this report, measurements at a subset of these stations are used for model validation (Figure 3.1a). These stations are the same stations used in the previous model validation for 2000-2001 (Jiang and Zhou, 2004c). One of those stations (N14) was dropped starting 2004, so the comparison invoked a nearby station (N16).

The water quality in BH was also extensively monitored through the Harbor Monitoring Project (e.g., Taylor et al., 2004). The program started in 1993, and water quality data were collected at 6 stations. Among the measured variables, chlorophyll, particulate organic nitrogen (PON) and dissolved oxygen (DO) are used for validating the results from the BEM runs.

The benthic metabolism and nutrient cycling were studied by taking sediment cores at 4 stations in Boston Harbor and 4 stations in Massachusetts Bay (Tucker et al., 2003; Tucker et al., 2004). Fluxes of nitrate, ammonia, denitrification, dissolved silica, phosphate and SOD through the sediment and water interface were measured four times

per year. Flux measurements at three stations in BH and three stations in MB were used for model validation.

3.2 Massachusetts Bay

Measured chlorophyll, DIN, PON, DON, $Si(OH)_4$, DO and DO saturation as environment health indices at 8 chosen stations (Figure 3.1a) were used for comparison of modeled results with data in the water column. The comparisons of modeled and observed surface and bottom concentrations of these variables are shown in Figures 3.2-3.4, and the comparisons of their vertical distributions are shown in Figures 3.5-3.14.

2002. Both modeled and observed chlorophyll concentrations in 2002 exhibited a similar pronounced seasonal cycle at these stations (Figure 3.2a, and third panels in Figures 3.5-3.7). The observed chlorophyll concentrations indicated a strong bloom in early February within coastal areas (N10, F01, and F06), which occurred in a warm winter with the mean temperature higher than 5ºC and weak wind mixing. A bay-wide spring bloom occurred in late March and April. The observed chlorophyll concentrations were low in the summer except for some episodic high values, and were high during late September and October at most stations, indicating a strong fall bloom.

The BEM reproduced the seasonal cycle of chlorophyll with a strong spring bloom in March (occurring 2 weeks earlier than the observed) and a fall bloom in late September and October (matching the observed in timing). The model also produced pronounced subsurface chlorophyll maxima during the spring bloom and relatively evenly-distributed vertical chlorophyll during the fall bloom, both of which were consistent with data. Modeled surface and bottom chlorophyll concentrations during spring and fall blooms were generally higher than the observed. The model did not predict the bloom observed in February. The cause was the designated optimal temperature of 8ºC used in the BEM that prevented spring phytoplankton group from blooming at temperature around 5ºC predicted and observed in MB in February, 2002. The model over-estimated the chlorophyll in the summer. The modeled chlorophyll concentrations were more evenly-distributed over the water column than the observed at most of stations except at N10.

The observed DIN in 2002 also showed a pronounced seasonal cycle consistent with the chlorophyll cycle (Figures 3.2b, second panels in Figures 3.5-3.7). In February, DIN concentrations were lower than that in other years, especially at coastal stations, following an undergoing phytoplankton bloom. The surface DIN was depleted from May to August, and the concentrations increased from September to the end of the year. The bottom DIN was generally high throughout the year except at F23 where DIN was depleted in the summer.

The comparison of modeled and observed DIN showed a good agreement except that modeled DIN concentrations were higher than observed before the spring bloom (Figure 3.2b). This agreement indicated that the model correctly reproduced the seasonal pattern of the nitrogen cycling including strong biological uptake during blooms and regeneration in the late spring and summer, even though modeled chlorophyll values were different from observed. At station F23, modeled DIN showed a different seasonal cycle from the observed with a continuous decrease in modeled DIN from February to August, and then a increase till the end of the year.

The observed $Si(OH)_4$ concentrations showed a similar seasonal cycle as that of the DIN concentrations except that the surface $Si(OH)_4$ was not depleted in the summer (Figure 3.2c). The observed $Si(OH)_4$ concentrations in February remained high, suggesting that the bloom was dominated by non-diatom species. Overall, modeled $Si(OH)_4$ agreed with data at most stations except at station F23.

The other two nitrogen pools, PON and DON, are compared in Figures 3.2d and 3.2e, respectively. Both of the modeled and observed PON and DON concentrations showed a weak seasonal variability with relatively low PON concentrations in the summer associated with low production and high regeneration. The observed DON showed significant increases at nearfield stations (N04, N10, and N14) in the fall. Modeled surface PON, surface DON and bottom DON agreed well with observed data, while the bottom PON concentrations were over-predicted by 2~3 fold in most of the year. One possible cause for this disagreement is the over-simplified zooplankton grazing model used in the BEM. In the model, the zooplankton grazing is imposed as an instantaneous removal of phytoplankton standing stock, and the removed phytoplankton biomass is

directly added into the settling particulate organic matter. Such a treatment of zooplankton grazing significantly shortens the time-scale of nutrient cycling, and can cause the over-prediction of near bottom PON and POC. The model did not reproduce the observed increase of DON at nearfield stations in the fall.

The comparison between modeled and observed DO concentrations is shown in Figure 3.2f and Figures 3.5-3.7. The observed DO concentrations exhibited a strong seasonal cycle at all stations. Both of the surface and bottom DO concentrations increased in the winter and early spring due to deep mixing produced by surface cooling and wind stirring, and increasing primary production. The observed DO peaked in February at shallow coastal stations (N10, F01 and F23) and in late March at offshore stations, and decreased steadily throughout the late spring and summer, primarily due to the decrease of saturation DO, which has an inverse relationship with water column temperature. Surface DO concentrations reached their minima in August and then increased from September to December. The bottom DO reached their minima in late September and early October, and then increased rapidly afterward. The increase of DO in the fall and winter was caused by the decrease of temperature and increase of mixing.

Overall, the model reproduced the seasonal cycle of observed DO concentrations reasonably well though there are some differences. First, the model under-estimated the peaks of surface DO concentrations during the winter-spring transition. Secondly, the modeled surface DO concentrations continued to decrease from August to October, opposite to the observed DO, and were lower than the observed in the fall. Finally, the model did not reproduce the episodic high DO values observed in the summer.

The comparison of modeled and observed saturation of DO is shown in Figure 3.2g, which indicated a pronounced seasonal cycle at these stations. Based on the observations, the surface waters were generally saturated in oxygen year around, with a relatively low saturation in the winter and a maximum saturation (110~120%) in March-April and the entire summer. The over-saturation of surface waters indicated was due to the primary production. The bottom DO saturation showed a seasonal cycle following that of bottom DO concentrations, and was below 100% with a minimum in October.

The model generally reproduced the seasonal cycles of DO saturation, and modeled values generally agreed with the observed except those at N10 and N07. Since the primary production in the winter was low, the under-estimation of DO saturation in November and December was likely due to the air-sea exchange algorithm of oxygen as noted in previous report (Jiang and Zhou, 2004c). The model also over-predicted the bottom DO saturation at shallow stations during the summer (N10, F23, F01 and F06), which might be due to over-estimated vertical mixing.

2003. The comparison of modeled and observed concentrations in 2003 is shown in Figure 3.3 and Figures 3.8-3.10. The characteristics of observed concentrations in 2003 were generally similar to those in 2002 with a few differences: (1) there was no bloom in February at most stations due to a cold winter in 2003 except F02; (2) both of the spring and fall blooms were stronger than those in 2002; (3) silicate concentrations remained high in the spring until mid-May; and (4) late fall increase of PON seen in 2002 was not observed.

The comparison between modeled and observed variables for year 2003 showed same agreements as those for 2002. The model reproduced the spring and fall blooms of phytoplankton well though it overestimated summer chlorophyll, especially near the bottom at shallow stations. Both of the modeled and observed chlorophyll indicated weaker blooms at N14 than at other stations. The modeled DIN concentrations tracked the observed ones very well except in February and March, when modeled DIN concentrations at inshore stations (F23, N10 and F01) were higher than the observed, likely due to the delay of modeled spring bloom at these stations. The model underestimated bottom DIN concentrations in May and June. The modeled $Si(OH)_4$ was also compared well with observed data. In February and March, the significant decreases in modeled $Si(OH)_4$ concentrations were consistent with the observed decreases of Si(OH)4 at the inshore stations (F23, N10 and N01) during the first two cruises of the year. Similar to year 2002, the modeled surface PON, surface DON and bottom DON concentrations were compared well with data, but the bottom PON concentrations were much higher than the observed. The modeled DO and DO saturation agreed with data well except those at the inshore stations in February and at nearfield stations in the

summer. During these periods, the modeled surface DO and DO saturation were lower than the observed, and bottom DO saturations at shallow stations were over-estimated.

2004. The comparison of modeled and observed variables in 2004 is shown in Figure 3.4 and Figures 3.11-3.13. Among all three years (2002-2004), the winter of 2004 was coldest, and the lowest chlorophyll concentrations were observed in February. A strong *Phaeocystis* bloom occurred in March and April, during which high chlorophyll concentrations and rapid DIN drawdowns were observed (Libby et al., 2005). The fall bloom was nearly missing except a weak enhancement of chlorophyll at F23. Consistent with the seasonal cycle of chlorophyll, the PON concentrations showed a single peak in the spring and were generally low in the rest of the year. The observed DO concentrations were smooth and showed a similar seasonal cycle at all stations, reflecting the small variation in productivity throughout the year. Moreover, the minimum bottom DO concentration in fall was 7.0 mg/l, which was much higher than those in 2002 (5.6 mg/l) and 2003 (5.6 mg/l) and likely due to low production and a cool summer in 2004.

The modeled results compared well with data by reproducing the strong spring and weak fall blooms, and the seasonal cycles of nutrients, DO, DON and PON. The model also reproduced the silicate drawdown observed in spring 2003, which implied the existence of a significant amount of diatom during the bloom of non-Si consuming *Phaeocystis*. There were some differences between the modeled results and observations same as in other years: (1) the model over-estimated surface chlorophyll concentrations in the summer; (2) the model over-estimated the bottom PON concentrations; and (3) the model over-estimated bottom DO saturation at shallow stations.

3.3 Boston Harbor

The 6 stations chosen for comparison represent the North Harbor (024, 130 and 140) and South Harbor (077, 141 and 124), respectively (Figure 3.1b). Measured chlorophyll, PON and DO concentrations were used for the validation.

2002. Modeled and observed surface and bottom chlorophyll, PON and DO concentrations are compared in Figure 3.14. The observed data indicated dramatically

different seasonal cycles from those in MB. Chlorophyll concentrations exhibited a strong spring bloom in February and a long summer bloom (July and August). Consistent with these, the observed PON concentrations showed a narrow strong peak in February and a broad peak in the summer. The DO concentrations increased in the winter and peaked in February. It decreased continuously in the spring and summer until reaching a minimum in August and September, and then increased again throughout the rest of the year.

The modeled chlorophyll compared reasonably well with data. The chlorophyll concentrations increased continuously from March to August with small vertical gradients. However, the modeled spring bloom in March was several weeks behind the observed; and the modeled summer bloom lasted much longer than the observed extending into the fall. Similar to the chlorophyll results, the modeled PON concentrations agreed generally with data, but were lower than the observed in February and higher than the observed in the summer and fall. The modeled DO concentrations showed a similar seasonal cycle as the observed, but were generally higher than the observed in the summer by 1~2 mg/l, which was likely due to the over-predicted summer bloom.

2003. Modeled and observed surface and bottom chlorophyll, PON and DO concentrations are compared in Figure 3.15. A similar seasonal cycle of chlorophyll as that of 2002 was observed except the spring bloom occurring in March, about the same time as the bloom in MB, and a weaker summer bloom than that of 2002. Consistent with this, the PON concentrations showed small seasonal trends. The DO concentrations also showed a similar seasonal cycle to those of 2002, but reached their minima in September.

The modeled results showed a similar agreement with data to that of 2002 except that the modeled DO concentrations in this year compared very well with data, likely due to small differences between the model-predicted and observed summer blooms.

2004. The modeled and observed surface and bottom chlorophyll, PON and DO concentrations are compared in Figure 3.16. Both of the modeled and observed results showed very similar features to those of 2003, and had a same degree of agreement. One

noticeable feature was that the minimum DO concentration was much higher than those of 2002 and 2003, which was likely due to relatively low temperature in the summer.

3.4 Primary productivity

2002. The comparison of vertically integrated primary production (PP) between modeled and observed values in 2002 is shown in Figure 3.17 and Table 3.2. The observed PP at stations N04 and N18 showed a seasonal cycle consistent with observed chlorophyll concentrations: an early bloom in February, a spring bloom in March-April and a fall bloom in August-September. At station F23, the observed PP showed two peaks in February and August, and was lower than 1 gC m^{-2} day^{-1} in the rest of the year. The modeled PP at both N04 and N18 generally agreed with observed data except that during the spring bloom the modeled PP increased earlier than the observed, and during the fall bloom modeled high PP lasted much longer than the observed. The modeled PP at F23 showed a similar pattern to the observed, but the predicted spring bloom was about 2~3 weeks behind the observed, and the production in the summer was higher than the observed. The over-prediction of production at F23 during summer and fall had been encountered during earlier simulations (HydroQual, 2000; HydroQual, 2003; Jiang and Zhou, 2004c).

2003. The comparison of modeled and observed PP in 2003 is shown in Figure 3.18 and Table 3.2. The observed PP showed a weak spring bloom in March and a strong fall bloom in September and October, and remained low throughout the rest of the year. The modeled PP showed similar seasonal variations to the observed at these monitoring stations, though the model tended to over-predict both spring and fall blooms at N04 and N18. The modeled summer PP at F23 was higher than the observed as well.

2004. The comparison of modeled and observed PP in 2004 is shown in Figure 3.19 and Table 3.2. The observed PP values at stations N04 and N18 showed a moderate spring bloom in April and were lower than 1 gC/m^2/day in the rest of the year. No fall bloom was observed. The observed PP at F23 was fairly constant except the low values in early February and August. The modeled PP showed some differences from the observed: (1) the model predicted a stronger and earlier (2 weeks) spring bloom than the

observed; (2) the modeled PP at N04 and N18 were higher than the observed during 2 summer events; and (3) in summer, the modeled PP at F23 was higher than the observed.

3.5 Sediment fluxes

The model performance in simulating the coupling between the water column and sediment is validated through fluxes of nitrate (JNO_3), ammonia (JNH_4), silicate (JSi), phosphate (JPO_4), denitrification (JN_2) and SOD.

2002. The comparison of modeled and observed sediment fluxes in 2002 is shown in Figure 3.20. In BH, the model reproduced the observed seasonal trends and values of nitrate and silicate fluxes, but over-estimated the fluxes of phosphate, SOD and ammonium, and under-estimated the denitrification rate except in Quincy Bay (BH08A).

In MB, the modeled fluxes agreed well with most observed values at all stations. A weak seasonal pattern of increasing fluxes from March to September could be identified in most modeled fluxes, which were not present in observed fluxes. The model over-estimated ammonium fluxes at MB03 and under-estimated the silicate fluxes at station MB05.

2003. The comparison of modeled and observed sediment fluxes in 2003 is shown in Figure 3.21. In BH, the model reproduced the observed seasonal trends and values of nitrate, silicate and SOD fluxes at most stations except in Quincy Bay (BH08A) where modeled fluxes were lower than the observed. The model reproduced the seasonal trends and values of phosphate flux except at BH03. The modeled over-estimated the ammonium flux and under-estimated the denitrification rate except in Quincy Bay (BH08A).

In MB, the modeled sediment fluxes agreed well with most of the observed values at all stations except that the model under-estimated the silicate flux in the spring and summer. Similar to year 2002, a weak seasonal pattern of increasing fluxes from March to September could be identified in most modeled fluxes, which was not present in observed values. The model over-estimated the ammonium flux at MB03.

2004. The comparison of modeled and observed sediment fluxes in 2004 is shown in Figure 3.22. In both BH and MB, the conclusions from the 2003 comparison can be applied to the 2004 comparison.

3.6 Statistical analysis

In order to quantitatively evaluate the differences between modeled and observed results, a regression analysis was carried out for key environmental variables and parameters, which include salinity, chlorophyll, DO, DIN, silicate and primary production. Correlation coefficients (r) and root-mean-squares (rms) of differences between modeled and observed surface and bottom salinity, chlorophyll, DO, DIN, and silicate at all sampled stations and depth-integrated primary production at N04 and N18. The rms is used to quantify the mean differences between modeled and observed values for each parameter.

The correlations between modeled and observed salinity, chlorophyll, DIN, DO and silicate for 2002-2004 are shown in Figures 3.23-3.25, and are summarized in Table 3.1. All correlation are significant with $p<0.01$. Overall, modeled salinity agreed with data very well in all three years. Modeled chlorophyll concentrations had significant correlations with observed values, though modeled chlorophyll concentrations had smaller variations than the observed.

The model simulated general values and variability of surface DIN reasonably well. Modeled bottom DIN concentrations did not reproduce the observed variations 2002 and 2003, though modeled mean DIN agreed with observed mean values. The model performed best in 2004 in terms of chlorophyll and nutrients because of less short-term (days to weeks) variability seen in both model results and observations, as compared to 2002-2003. The modeled silicate concentrations at both surface and bottom also had good correlations with observed values in these years with the rms values generally lower than those of DIN. Modeled and observed nutrient concentrations at the lower end of concentrations were less scattered, which suggested that the model was able to capture the major nutrient drawdown by phytoplankton, though modeled chlorophyll values showed substantial deviations from observed values.

Modeled and observed DO concentrations correlated quite well with the rms value less than 1 mg/l. The analysis also indicated that the model reproduced the occurrences of low DO as observed in all three years, as evident from the good correlations at the lower end of DO concentrations. The highest correlations and least rms between modeled and observed values were found in 2004, similar to chlorophyll.

The correlations between modeled and observed primary production are shown in Figure 3.26. To calculate these correlations, observed PP were interpolated over the year to derive monthly mean values (excluding January since there was no observation in January), and modeled results were averaged to derive monthly means for N04 and N18 (total 22 data points in each year). The results at F23 were not used because only 6 measurements per year were made. These results indicated that the modeled PP had significant correlations with the observed values (with $p<0.05$ for 2002, $p<0.01$ for 2003, and $p<0.05$ for 2004, respectively), similar to the regression results of chlorophyll. Modeled results showed smaller variations than the observed did. Modeled PP had the lowest correlation with data in 2002.

Table 3.1. Summary of correlations between modeled and observed results*.

Years	Variables	Surface		Bottom	
		Correlation coefficient (r)	RMS	Correlation coefficient (r)	RMS
2002	Salinity	0.85	0.3	0.84	0.25
	Chlorophyll	0.17	2.8	0.25	2.5
	DO	0.69	1.0	0.76	0.9
	DIN	0.62	3.9	0.29	4.4
	$Is(OH)_4$	0.60	2.3	0.55	3.2
2003	Salinity	0.73	0.55	0.8	0.38
	Chlorophyll	0.45	2.6	0.56	2.3
	DO	0.85	0.9	0.92	0.7
	DIN	0.75	3.1	0.26	5.2
	$Is(OH)_4$	0.6	2.5	0.52	3.0
2004	Salinity	0.63	0.58	0.71	0.37
	Chlorophyll	0.47	1.6	0.71	1.5
	DO	0.9	0.64	0.9	0.6
	DIN	0.91	2.2	0.78	3.2
	$Is(OH)_4$	0.87	2.2	0.71	2.8

* The number of samples n>400 in 2002-2003 for each parameter except surface DIN (n=384 for 2002 and n=324 for 2003, respectively) and n>200 in 2004 for each parameter.

Table 3.2 Modeled and observed primary production at N04 and N18

	2002				2003				2004			
	N04		N18		N04		N18		N04		N18	
	Mdl.	Obs.	Mdl.	Obs.	Mdl.	Obs.	Mdl.	Obs.	Mdl.	Obs.	Mdl.	Obs.
January	0.60	NA	0.49	NA	0.38	NA	0.29	NA	0.28	NA	0.31	NA
February	1.23	1.55	1.06	2.01	1.20	0.54	0.88	0.32	0.64	0.46	0.53	0.33
March	2.73	1.21	2.22	1.07	1.98	0.98	1.58	1.02	2.10	1.25	1.94	0.50
April	2.26	2.72	1.97	3.28	1.25	0.87	1.51	0.40	1.05	1.83	1.14	1.20
May	1.32	0.78	1.18	0.70	0.37	0.30	0.87	0.31	1.42	0.70	0.77	0.77
June	1.33	0.80	0.98	1.01	0.97	0.37	1.05	0.42	0.89	0.66	1.24	0.51
July	1.45	0.94	1.54	1.78	0.69	0.76	1.55	0.59	0.67	0.52	1.20	0.48
August	1.63	2.15	1.58	2.83	1.35	0.78	1.81	0.57	0.95	0.46	1.05	0.75
September	2.44	2.36	1.97	1.38	1.32	0.59	1.66	0.72	1.07	0.58	1.43	0.48
October	2.43	0.56	2.14	0.32	2.78	0.89	2.52	2.00	0.47	0.54	0.73	0.56
November	1.32	0.76	1.20	0.38	1.60	1.57	1.32	1.44	0.20	0.30	0.15	0.28
December	0.35	0.24	0.30	0.27	0.63	0.58	0.54	0.37	0.15	0.22	0.14	0.15

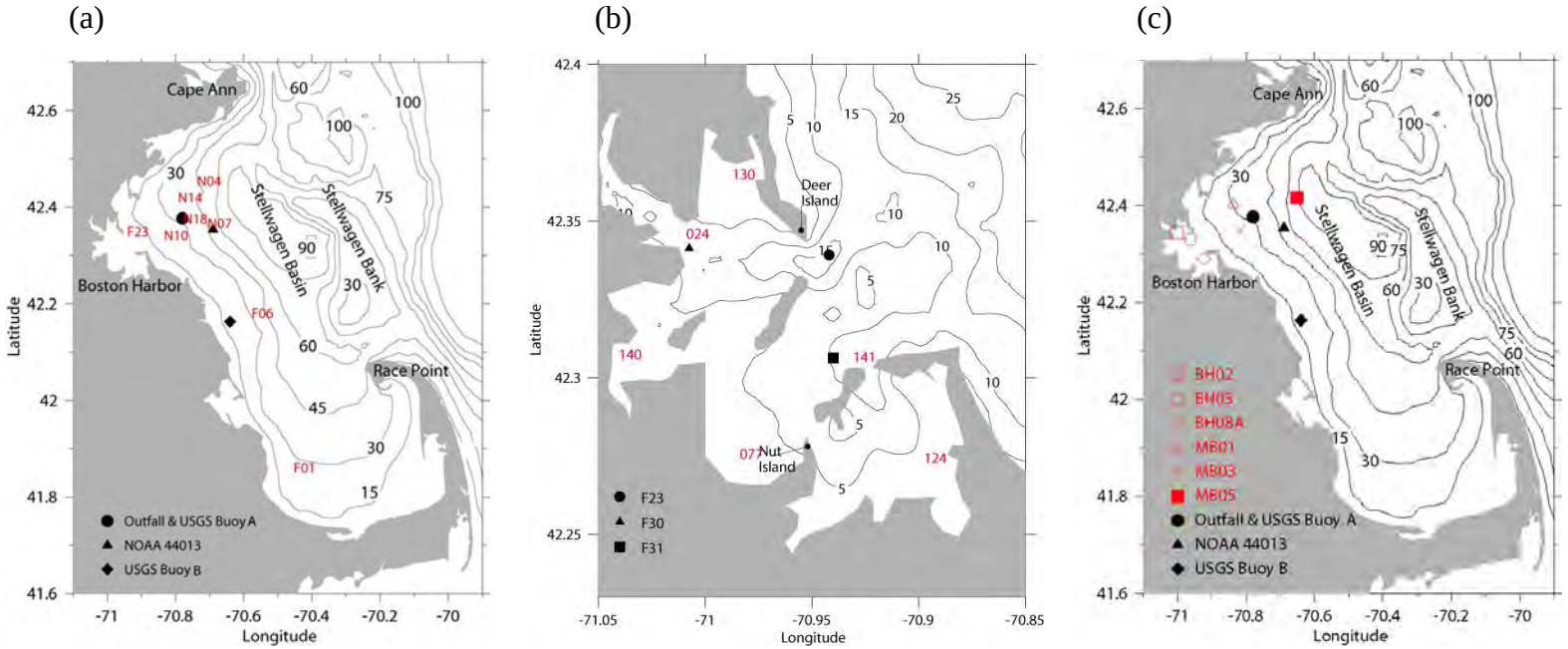

Figure 3.1 Station maps for data comparison: (a) MB, (b) BH, and (c) stations for sediment fluxes. The station N18 was only used for primary production comparison. The station N14 was not occupied in 2004 and the results at a nearby station N16 (not shown) were used for the comparison.

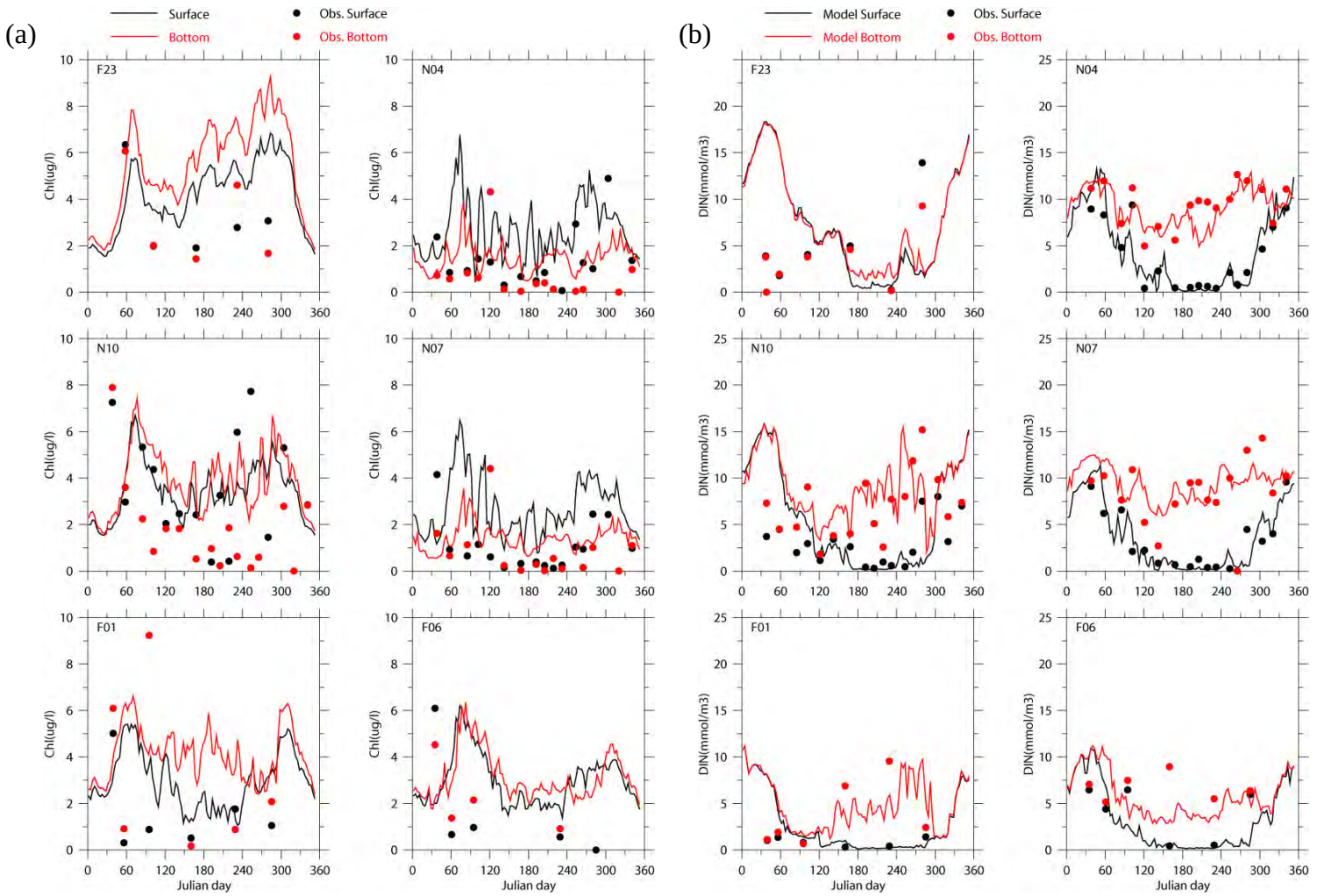

Figure 3.2. Time series of modeled and observed variables in 2002: (a) chlorophyll, (b) DIN, (c) SiO_4, (d) PON, (e) DON, (f) DO and (g) DO saturation (to be continued on next page).

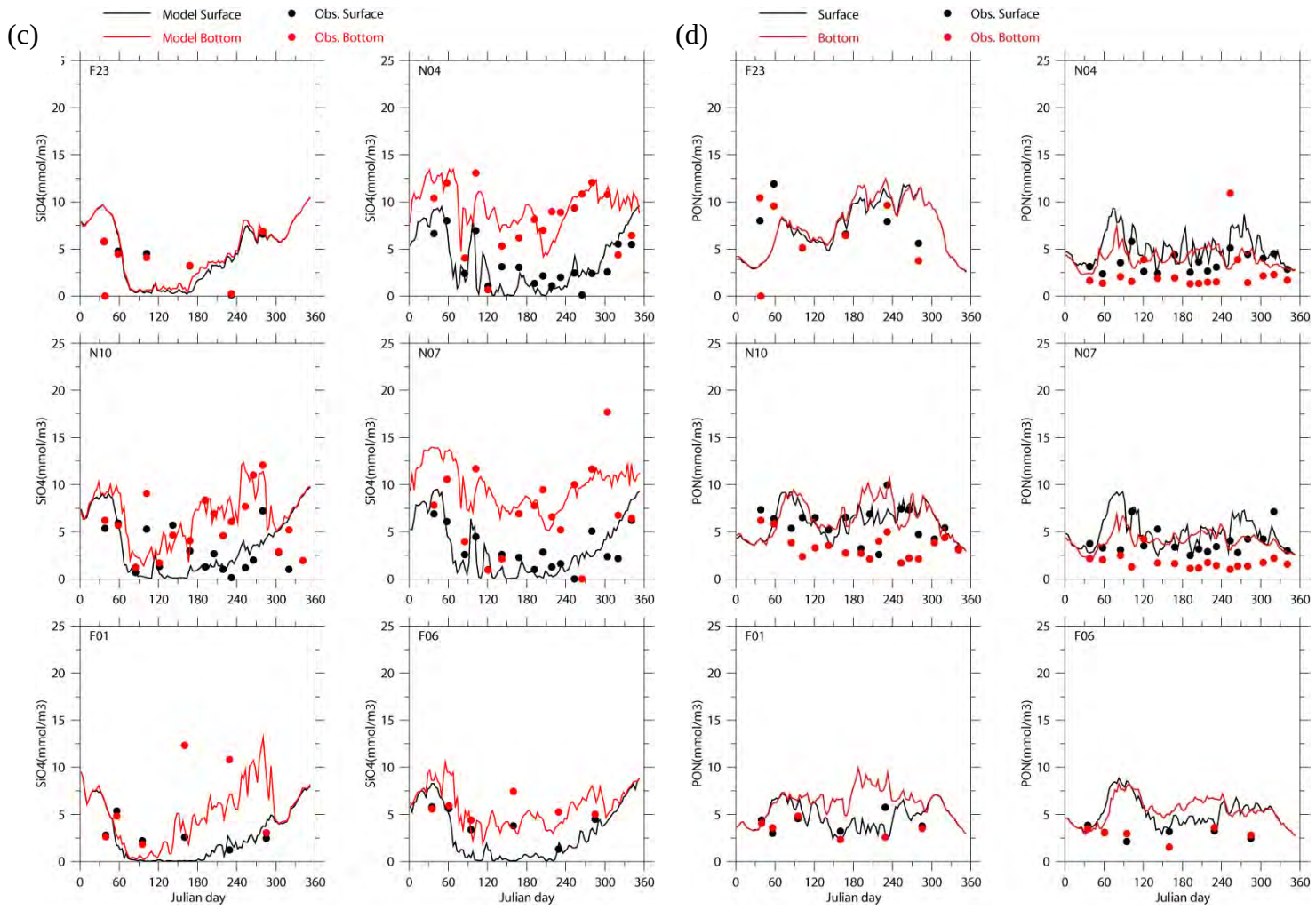

Figure 3.2. Continued.

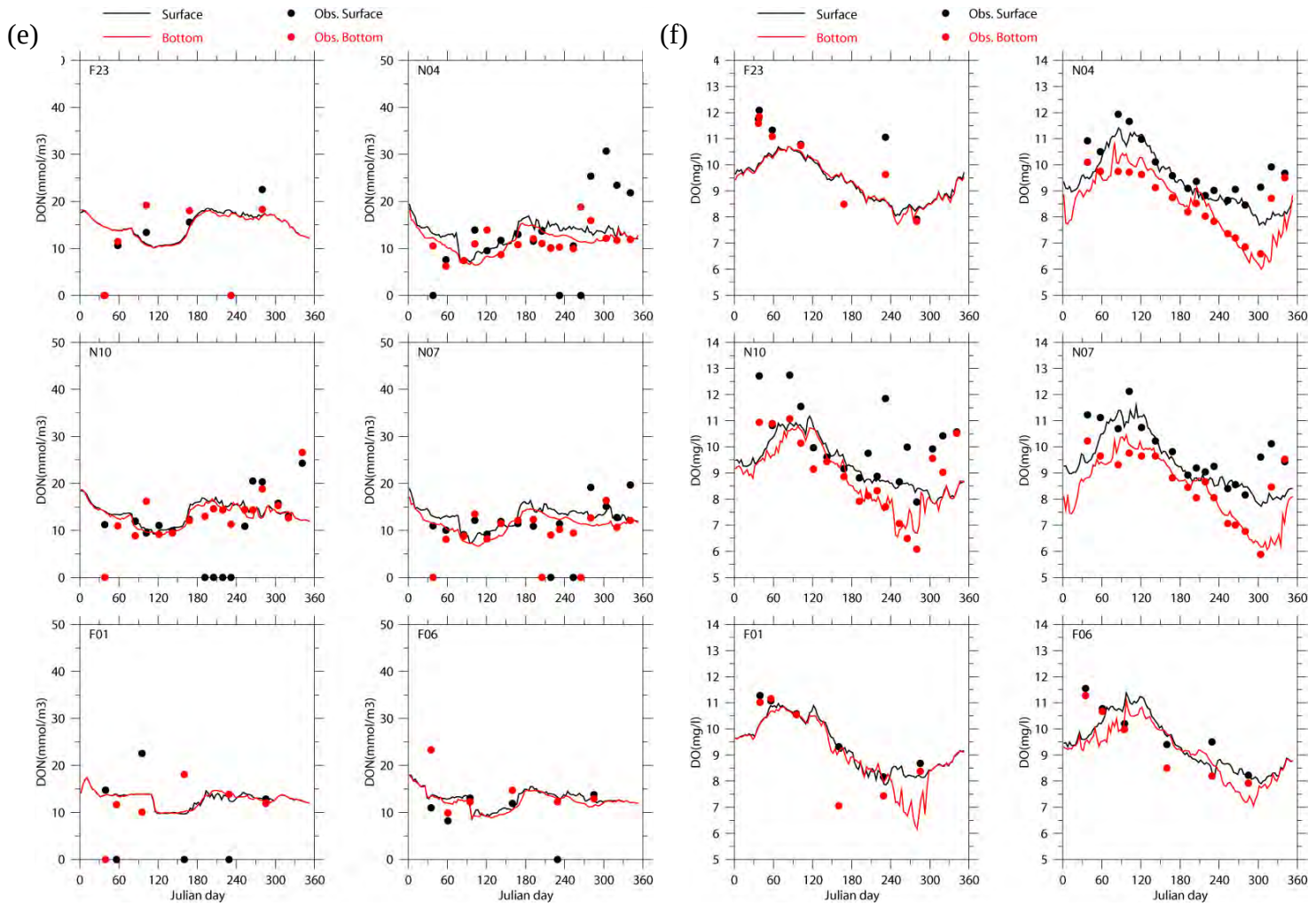

Figure 3.2. Continued.

(g)

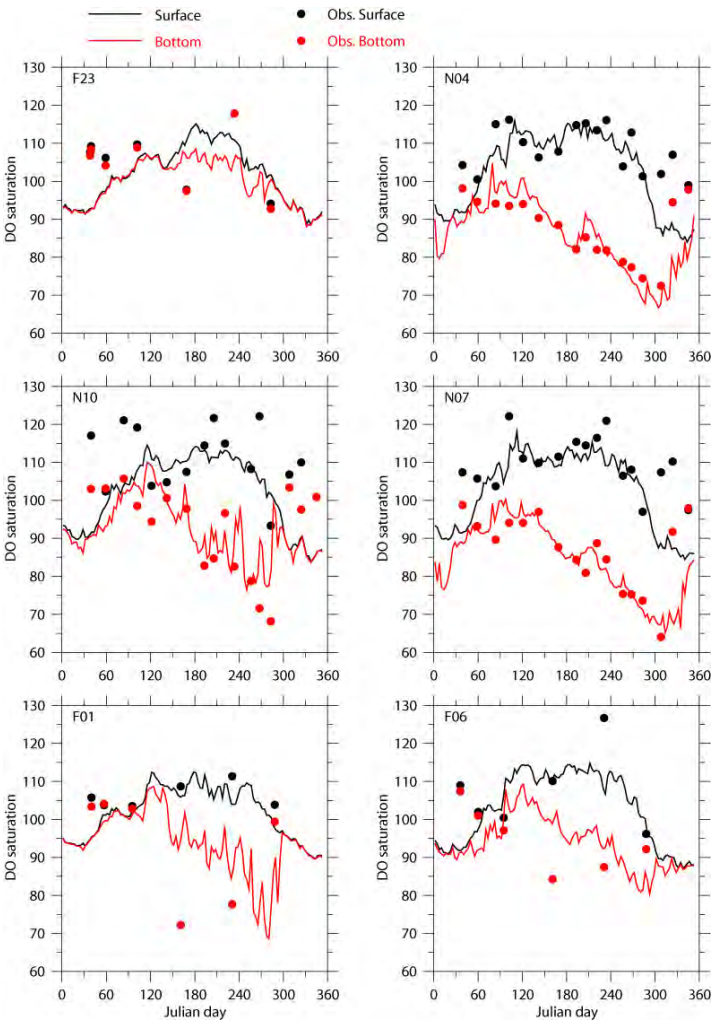

Figure 3.2. Continued.

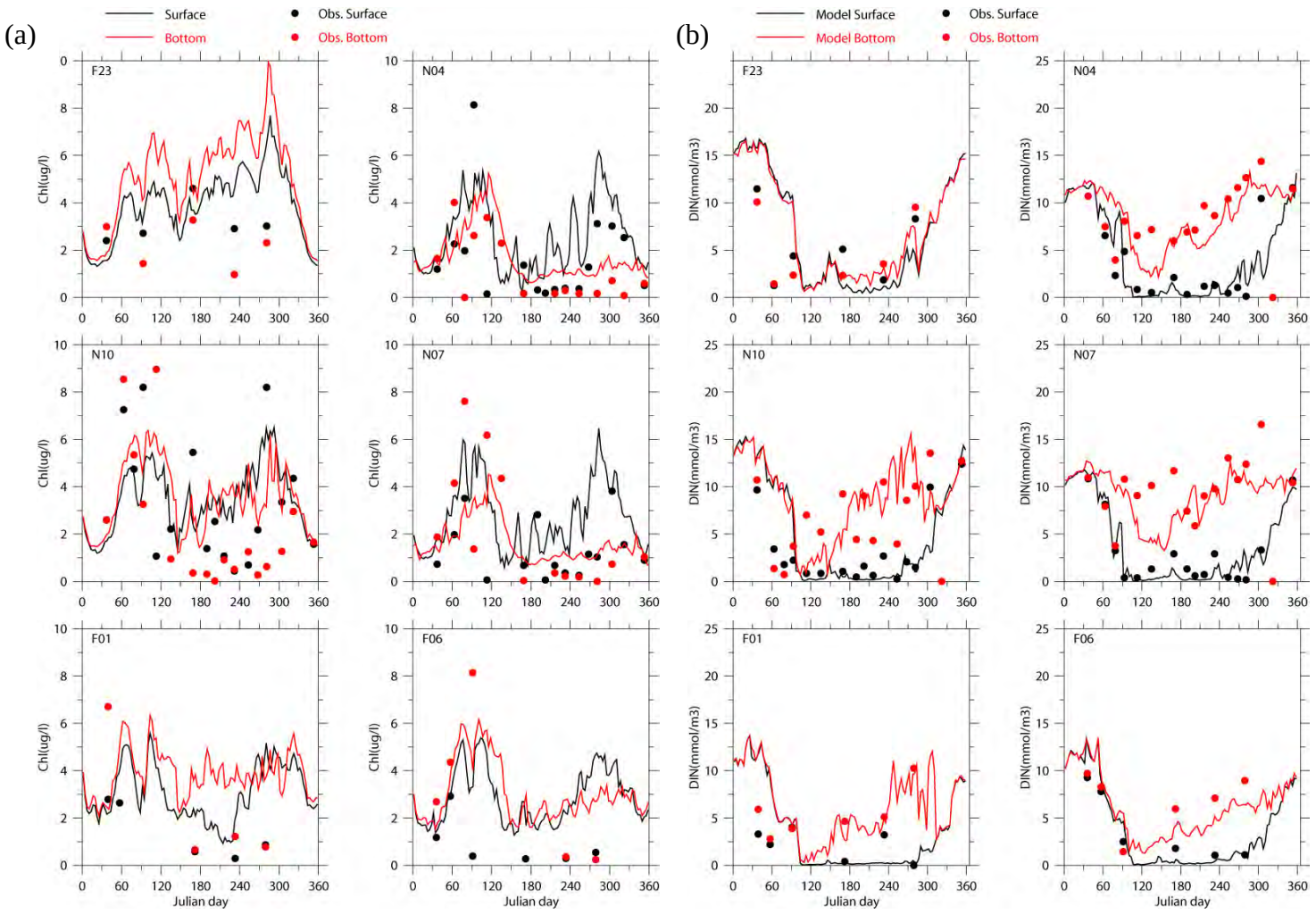

Figure 3.3. Time series of modeled and observed variables in 2003: (a) chlorophyll, (b) DIN, (c) SiO_4, (d) PON, (e) DON, (f) DO and (g) DO saturation (To be continued on next page).

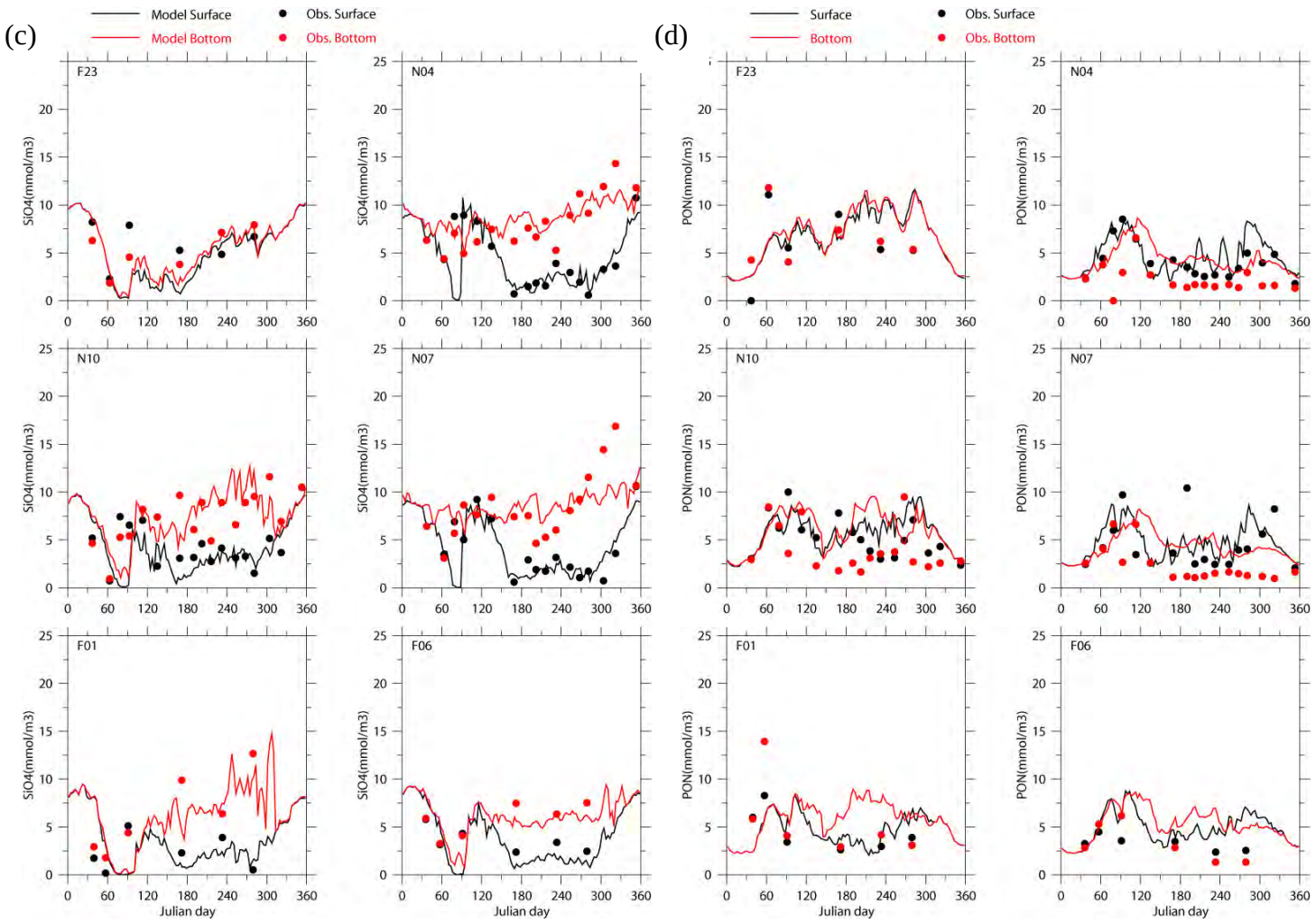

Figure 3.3. Continued.

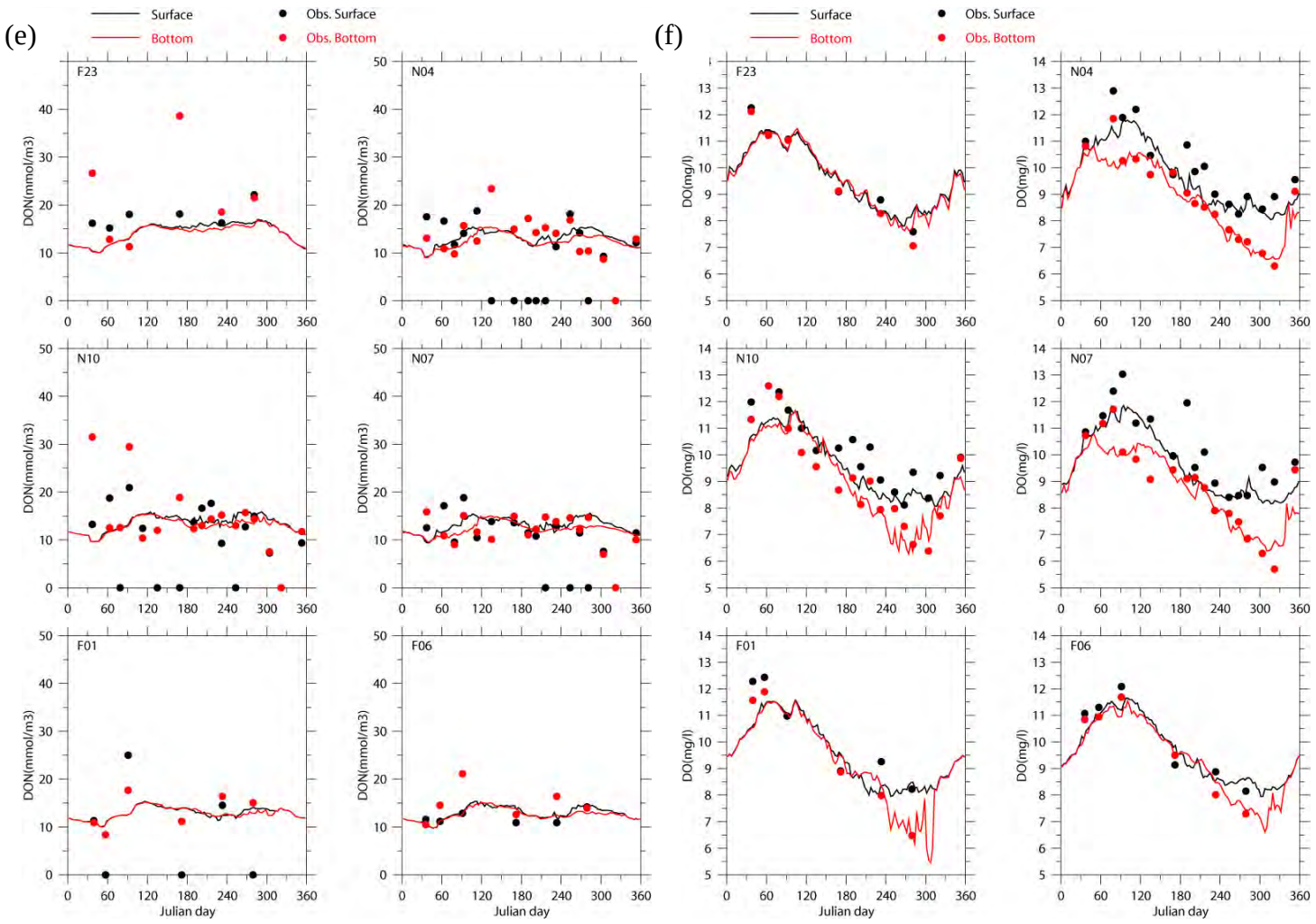

Figure 3.3. Continued.

(g)

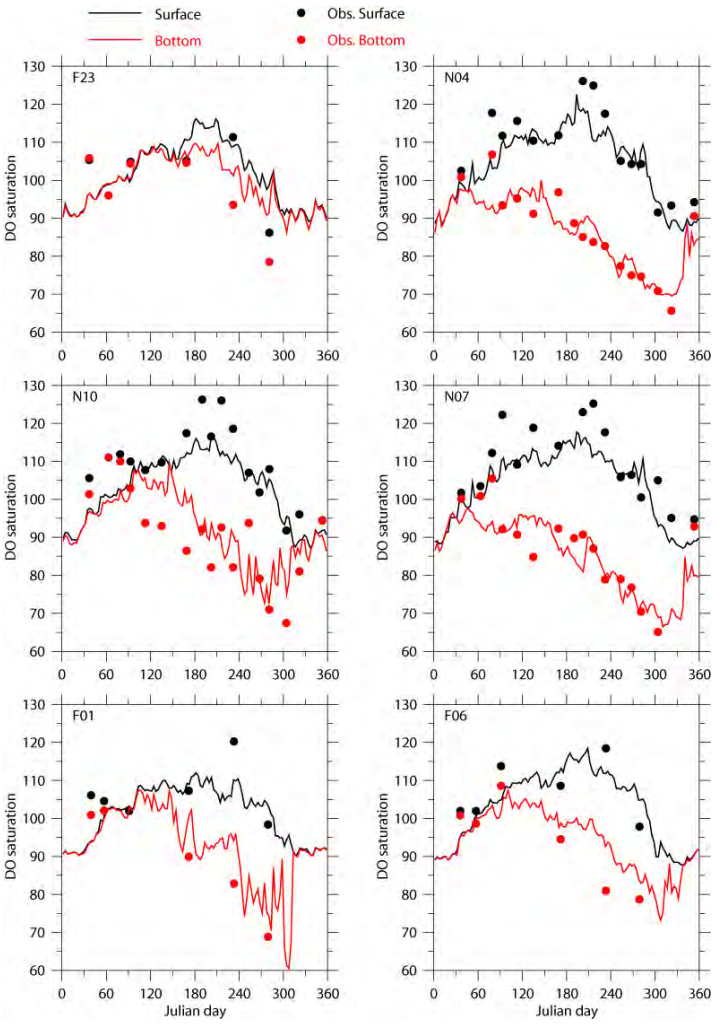

Figure 3.3. Continued.

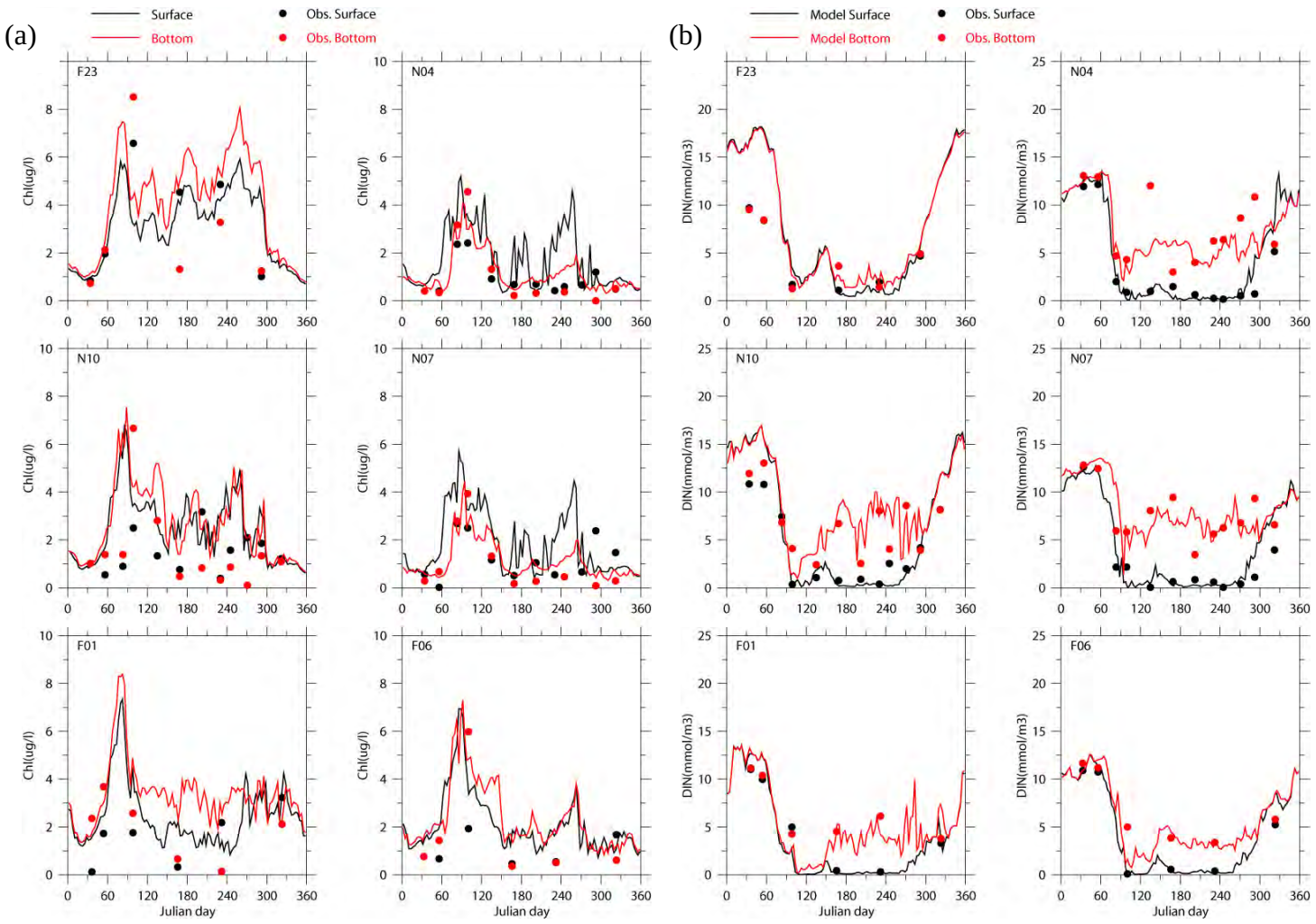

Figure 3.4. Time series of modeled and observed variables in 2004: (a) chlorophyll, (b) DIN, (c) SiO_4, (d) PON, (e) DON, (f) DO and (g) DO saturation (To be continued on next page).

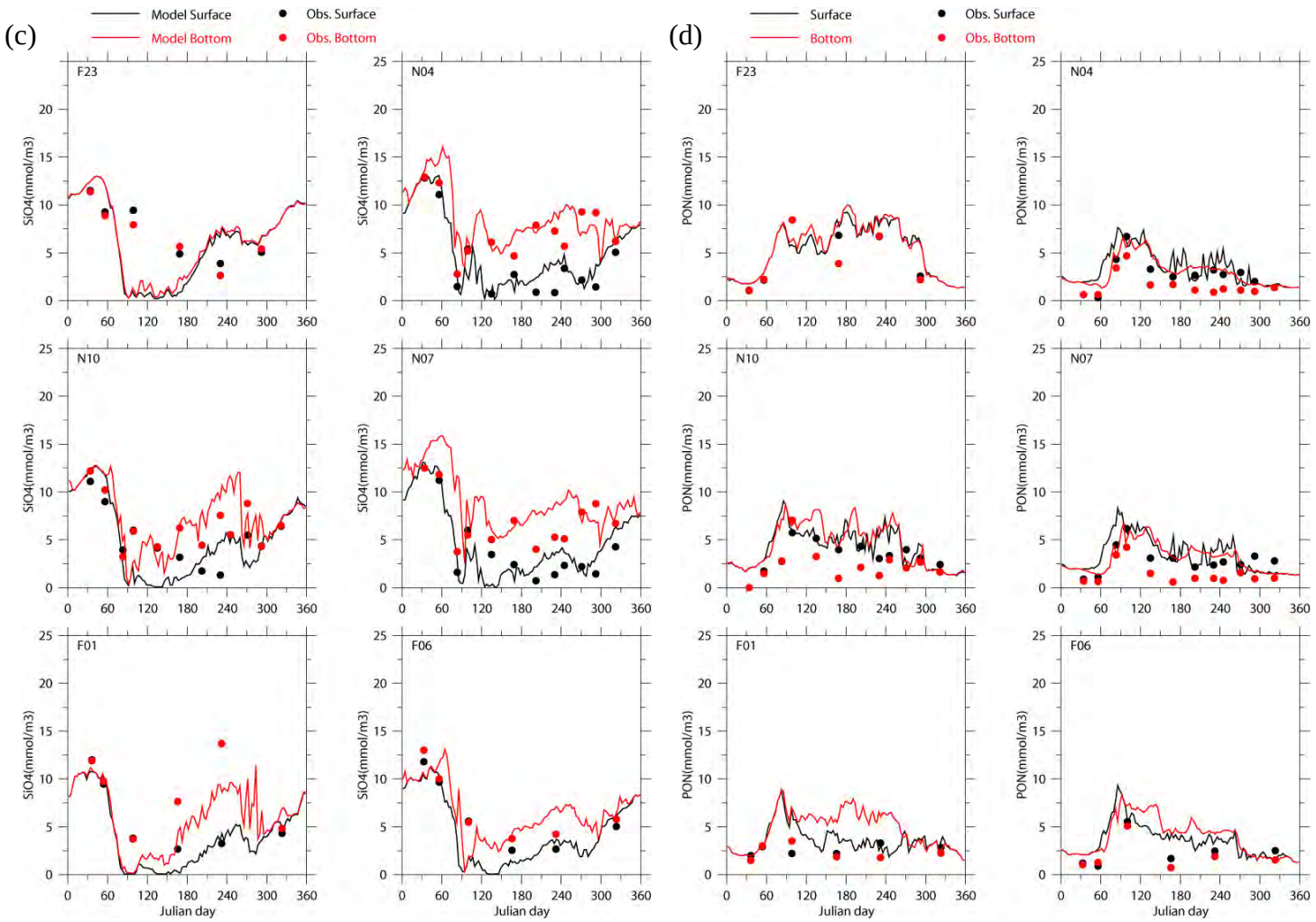

Figure 3.4. Continued.

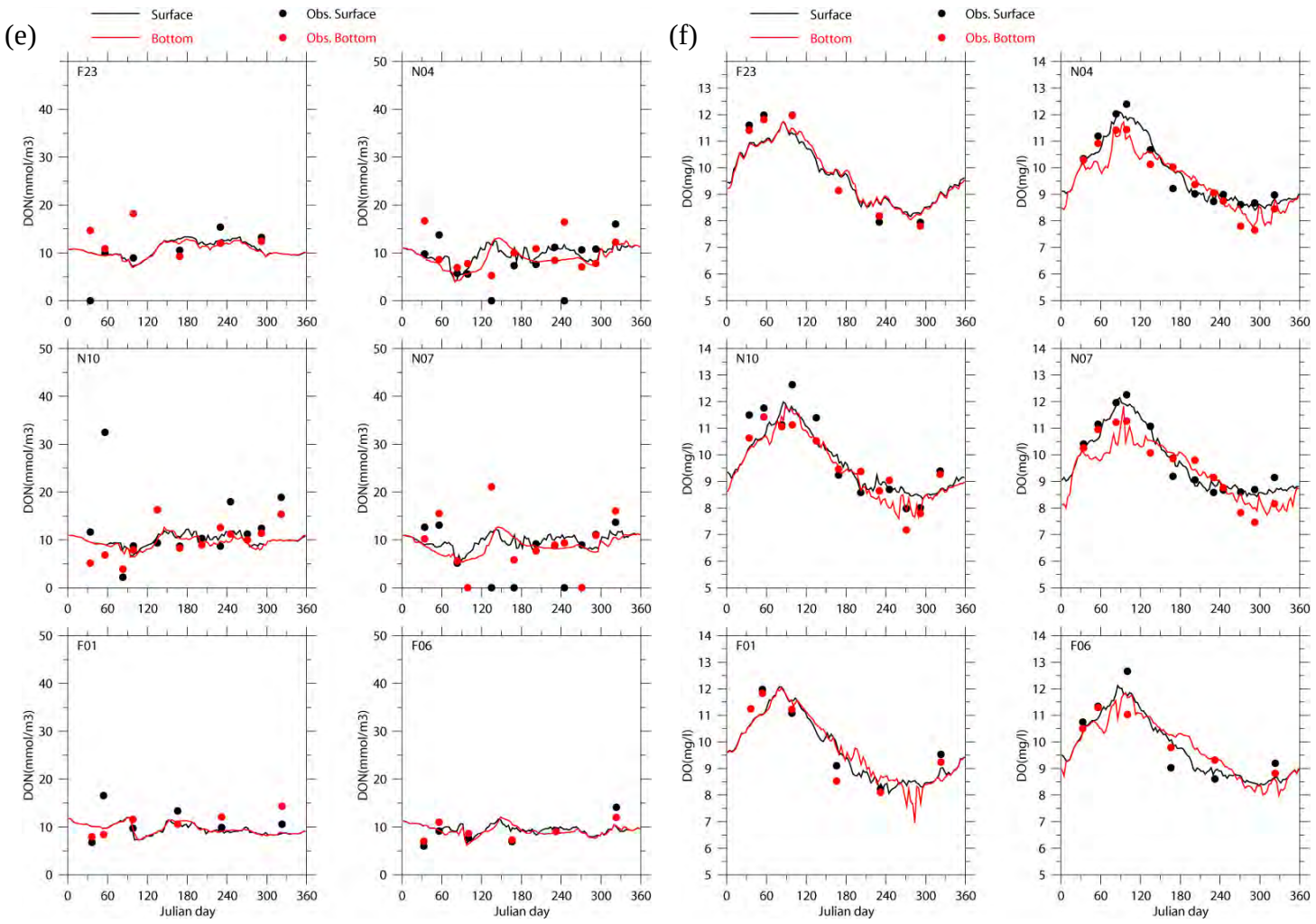

Figure 3.4. Continued.

(g)

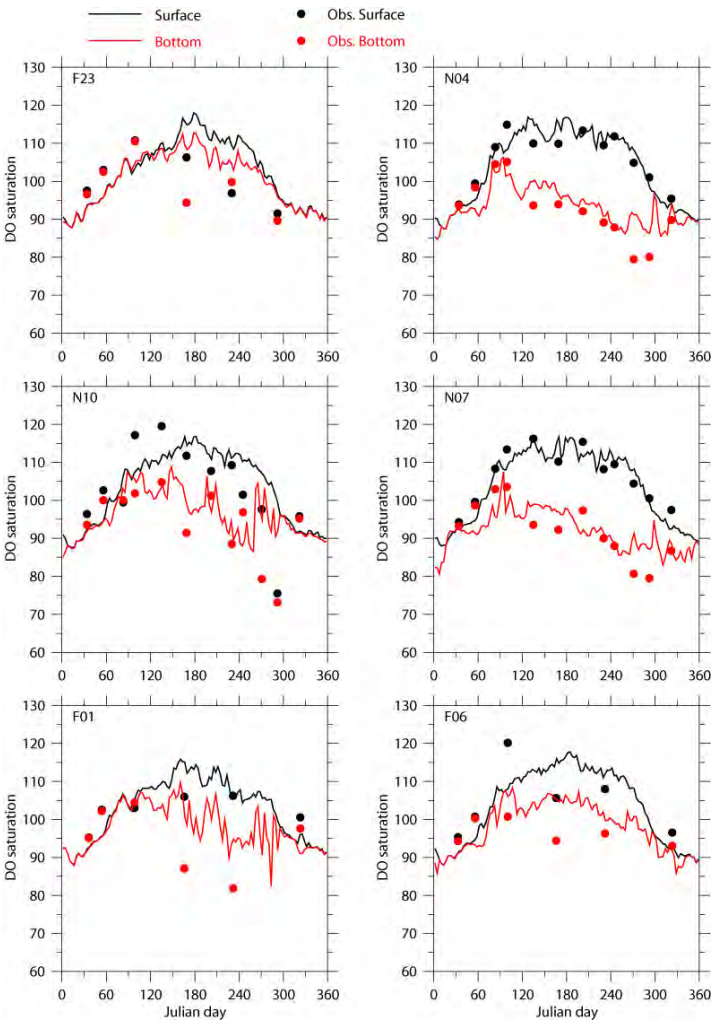

Figure 3.4. Continued.

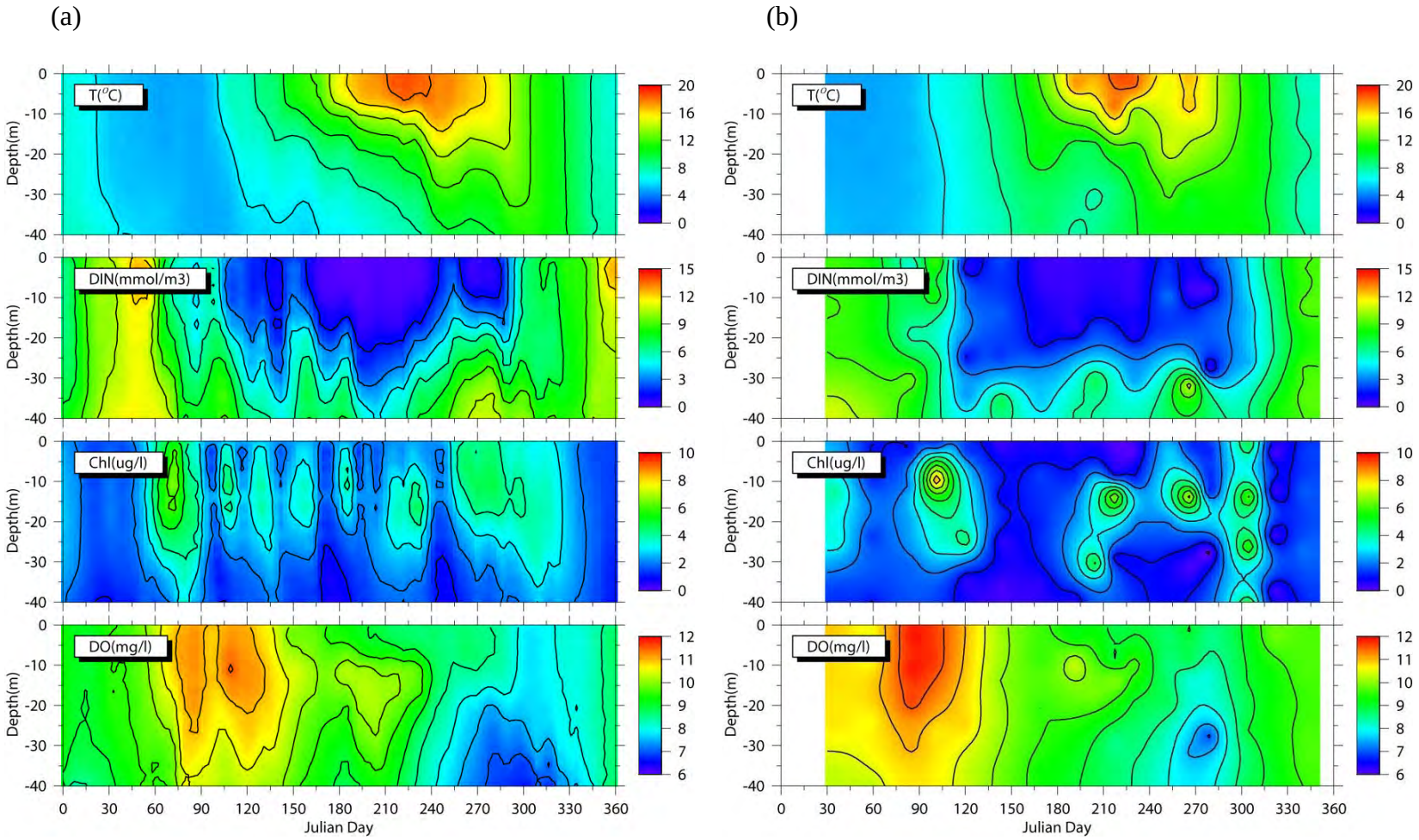

Figure 3.5. Time series of (a) modeled and (b) observed vertical distributions of temperature, DIN, Chl and DO at station N04 in 2002.

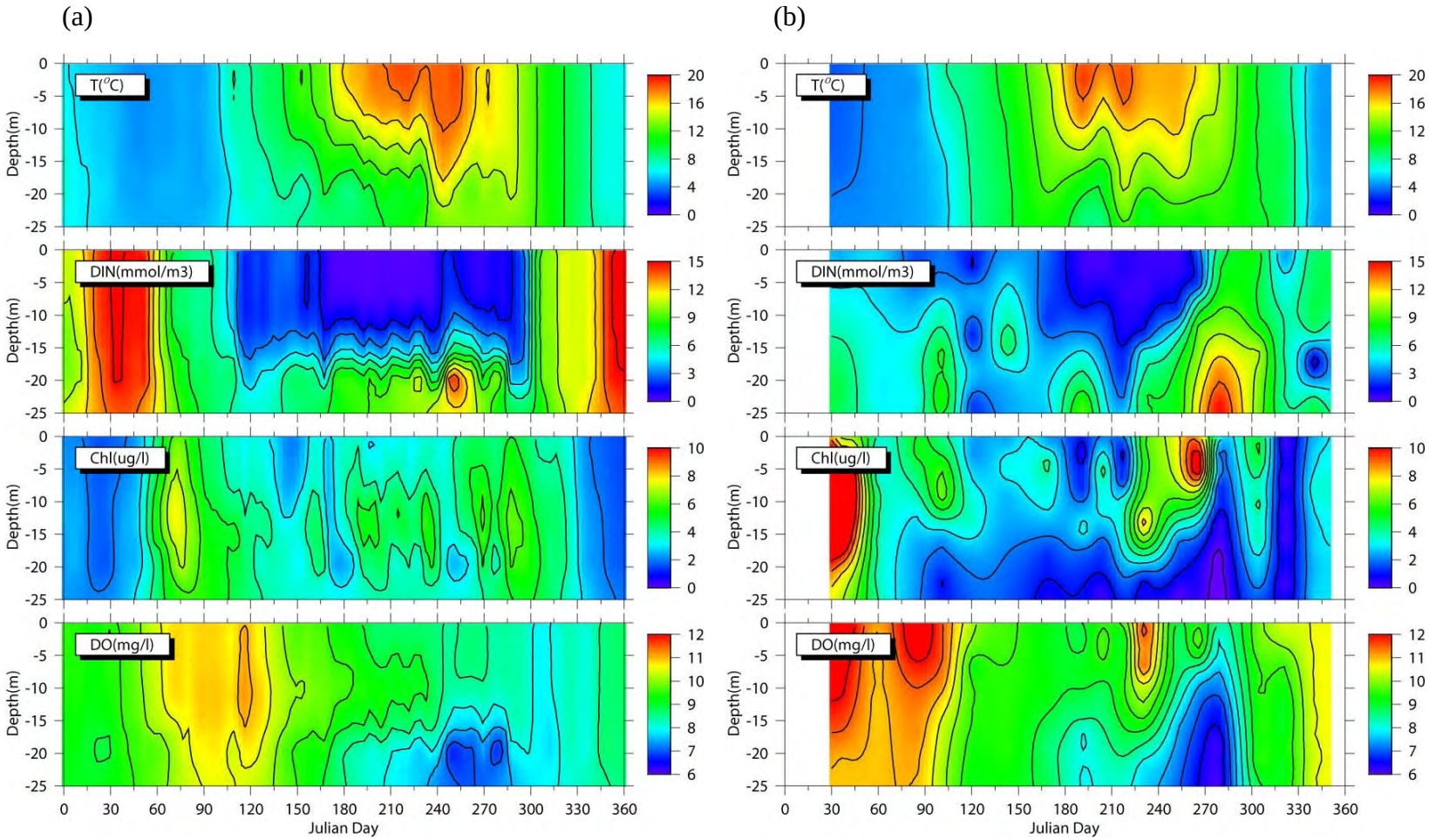

Figure 3.6. Time series of (a) modeled and (b) observed vertical distributions of temperature, DIN, Chl and DO at station N10 in 2002.

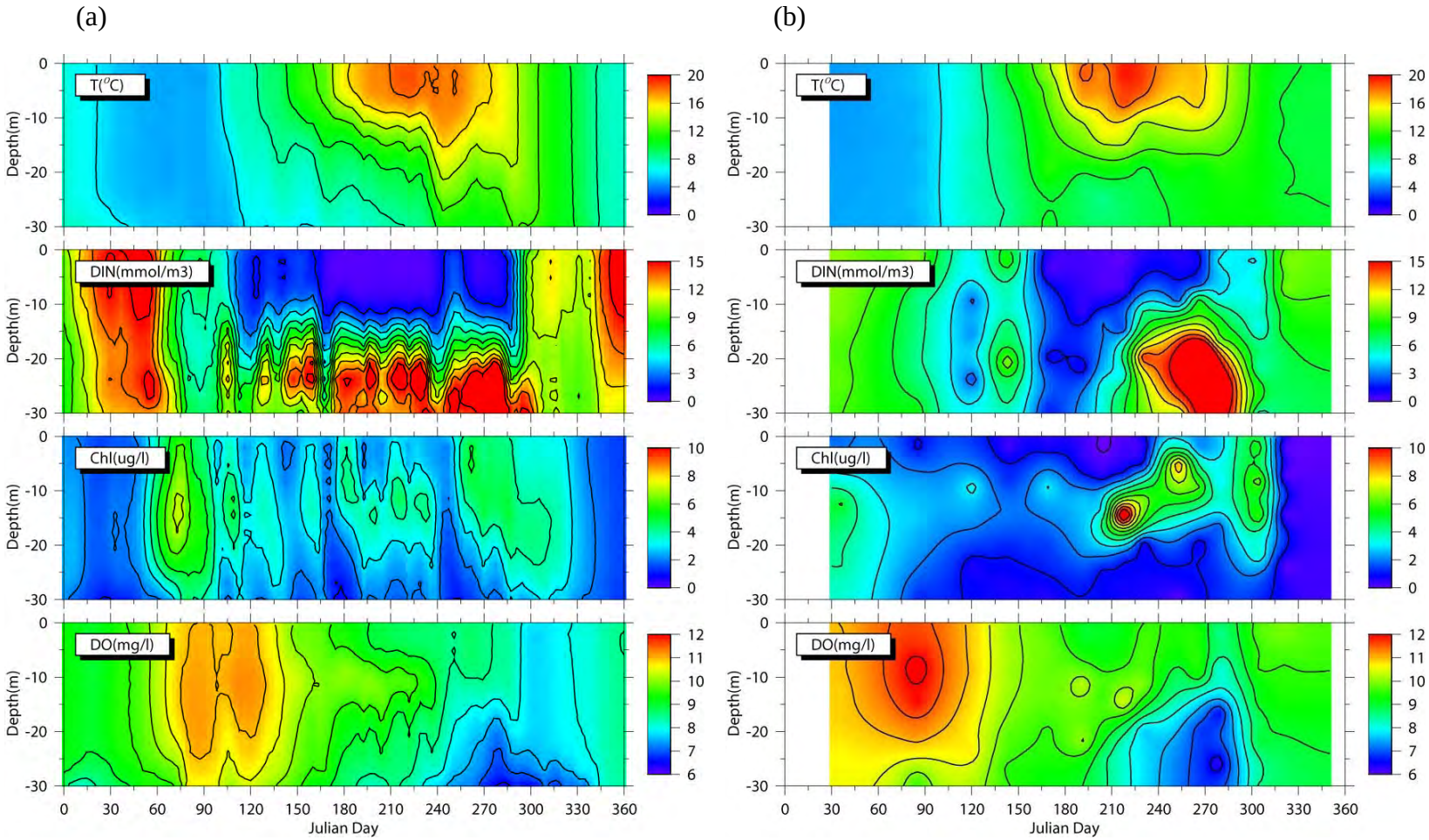

Figure 3.7. Time series of (a) modeled and (b) observed vertical distributions of temperature, DIN, Chl and DO at station N14 in 2002.

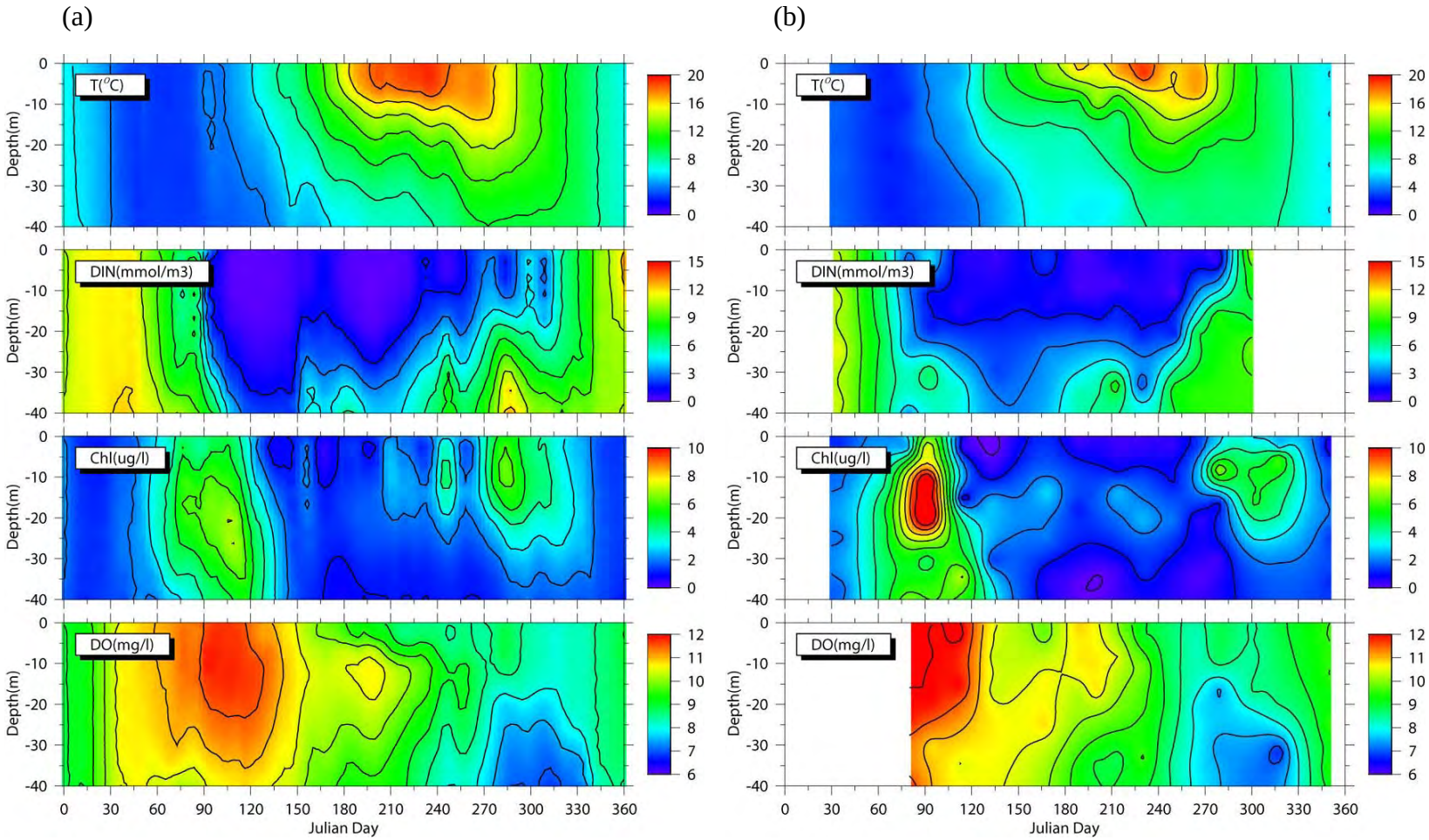

Figure 3.8. Time series of (a) modeled and (b) observed vertical distributions of temperature, DIN, Chl and DO at station N04 in 2003.

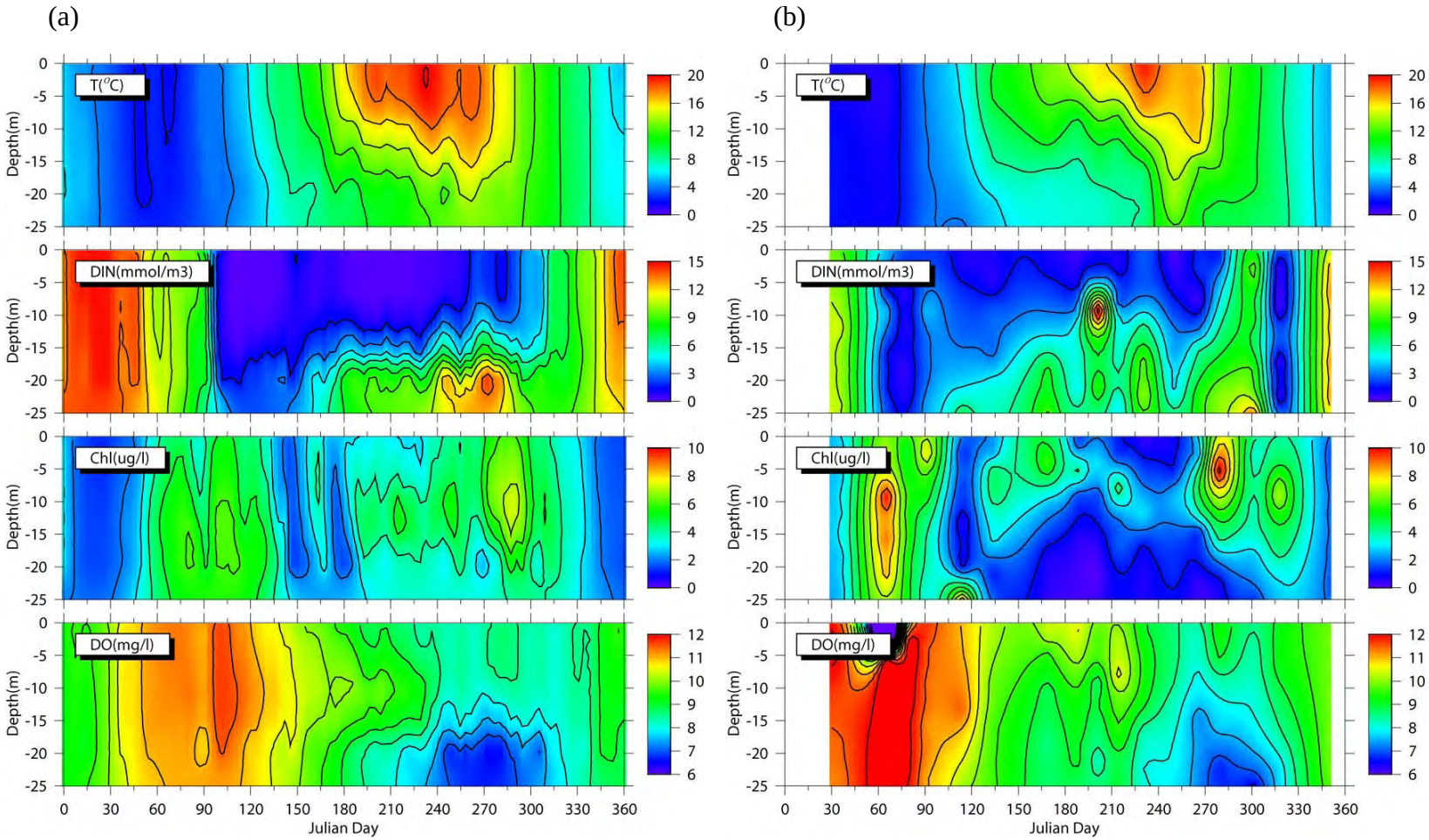

Figure 3.9. Time series of (a) modeled and (b) observed vertical distributions of temperature, DIN, Chl and DO at station N10 in 2003.

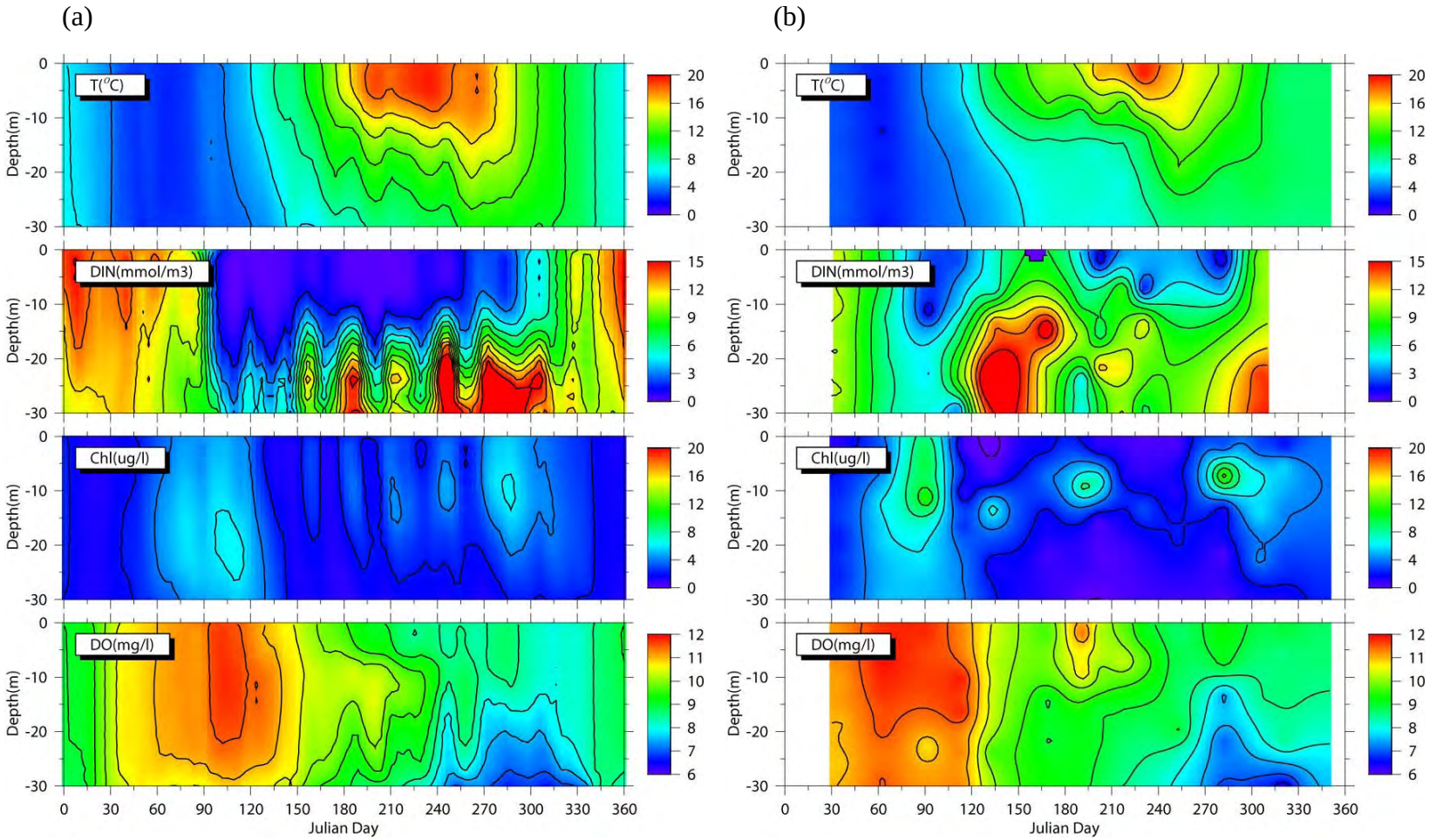

Figure 3.10. Time series of (a) modeled and (b) observed vertical distributions of temperature, DIN, Chl and DO at station N14 in 2003.

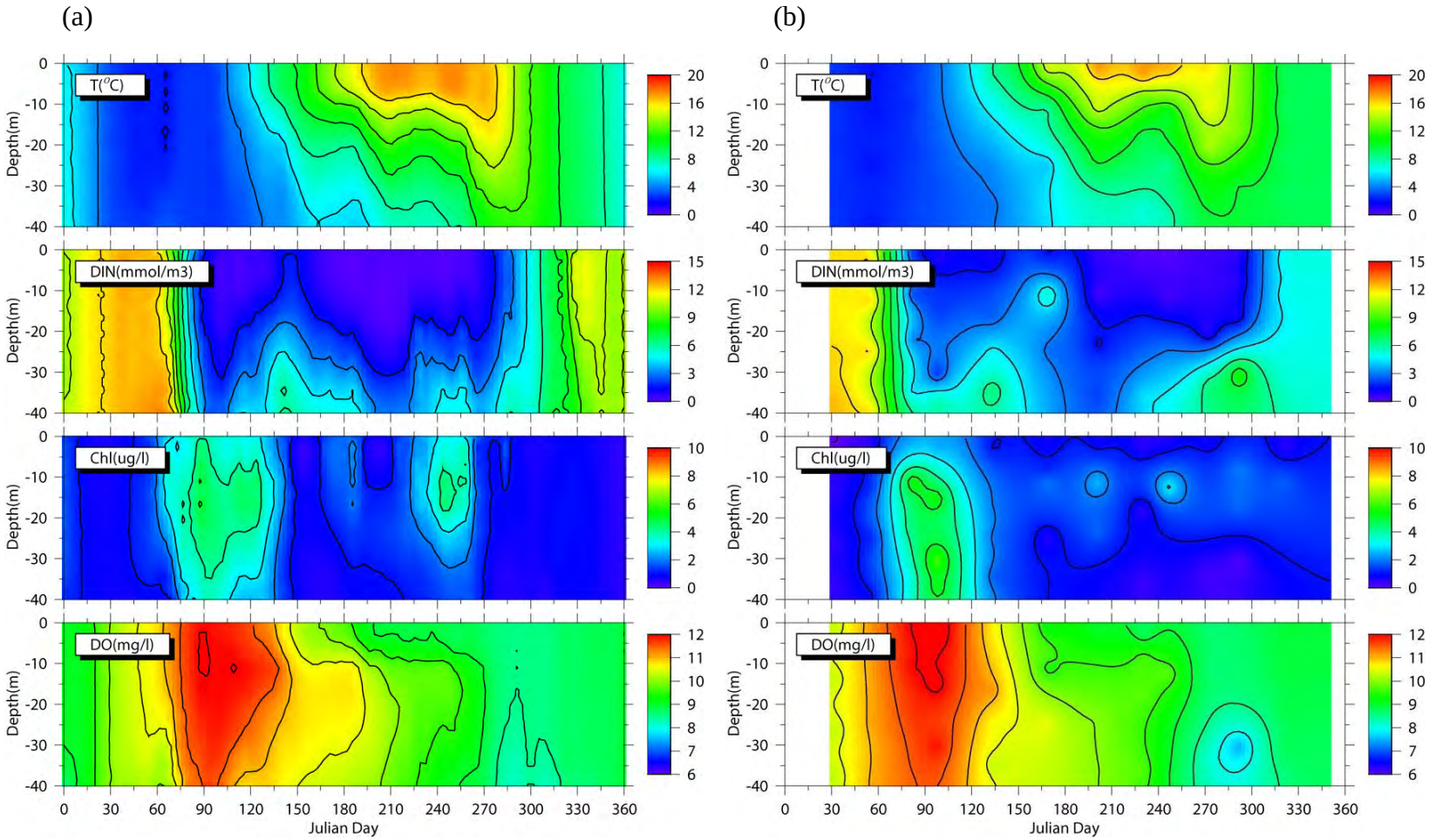

Figure 3.11. Time series of (a) modeled and (b) observed vertical distributions of temperature, DIN, Chl and DO at station N04 in 2004.

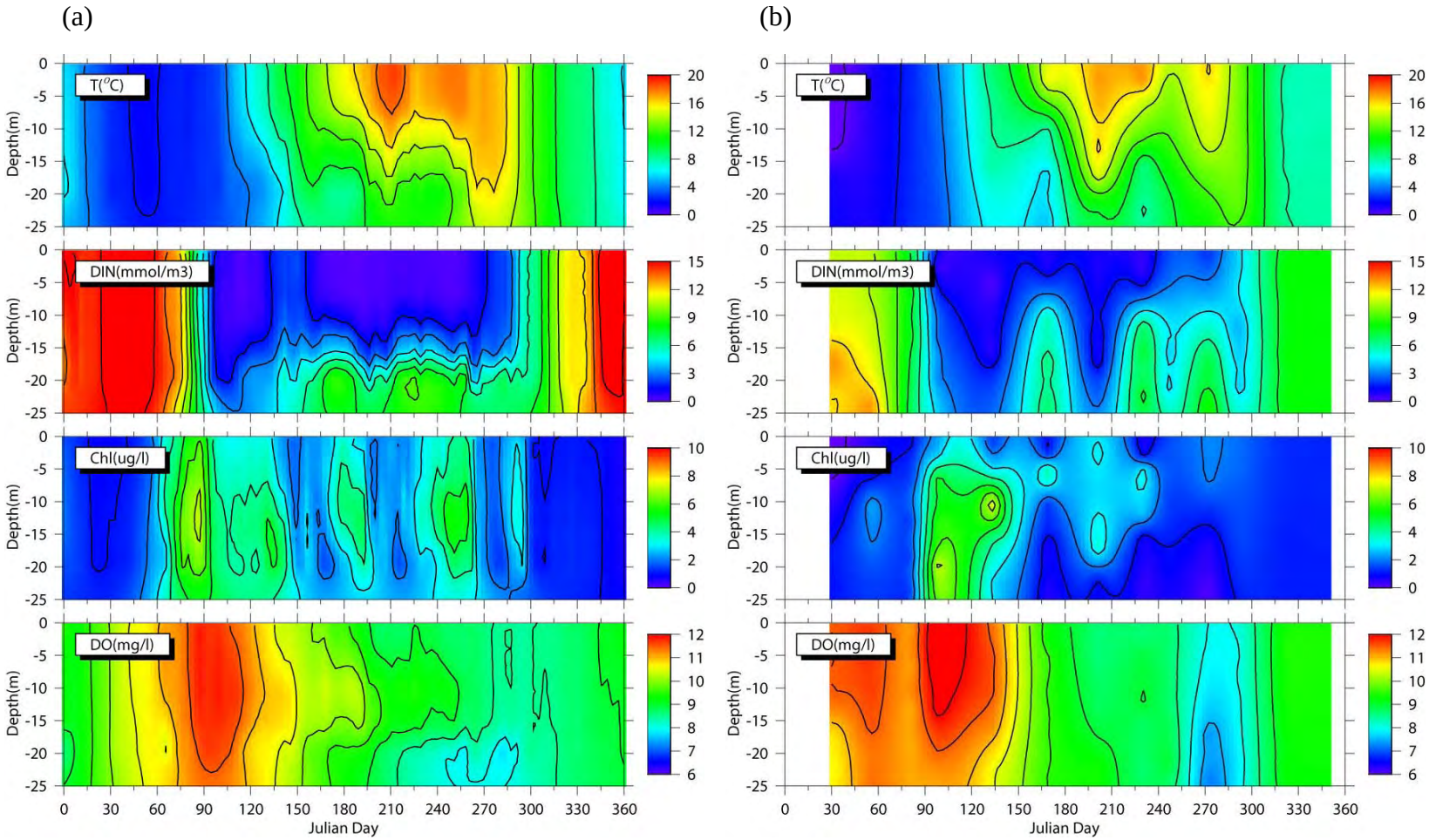

Figure 3.12. Time series of (a) modeled and (b) observed vertical distributions of temperature, DIN, Chl and DO at station N10 in 2004

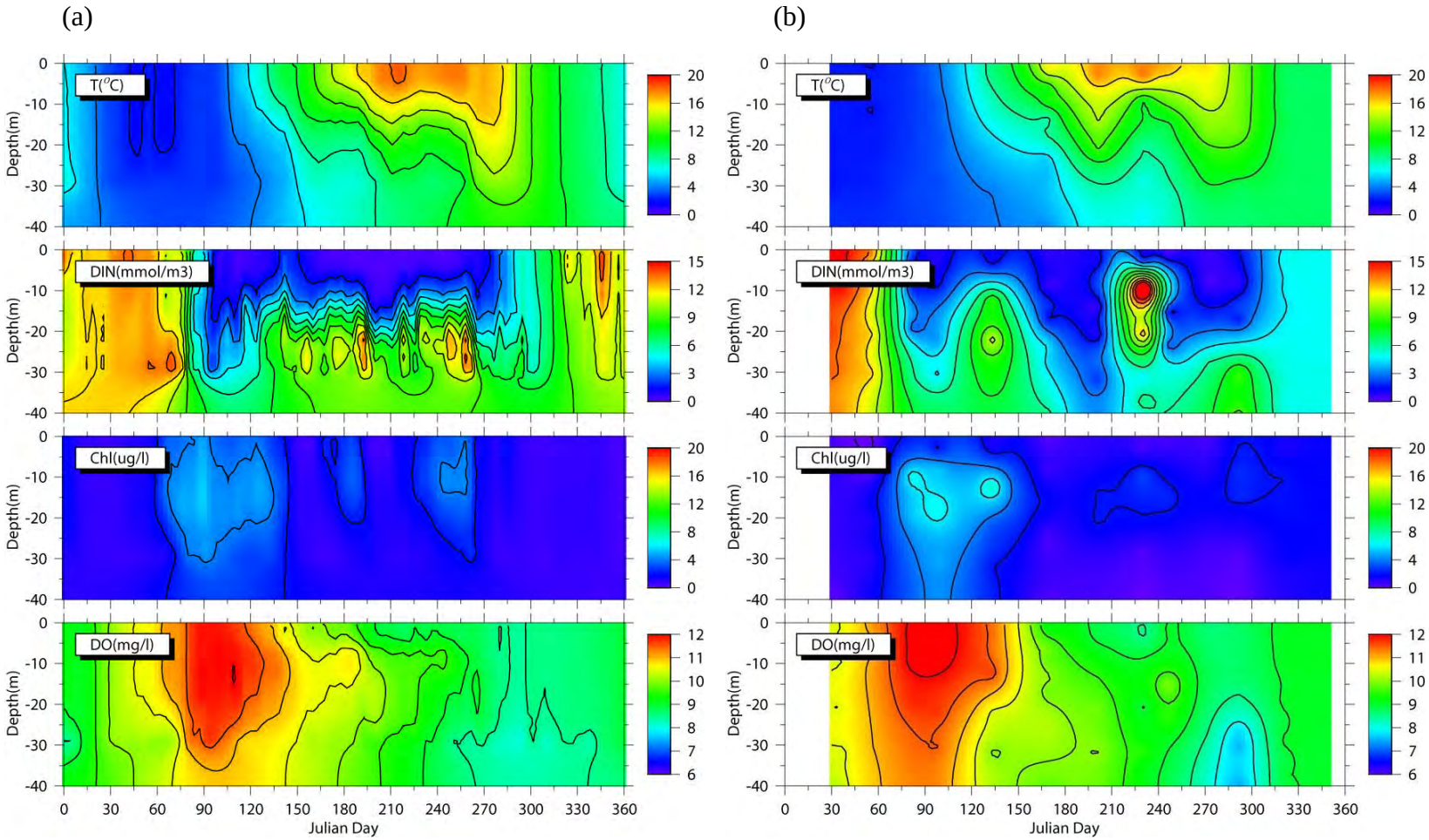

Figure 3.13. Time series of (a) modeled and (b) observed vertical distributions of temperature, DIN, Chl and DO at station N16 in 2004.

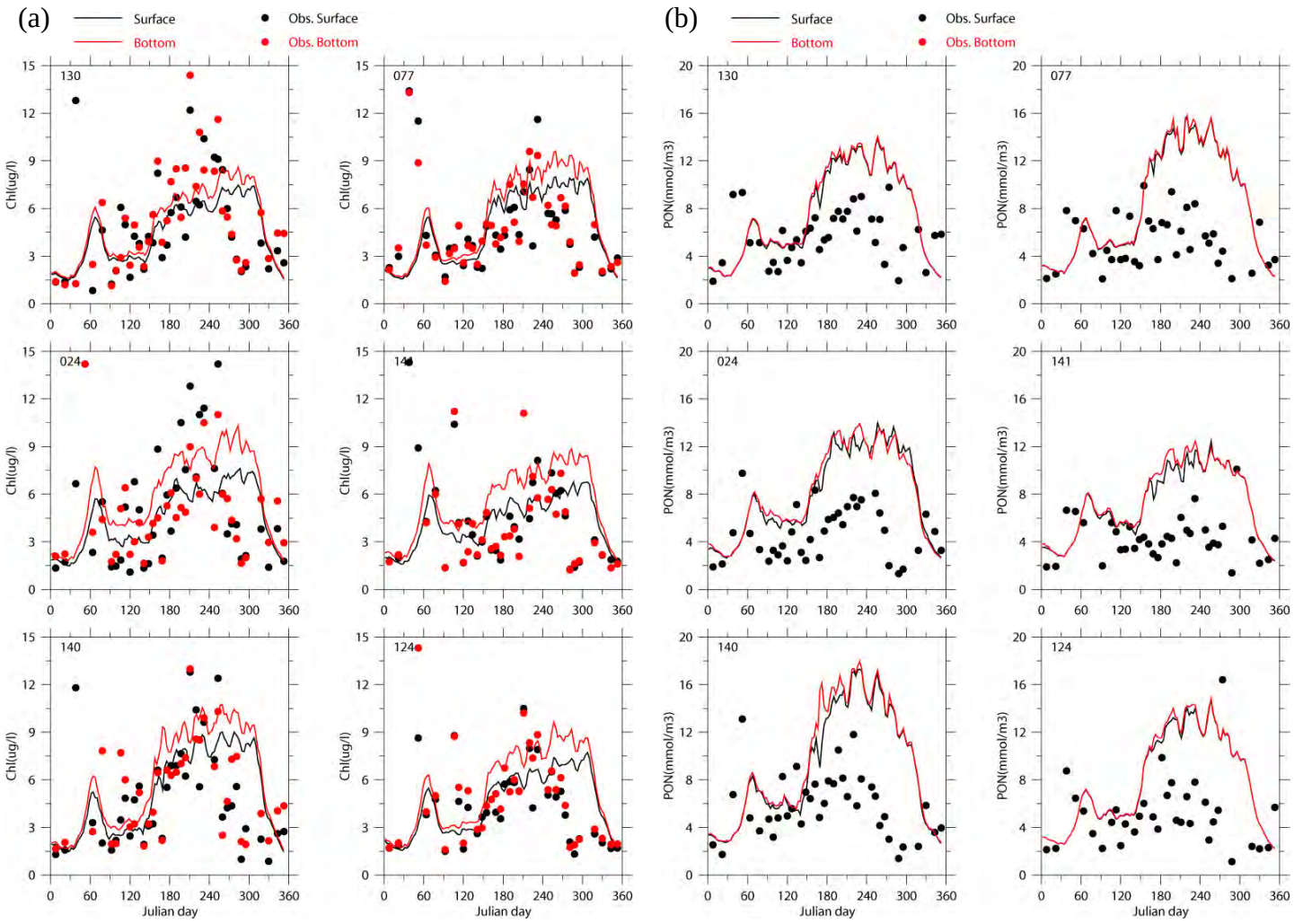

Figure 3.14. Time series of modeled and observed (a) chlorophyll, (b) PON and (c) DO in BH during 2002 (To be continued on next page).

(c)

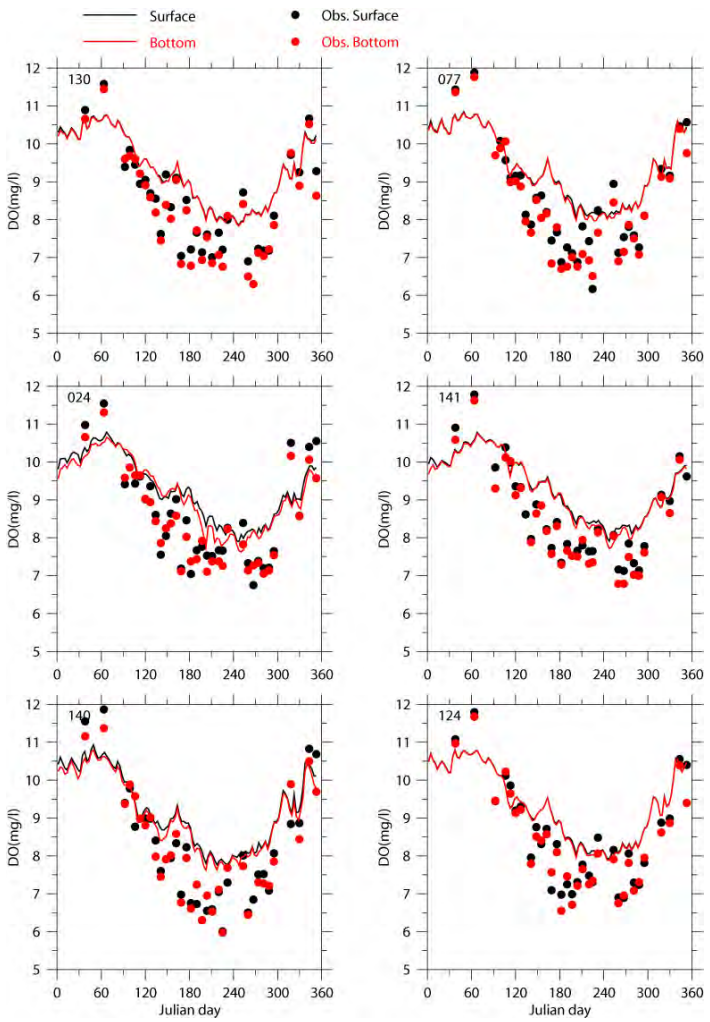

Figure 3.14. Continued.

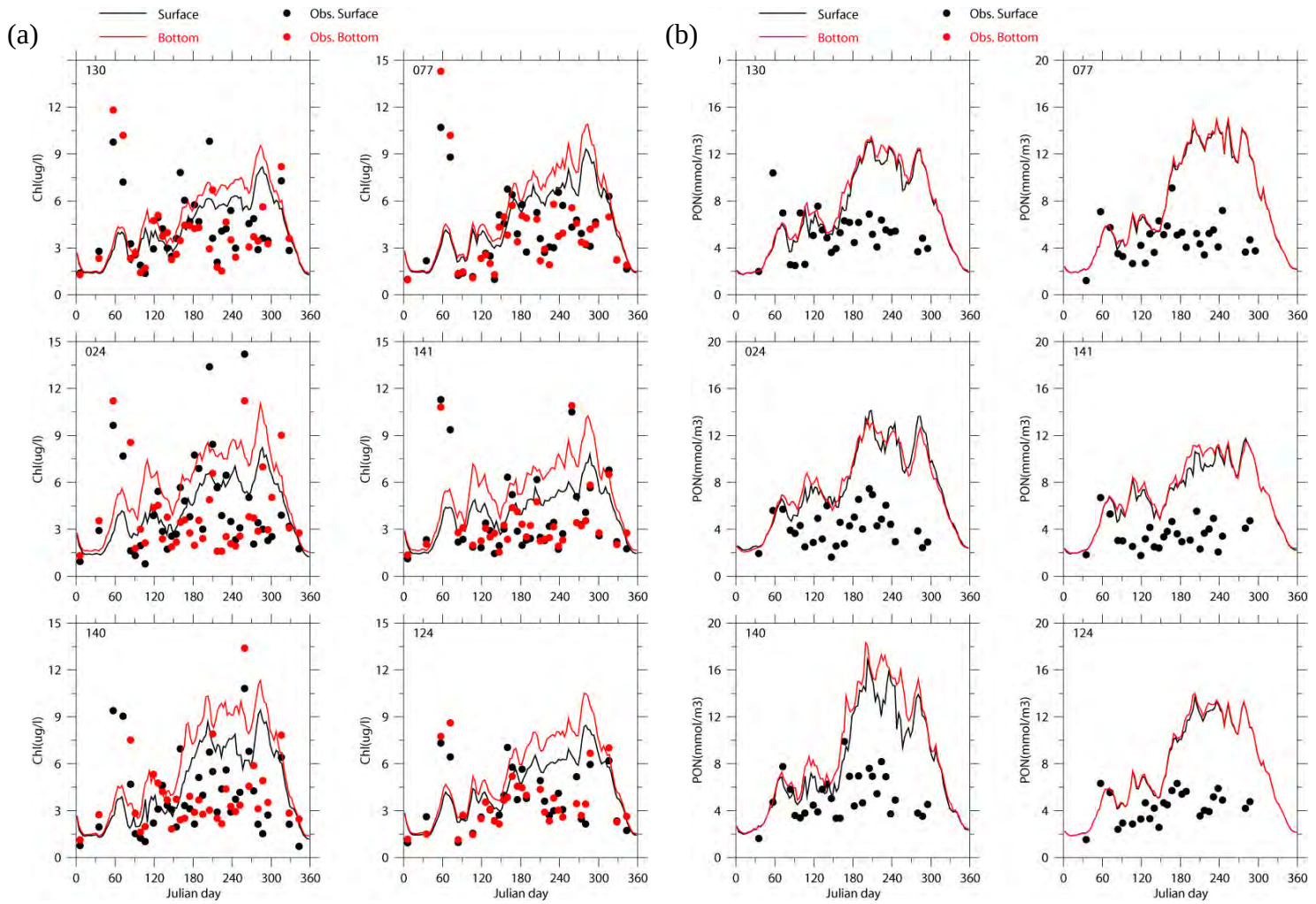

3.15. Time series of modeled and observed (a) chlorophyll, (b) PON and (c) DO in BH during 2003. (To be continued on the next page).

(c)

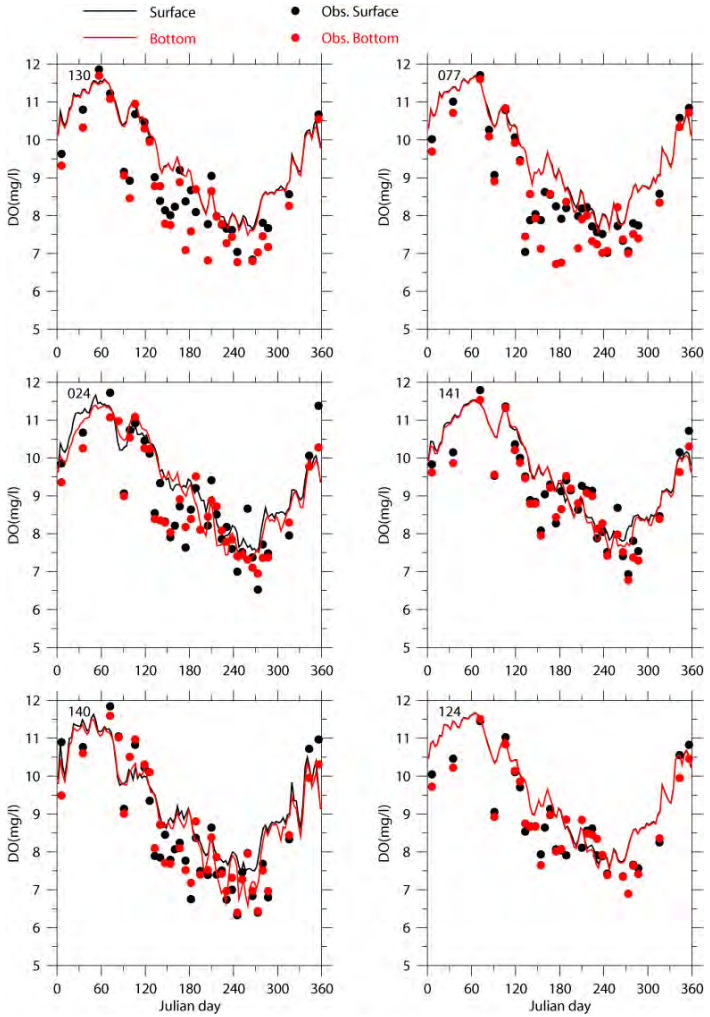

Figure 3.15. Continued.

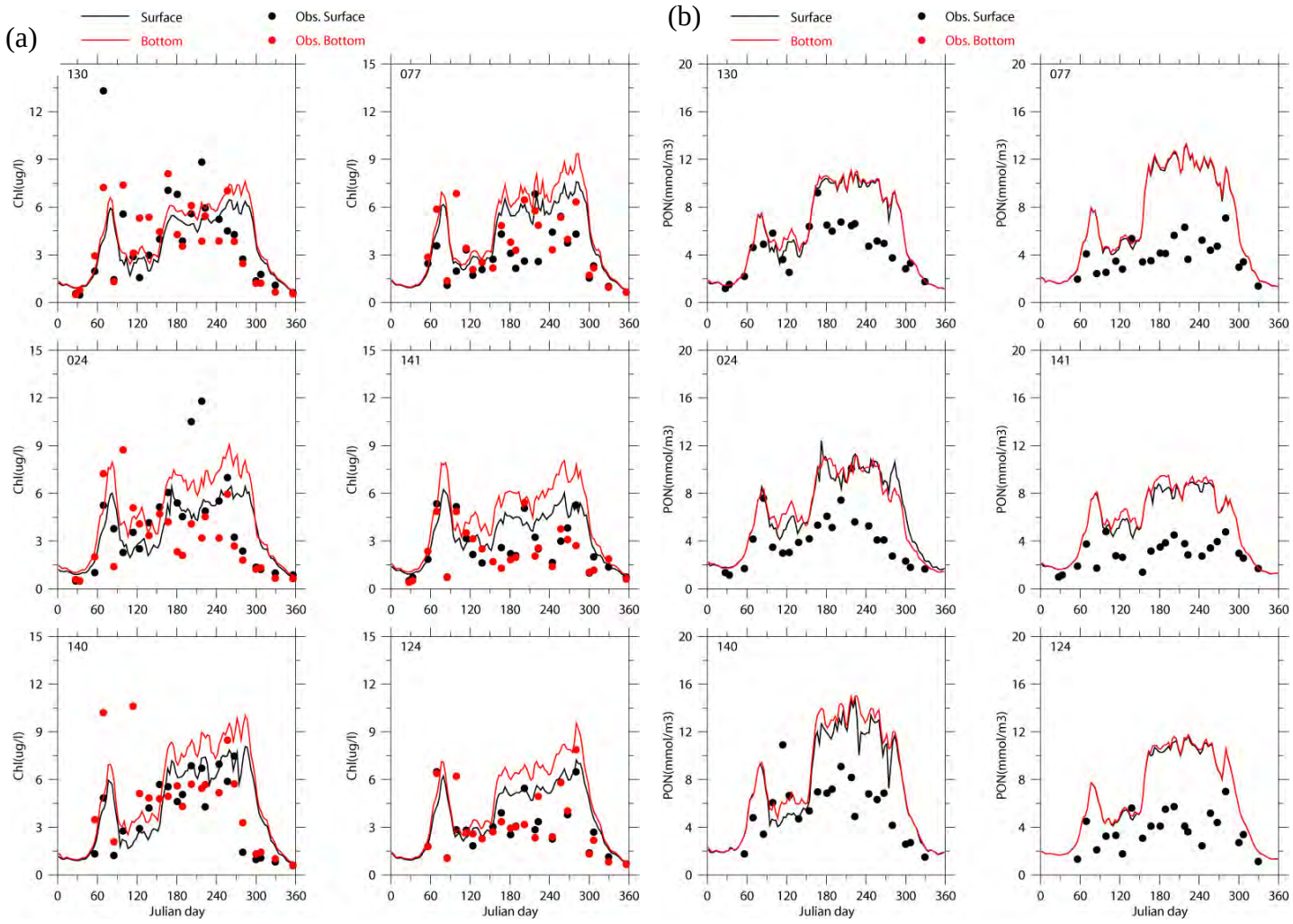

Figure 3.16. Time series of modeled and observed (a) chlorophyll, (b) PON and (c) DO in BH during 2004 (To be continued on next page).

(c)

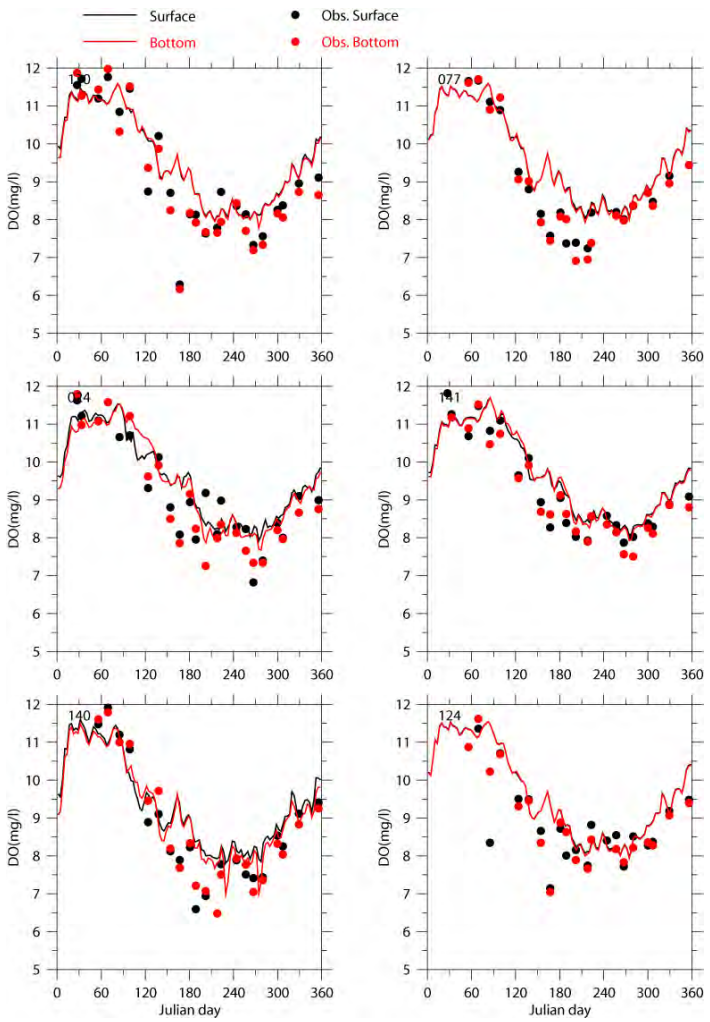

Figure 3.16. Continued.

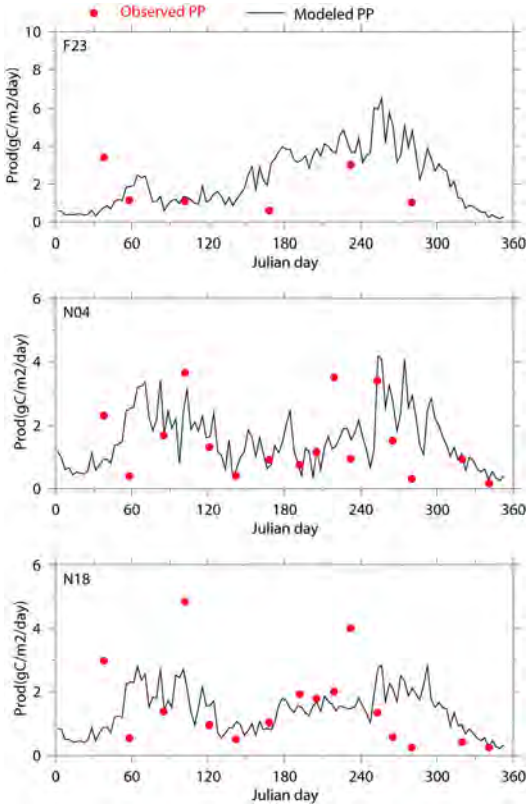

Figure 3.17. Modeled and observed primary production (PP) in 2002.

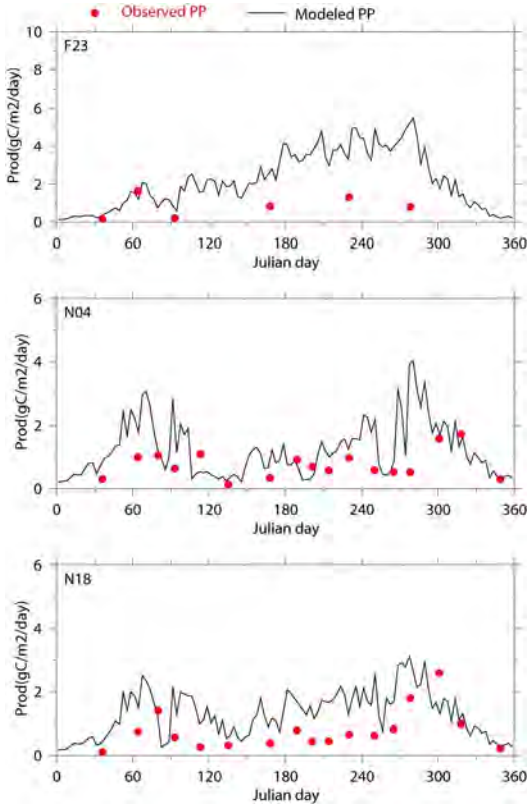

Figure 3.18. Modeled and observed primary production (PP) in 2003.

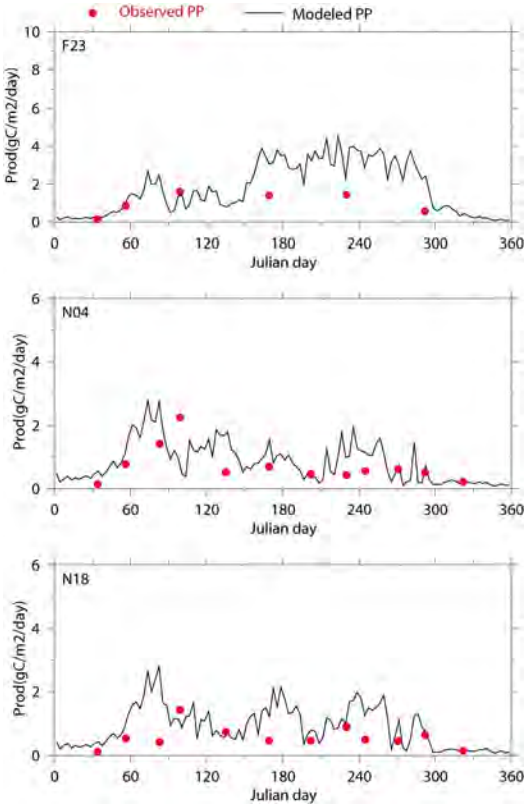

Figure 3.19. Modeled and observed primary production (PP) in 2004.

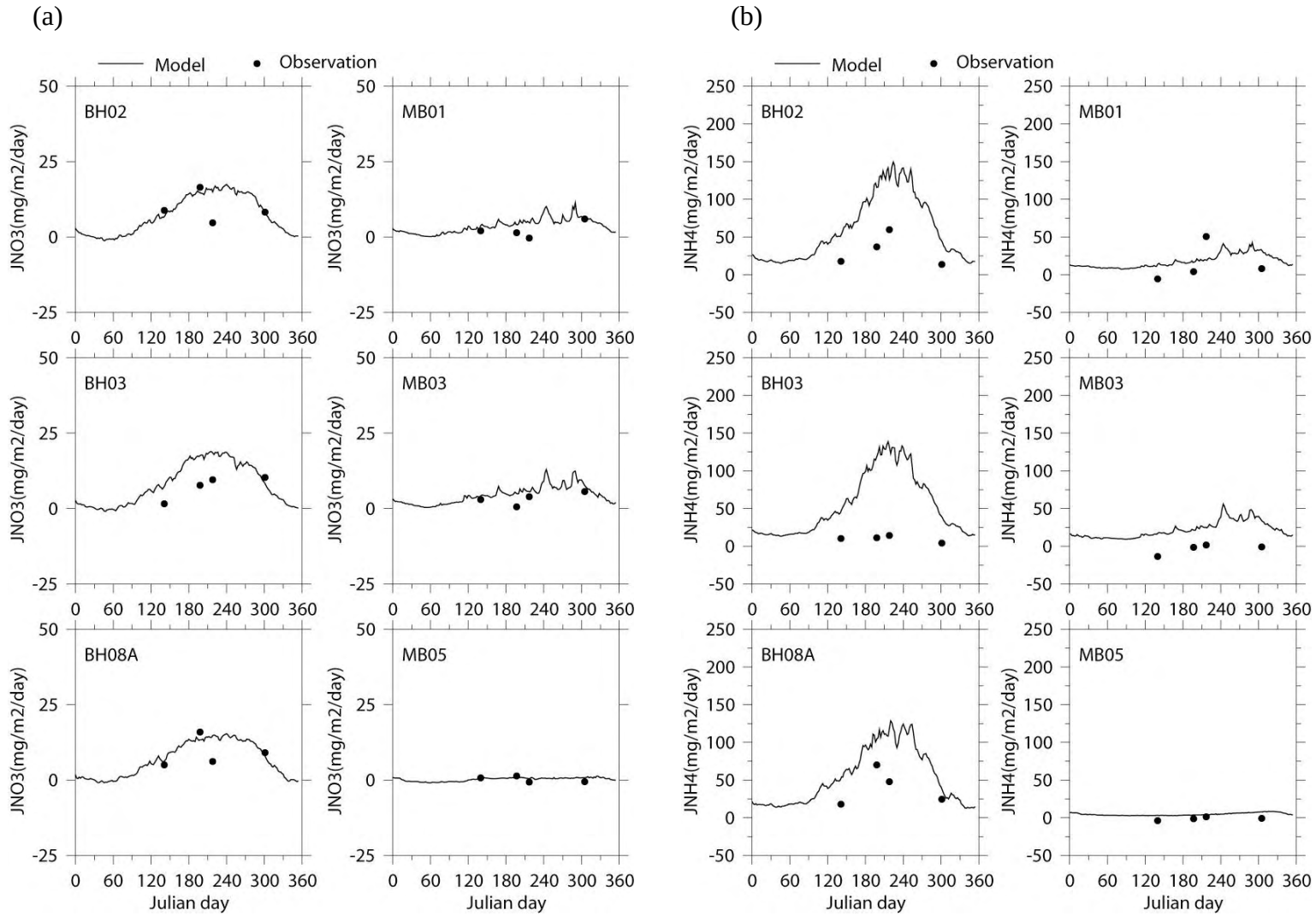

Figure 3.20. Nutrient fluxes and sediment oxygen demand in 2002: (a) JNO_3, (b) JNH_4, (c) JSi, (d) JPO_4, (e) SOD and (f) JN_2. (To be continued on next page).

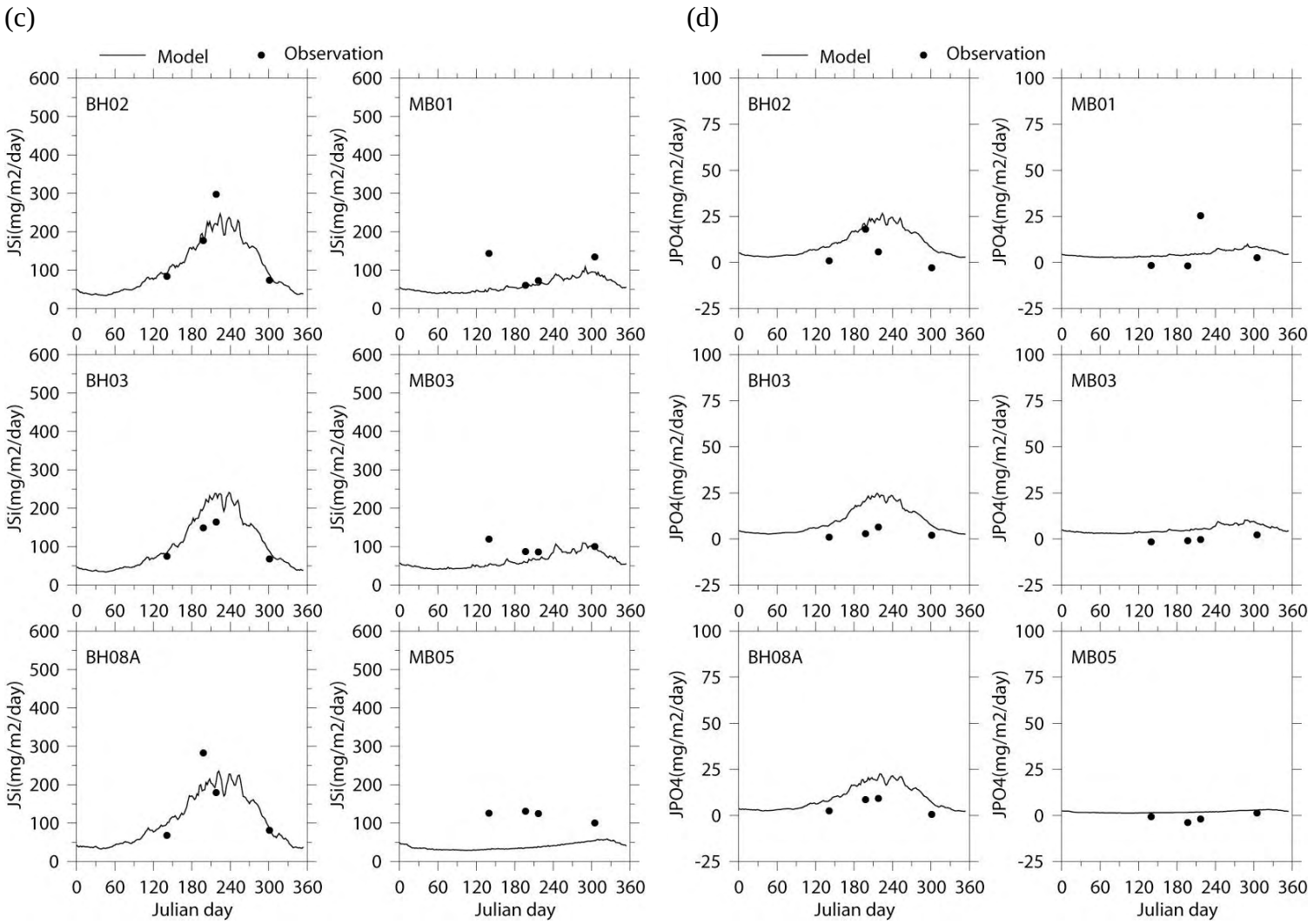

Figure 3.20. Continued.

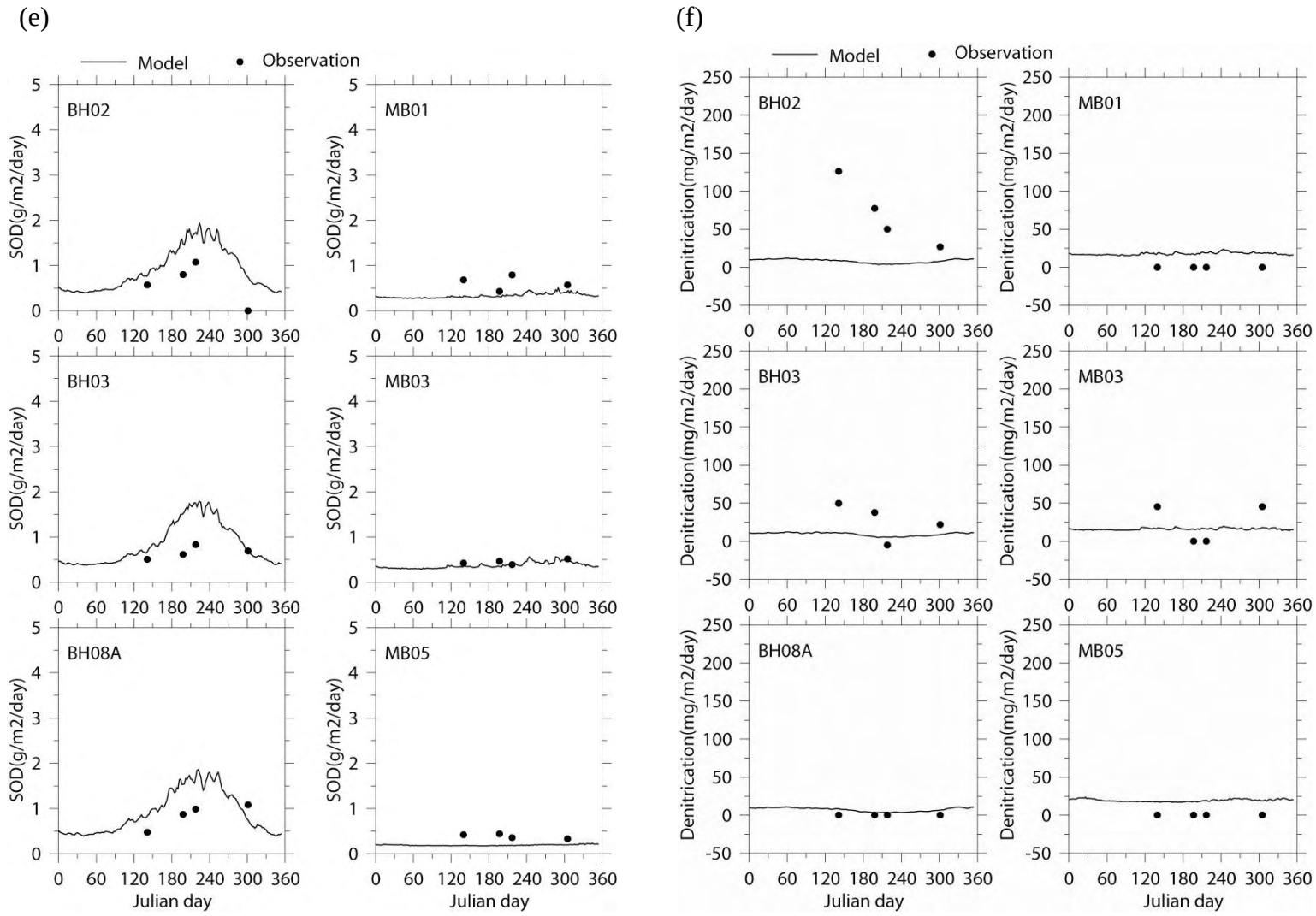

Figure 3.20. Continued.

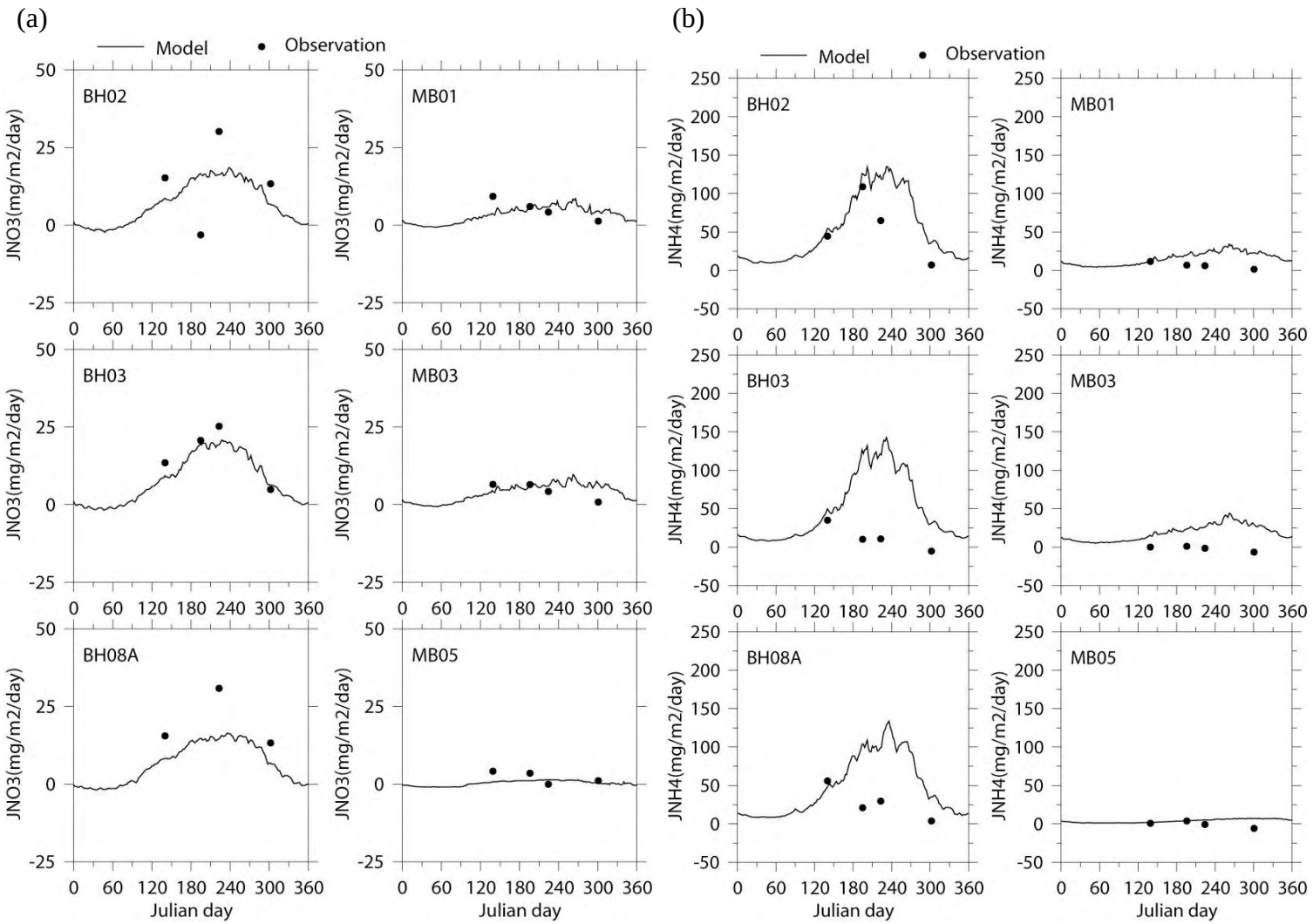

Figure 3.21. Nutrient fluxes and sediment oxygen demand in 2003: (a) JNO_3, (b) JNH_4, (c) JSi, (d) JPO_4, (e) SOD and (f) JN_2. (To be continued on next page).

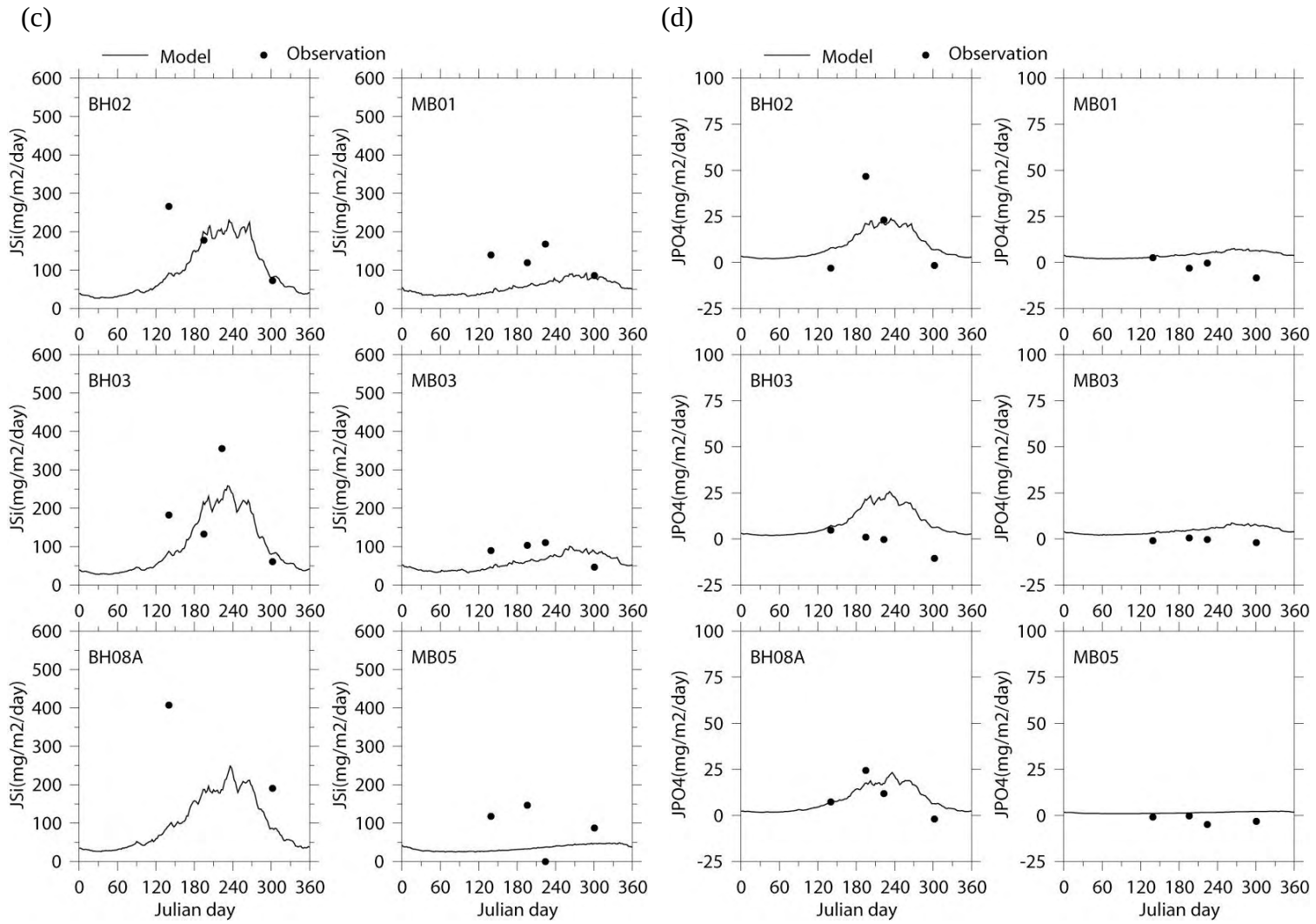

Figure 3.21. Continued.

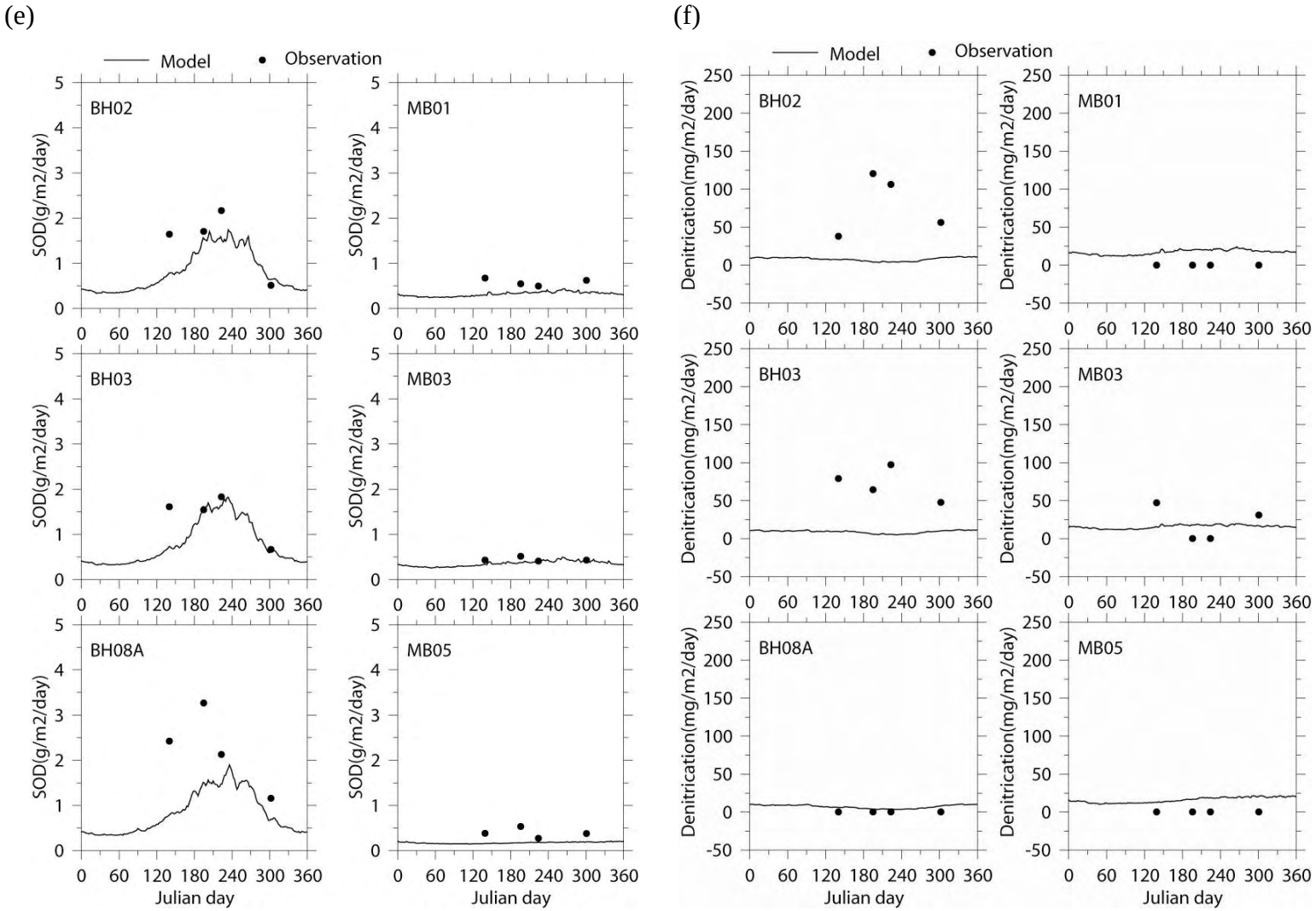

Figure 3.21. Continued.

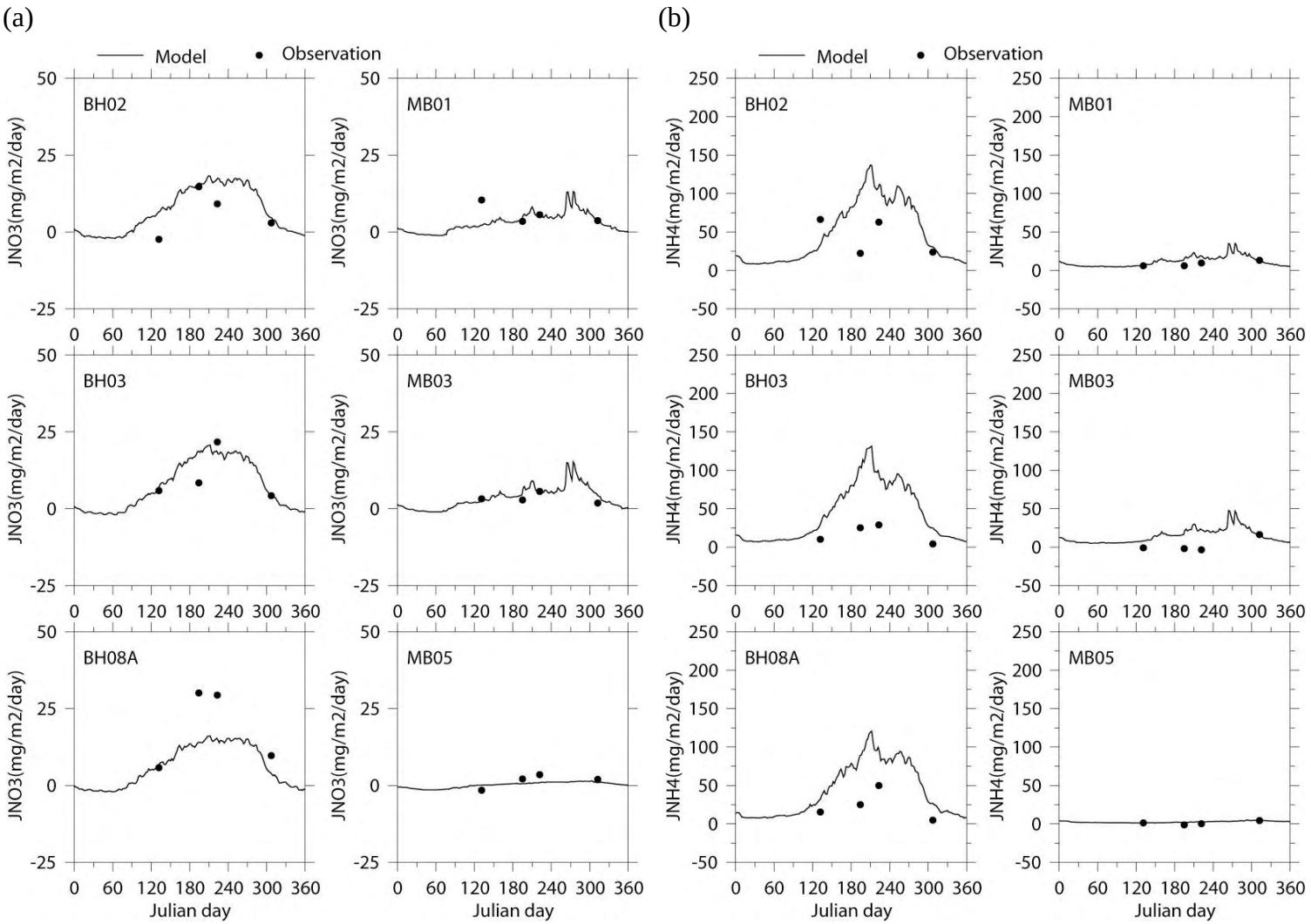

Figure 3.22. Nutrient fluxes and sediment oxygen demand in 2004: (a) JNO_3, (b) JNH_4, (c) JSi, (d) JPO_4, (e) SOD and (f) JN_2. (To be continued on next page).

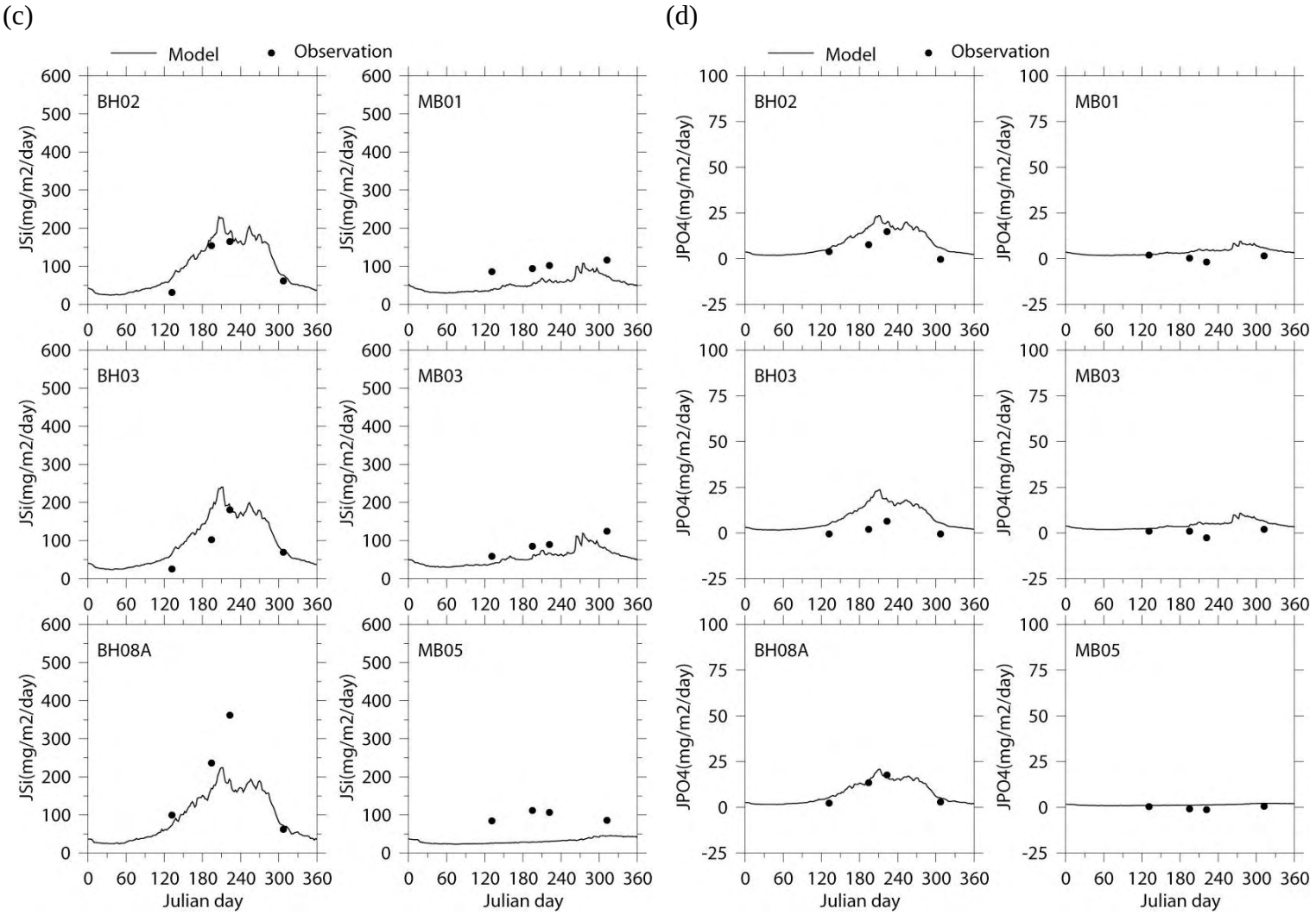

Figure 3.22. Continued.

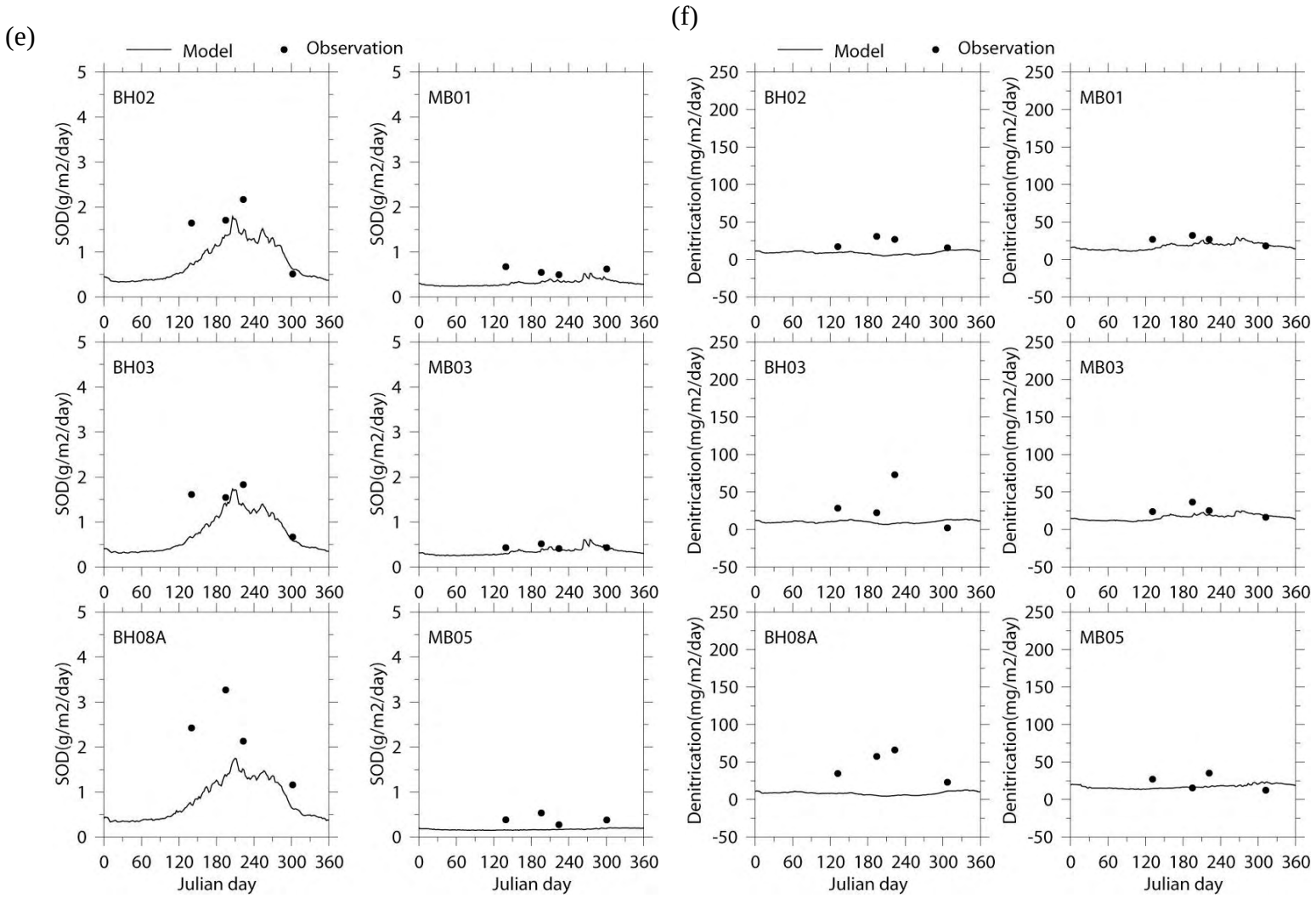

Figure 3.22. Continued.

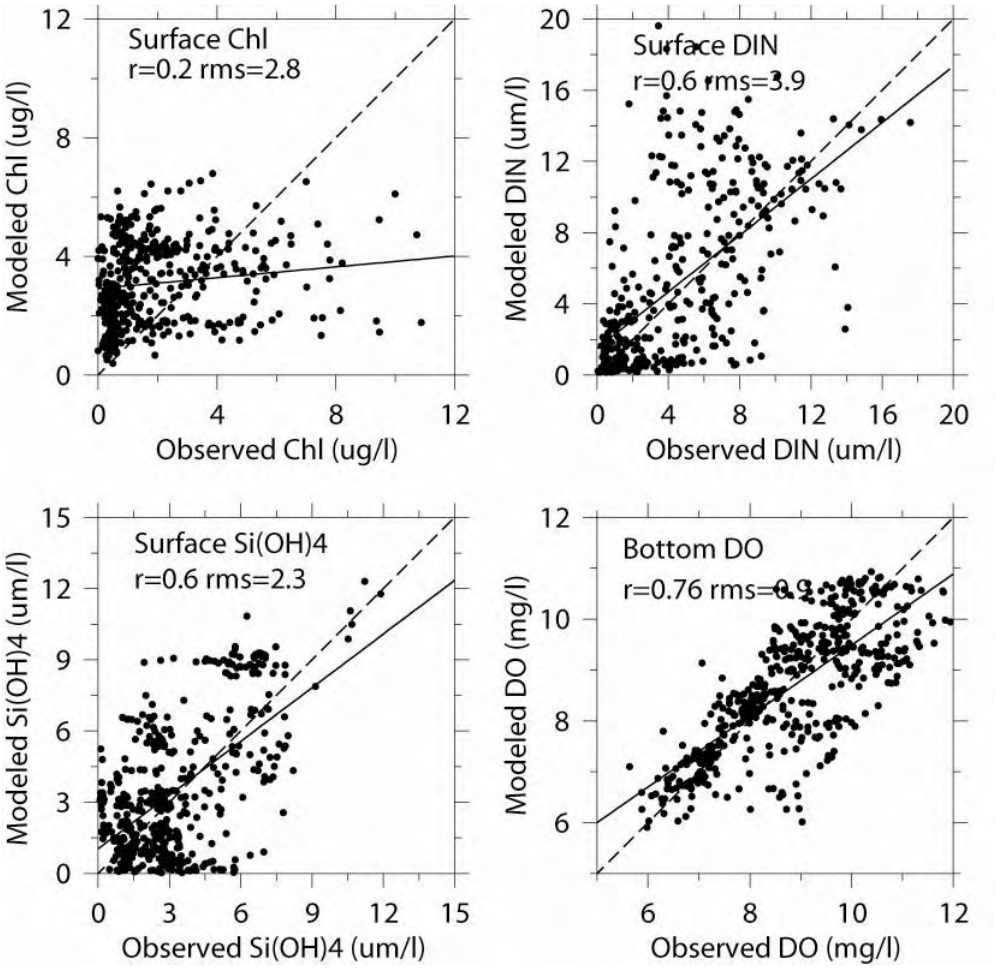

Figure 3.23. Correlation between modeled and observed concentrations for key parameters in 2002. Solid lines indicate best linear fit and dash lines indicate 1:1 relationship. Also shown are the correlations coefficients (r) and root-mean-square (rms).

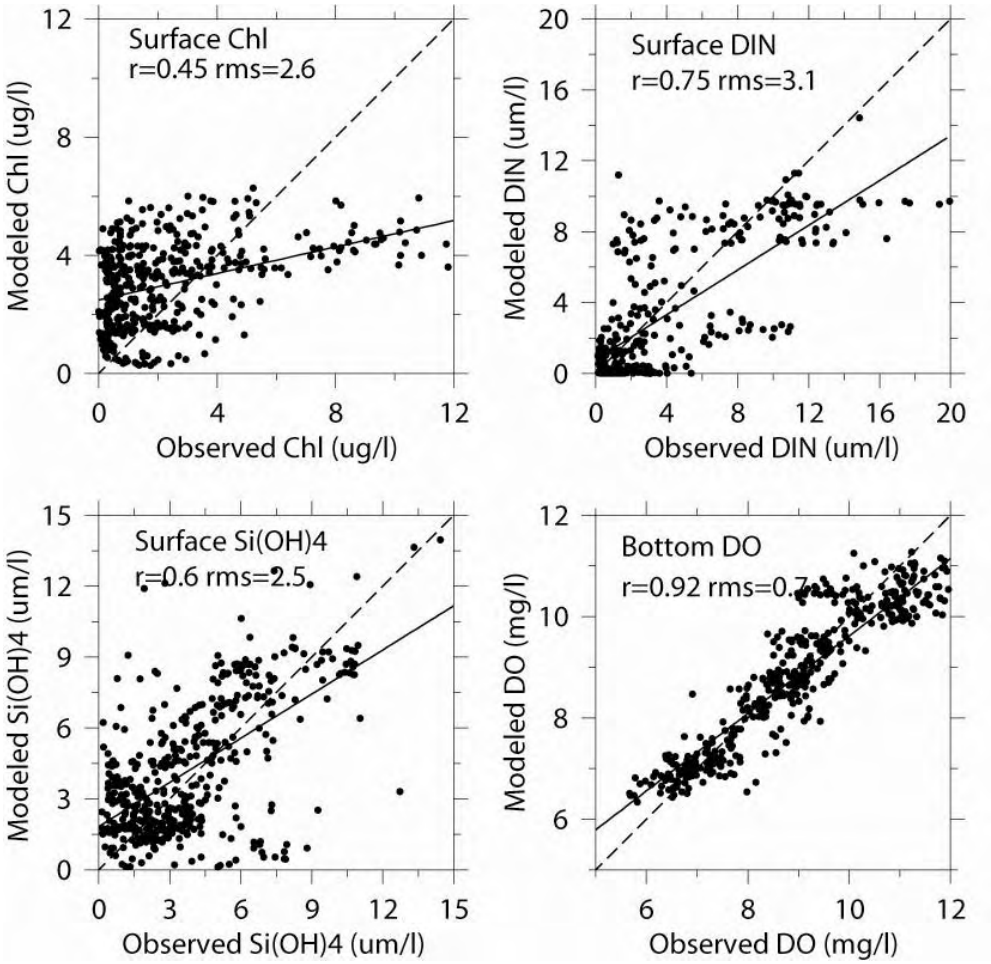

Figure 3.24. Correlation between modeled and observed concentrations for key parameters in 2003. Solid lines indicate best linear fit and dash lines indicate 1:1 relationship. Also shown are the correlations coefficients (r) and root-mean-square (rms).

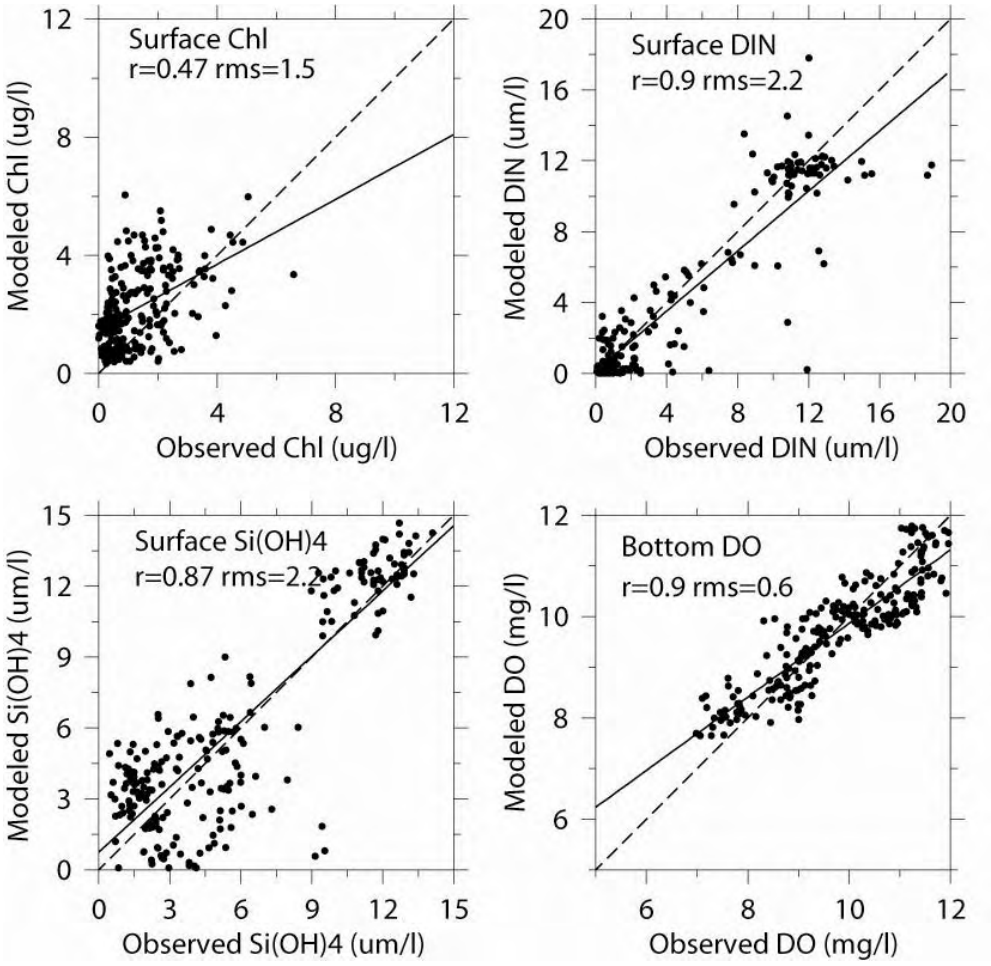

Figure 3.25. Correlation between modeled and observed concentrations for key parameters in 2004. Solid lines indicate best linear fit and dash lines indicate 1:1 relationship. Also shown are the correlations coefficients (r) and root-mean-square (rms).

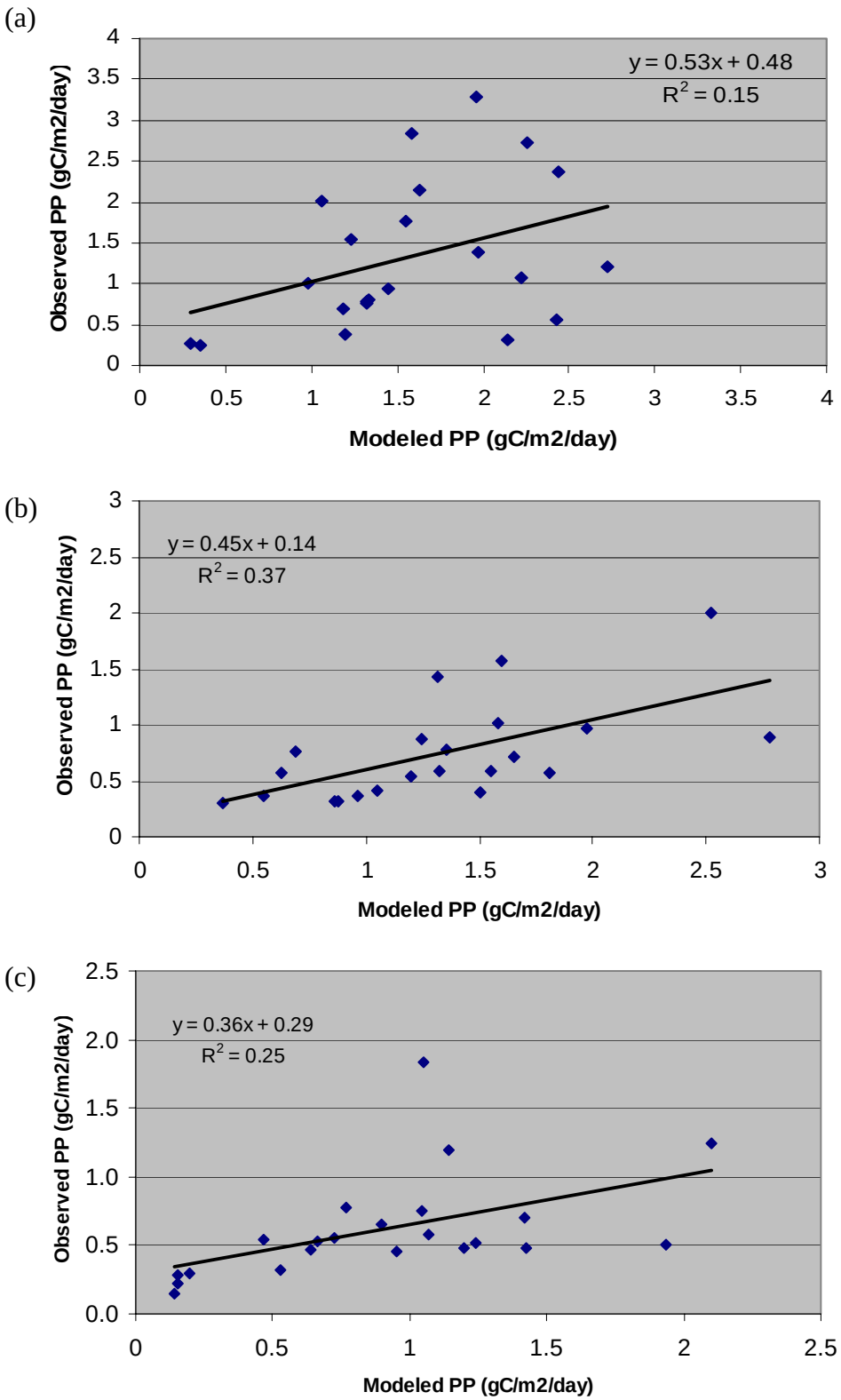

Figure 3.26. Correlations between modeled and observed primary productivity (PP): (a) 2002, (b) 2003 and (c) 2004. Also shown are the best linear fits (solid lines) and the values of R^2.

4. SENSITIVITY EXPERIMENTS

In this section, we will analyze the model sensitivities to the air-sea O_2 exchange formulation, phytoplankton growth formulation and sewage effluent changes listed in Table 4.1.

4.1 Air-sea O_2 exchange formulation

As noted in the 2000-2001 simulation (Jiang and Zhou, 2004c), current air-sea O_2 formulation tends to under-estimate the air-sea exchange, which in turn leads to an under-saturated O_2 condition in winter. In this section, we compare the modeled results from the current formula and an alternative formula.

The air-sea exchange (F_{O2}) is determined by,

$$F_{O2}=k*(DO_{sat}-DO), \tag{4.1}$$

where DO_{sat} is the saturation concentration of oxygen at the sea surface as calculated by Hyer et al. (1971), k (unit: m/day) is the piston velocity for air-sea O_2 exchange. The piston velocity largely depends on wind speed (w, m/sec) and water temperature. In the current BEM, an empirical formula by Banks and Herrera (1977) is used for piston velocity. At 20ºC water temperature, the formula is as follows,

$$k = \max(1,0.728\sqrt{w} - 0.317w + 0.0372w^2)\,. \tag{4.2}$$

An alternative formula is proposed by Wanninkhof (1992), which has been widely used in recent modeling studies. At 20ºC water temperature, the formula can be written as,

$$k = 0.1w^2\,. \tag{4.3}$$

The comparison of these two formulas is shown in Figure 4.1. The sensitivity analysis was conducted by comparing the model results for year 2002 between the experiment using Equations 4.2 (referred to CONTROL) and that using Equation 4.3 (referred to W92) . The modeled bottom DO concentrations in MB are shown in Figure 4.2. The W92 formula generally yields higher piston velocity than that by Equation 4.2. Because surface water was under-saturated and receiving oxygen from the air in winter, a higher exchange rate in the W92 experiment led to higher modeled surface DO concentrations

by 0.5~0.7 mg/l than that produced by the Control experiment. The modeled DO values in the W92 experiment compared better with the observed DO concentrations, though the modeled DO values were still lower than the observed. In the summer, the W92 experiment produced surface DO concentrations slightly lower than the CONTROL experiment (Figure 4.3). This improved modeled surface DO concentrations during the summer in BH, which were over-estimated by approximately 2 mg/l in the CONTROL experiment.

4.2 Phytoplankton growth formulation

As noted in section 3.2 and the report for the 2000-2001 simulation, modeled chlorophyll tends to be more evenly distributed over the water column. In particular, the bottom chlorophyll concentrations simulated were generally higher than the observed. This could be due to several reasons: (1) low light attenuation coefficient, (2) inadequate vertical profile of growth rates, (3) inadequate carbon to chlorophyll ratios and (4) over-estimated vertical mixing. In this section, we test effects of different formulas for phytoplankton growth rates using the 2003 simulation.

The maximum phytoplankton growth rate ($\mu_{\max}$) in the BEM under nutrient saturated condition is defined as (Laws and Chalup, 1990),

$$\mu_{\max} = \frac{G_{pre}(1-k_{RG})(1-f_{SC})I}{G_{pre}/G_{pr0} + I\left[1+G_{pre}/\left(I_S G_{pr0}\right)\right]}, \tag{4.4}$$

where I is the solar radiation (mol quanta m^{-2} d^{-1}) as a function of depth and time, and I_s is the radiation when the photosynthetic rate reaches 50% of the maximum photosynthetic rate. Other parameters are defined in Table 2.2. The maximum growth rate ($\mu^0_{\max}$) is achieved when light is not limiting. This formula (referred to as LC90 hereafter) predicts a slow decrease of the growth rate as a function of depth (Figure 4.4), which tends to over-estimate growth rates at depth. The numerical experiment using this formula is referred to as CONTROL hereafter.

An alternative formula was proposed by Platt et al. (1980) (the numerical experiment

is referred to as PL80 hereafter), i.e.,

$$\mu_{\max} = g_{\max}\left[1 - \exp(-\alpha I / g_{\max})\right], \tag{4.5}$$

where $g_{\max}$ is the maximum growth rate, and α is the initial slope of the *P-I* curve. No photo-inhibition was implemented. We chose a slightly higher maximum growth rate ($\mu^0_{\max}$) than used in Equation 4.4. A higher α will produce a faster decrease of growth rate with depth. We chose a relatively low value of $\alpha = 0.03$ day^{-1} (W m^{-2})$^{-1}$ (Evans and Garcon, 1997), which still resulted in a faster decrease of growth rate with depth than the Equation 4.4.

The comparisons of modeled bottom chlorophyll concentrations in MB and BH are shown in Figures 4.5 and 4.6, respectively. The PL80 experiment generally produced lower bottom chlorophyll concentrations in summer and fall, which were compared better with data, especially in BH. The modeled bottom DIN concentrations in the PL80 experiment were higher than those in the CONTROL experiment, and also were compared slightly better with data (Figure 4.7). The improvement of bottom chlorophyll in the PL80 experiment can be further illustrated from the vertical profiles at N04 and N10 (Figures 4.8-4.9) which were compared to the results of CONTROL experiments and observations (Figures 3.9-3.10). The modeled DIN concentrations in the mixed layer during the second half of the year were also improved. No substantial differences in the surface chlorophyll and DIN between the two experiments were found. Given the improvements of chlorophyll and DIN concentrations, the modeled PP in the PL80 experiment were also improved, especially during the second half of the year (Figure 4.10). In brief, this test demonstrated that both modeled chlorophyll and PP can be improved by adjusting the vertical profile of growth rates.

4.3 Effects of effluent on phytoplankton growth

In order to understand the contribution of sewage effluent to phytoplankton biomass in MB, an experiment was conducted using parameters and forcing data in year 2001 except the nutrient concentrations in the effluent, which were set to zero (referred to No-sewage hereafter), and compared to the standard experiment (referred to as CONTROL

hereafter). The comparison between the CONTROL and No-sewage experiments suggested that the contributions of effluent nutrients to surface chlorophyll and PP were small in spring and winter, and largest in summer, reaching 1~2 μg/l and 1gC/m2/day, respectively (Figures 4.11-4.12). The influence of effluent was limited to the nearfield and the vicinity of BH, consistent with those results from previous simulations using a passive tracer in the hydrodynamic model (Signell et al., 1996).

The spatial pattern of effluent's influences can be better illustrated by examining the differences of subsurface chlorophyll and nutrients between the CONTROL and No-sewage experiments (Figures 4.13-15). In a northerly or northeasterly wind case (Figure 4.13), the southward coastal current transported the effluent plume downstream as it was diffused. No significant phytoplankton growth was induced by effluent nutrients. However, during a southwesterly or southerly wind case, a northward flow along the western coast was typically formed, which transported nutrients toward the northern coast (Figure 4.14). When this type of wind condition lasted several days, nutrients transported to the northern coast significantly enhanced the phytoplankton growth in that area with chlorophyll differences up to 1~2 μg/l (Figure 4.15).

The results also revealed frequent occurrences of meso-scale eddies in this area, for example, the meso-scale eddy off Hingham (Figure 4.15), and another right on the top of the outfall (Figure 4.16). Both eddies had the spatial scale of 5~10km and a time scale of 2-5 days. These meso-scale eddies would have significant impacts on local biogeochemical processes and transport of nutrients and biota.

Table 4.1. Summary of the numerical experiments.

Experiment Aliases	Descriptions
CONTROL	Standard simulations for 2001, 2002, and 2003
W92	2002 simulation Air-sea O_2 exchange formulation by Wanninkhof (1992)
PL80	2003 simulation Phytoplankton growth formulation by Platt et al. (1980)
No-sewage	2001 simulation Set nutrient concentrations in the effluent as zero

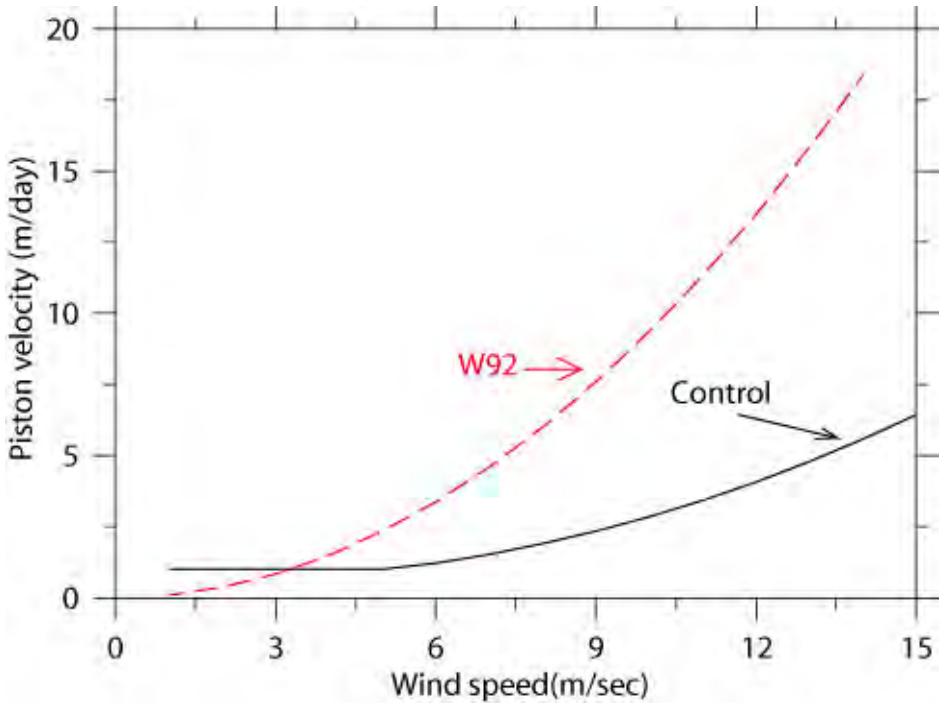

Figure 4.1 The piston velocity calculated by Hyer et al. (1971) (Control) and Wanninkhof (1992) (W92).

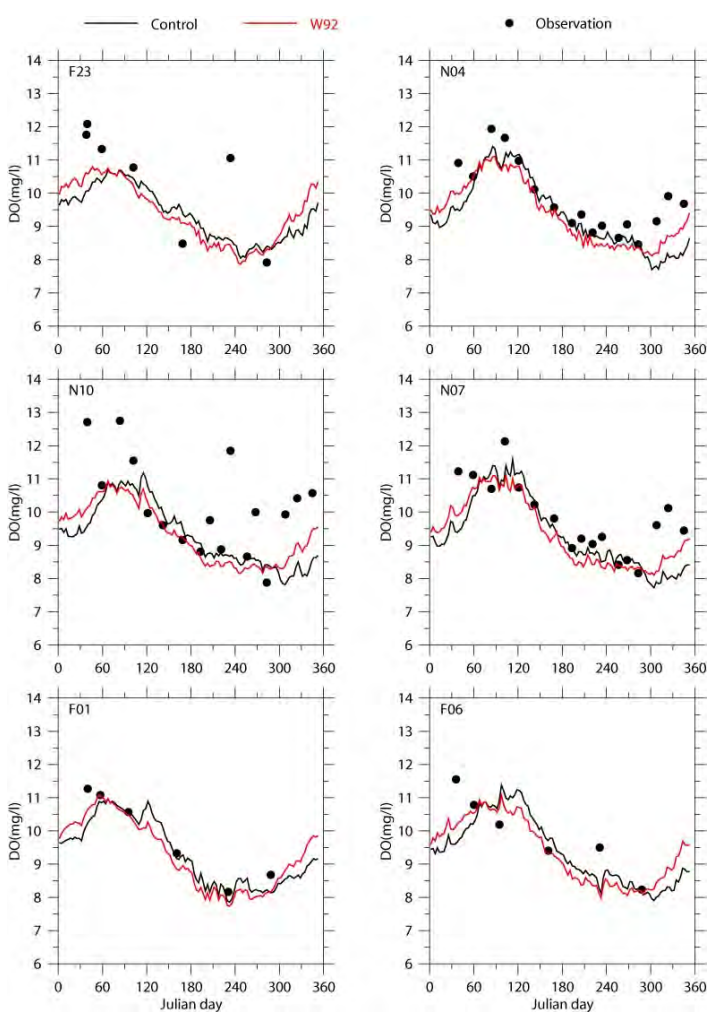

Figure 4.2. Comparison of surface DO concentrations between the CONTROL and W92 experiments in 2002.

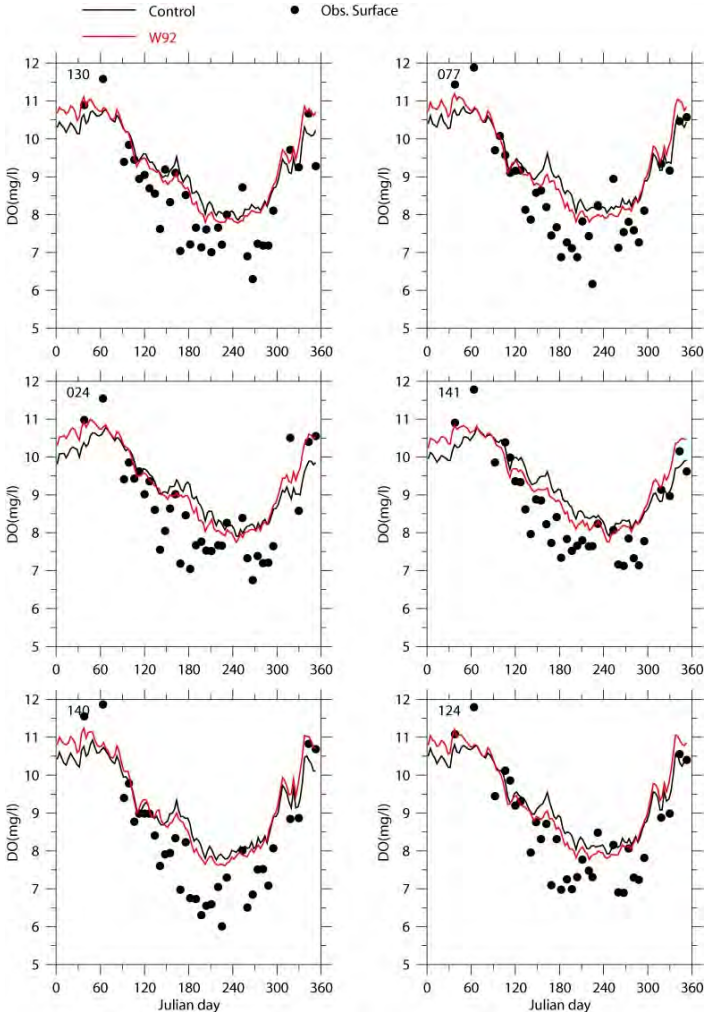

Figure 4.3. Comparison of surface DO concentrations in BH between the CONTROL and W92 experiments in 2002.

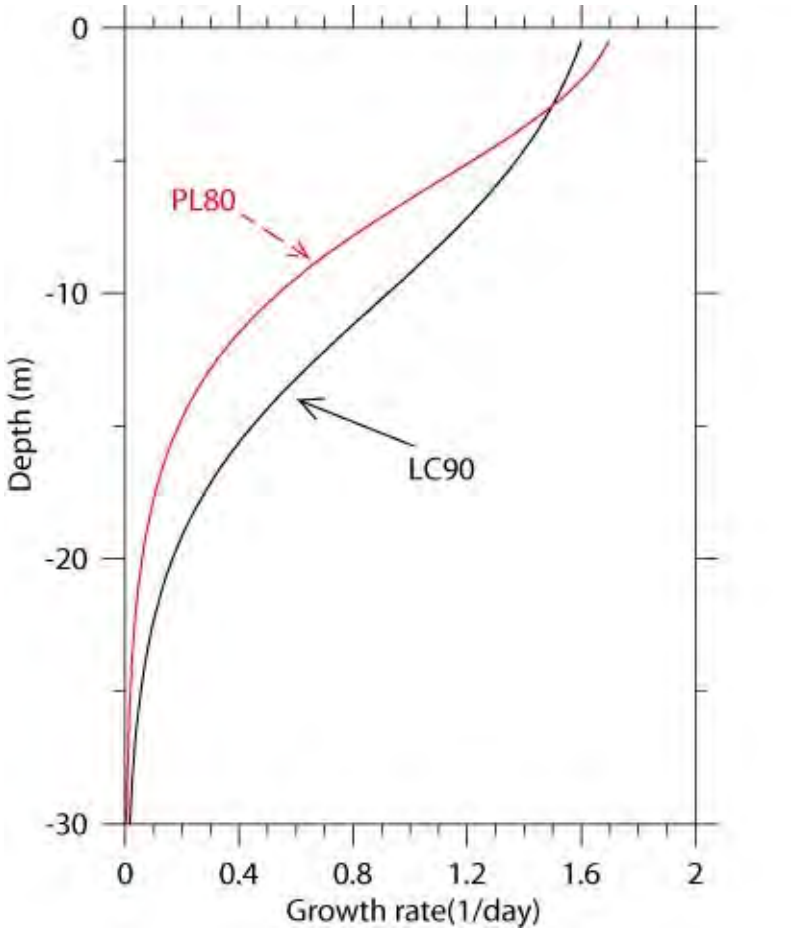

Figure 4.4. Vertical profiles of growth rates of Platt et al. (1980) and Laws and Chalup (1990).

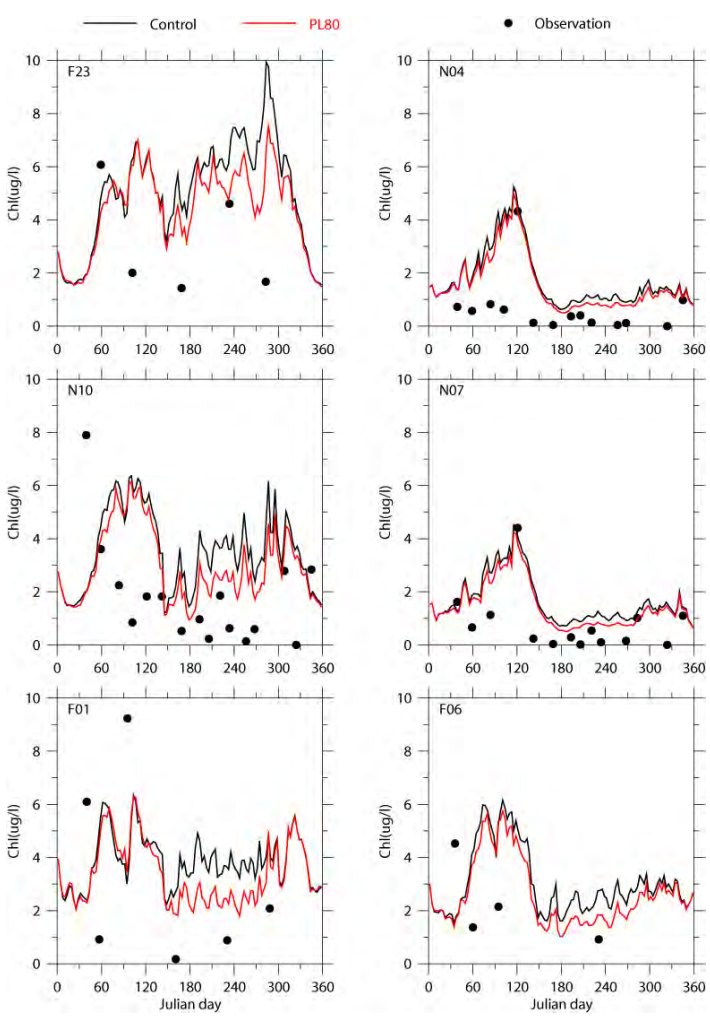

Figure 4.5. Comparison of bottom chlorophyll concentrations in MB between the CONTROL and PL80 experiments in 2003.

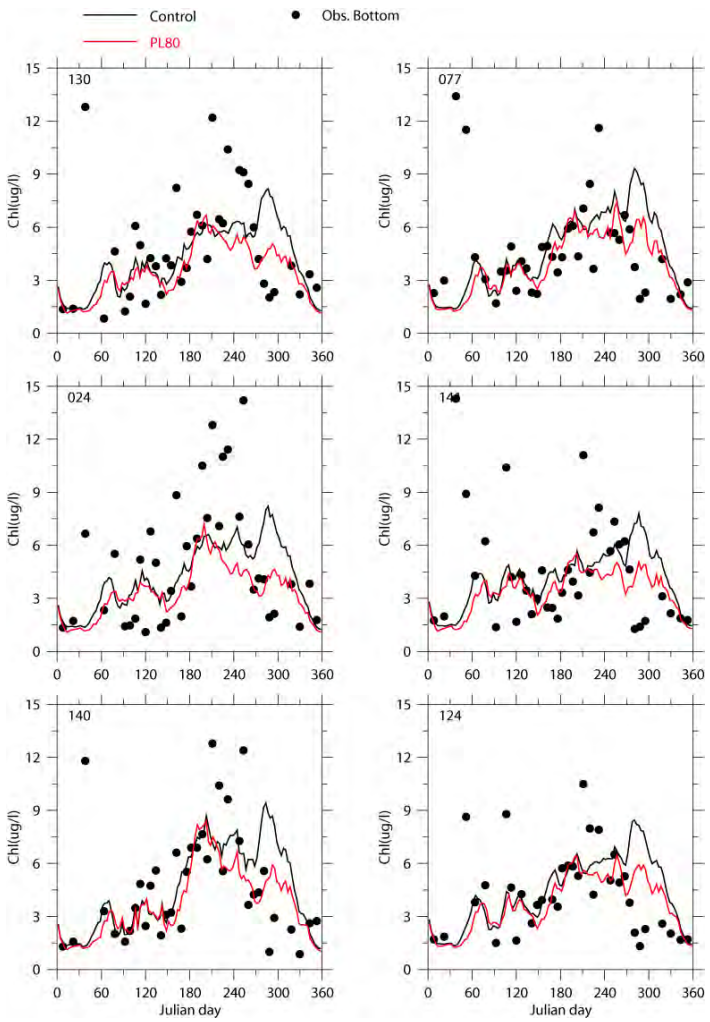

Figure 4.6. Comparison of surface chlorophyll concentrations in BH between the CONTROL and PL80 experiments in 2003

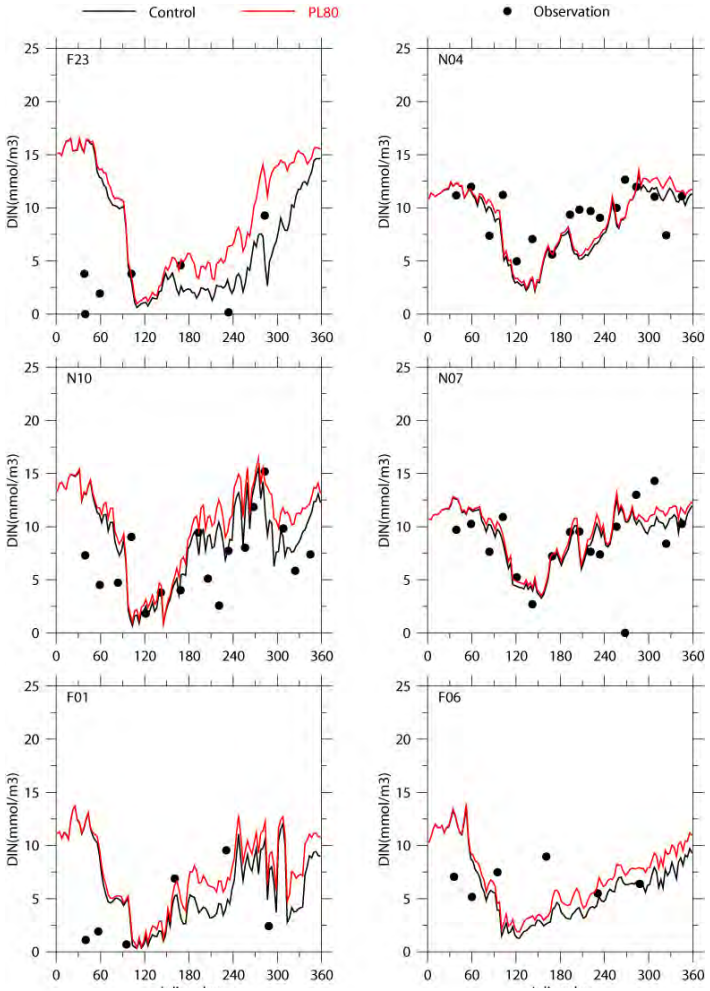

Figure 4.7. Comparison of bottom DIN concentrations in MB between the CONTROL and PL80 experiments in 2003.

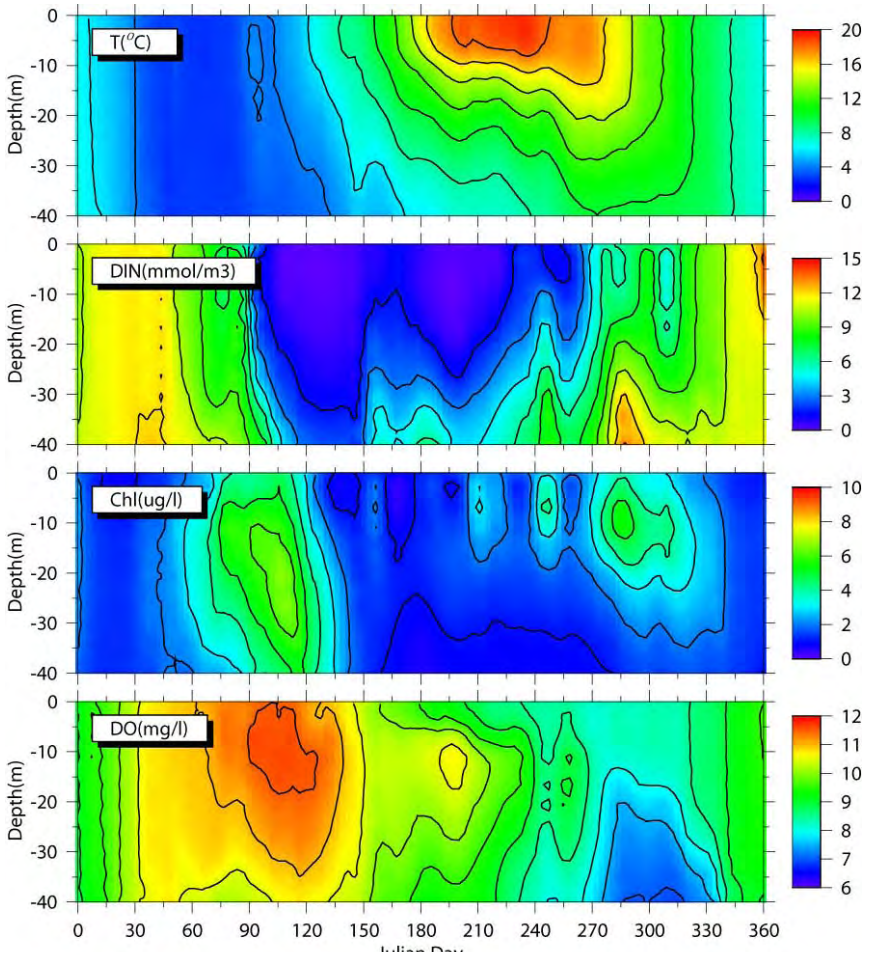

Figure 4.8. Modeled temperature, DIN, chlorophyll and DO at N04 from the PL80 experiment in 2003.

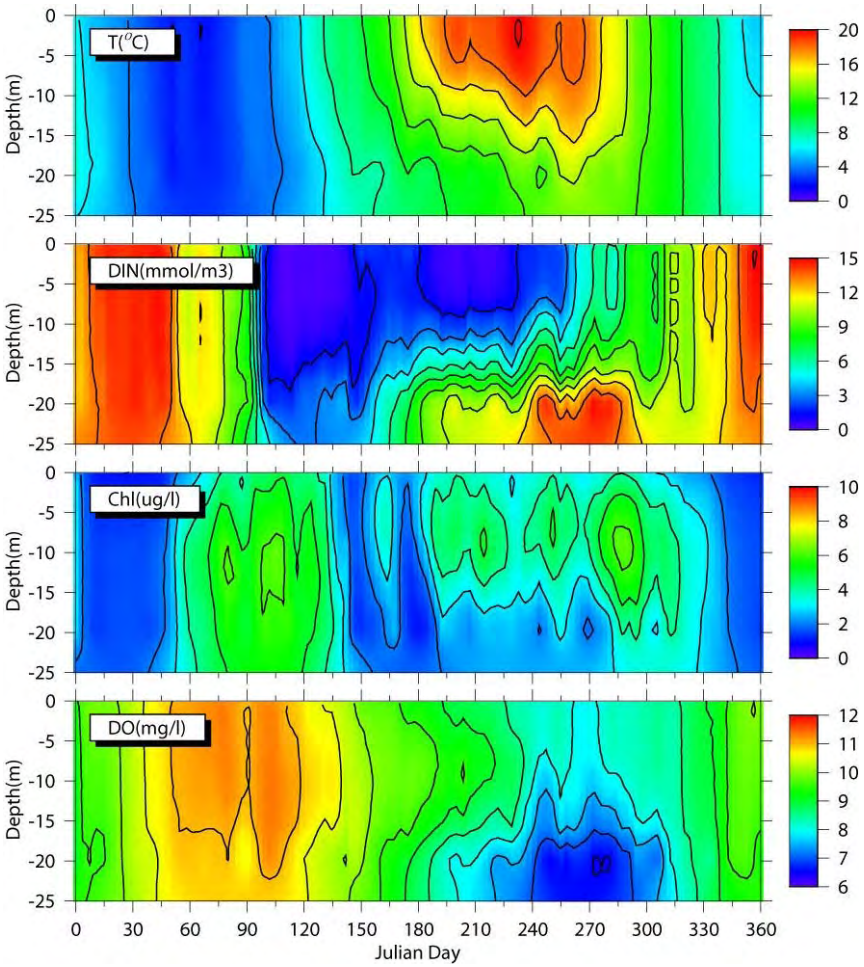

Figure 4.9. Modeled temperature, DIN, chlorophyll and DO at N14 from the PL80 experiment in 2003.

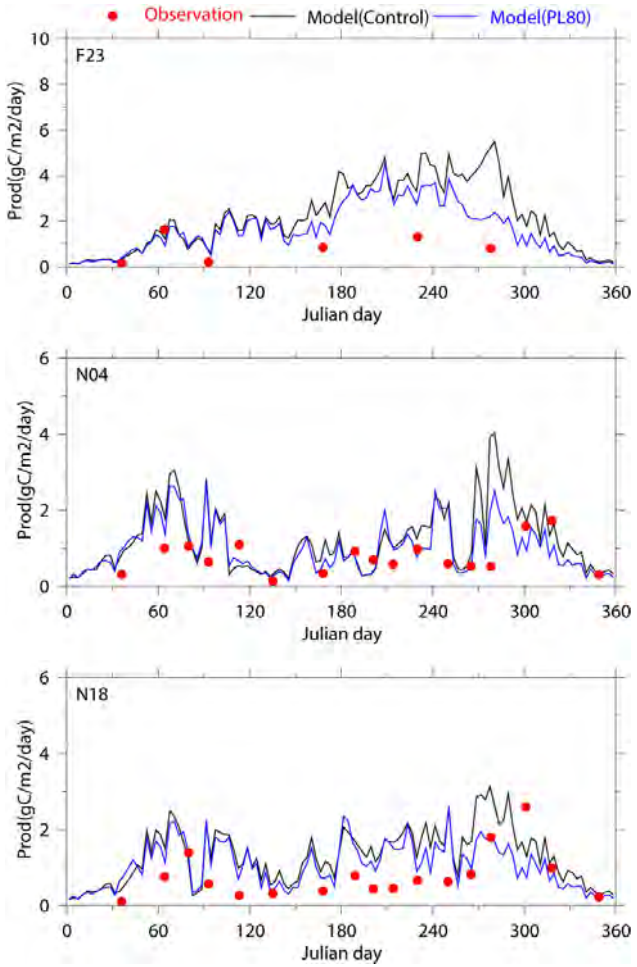

Figure 4.10. Comparison of primary production between the Control and PL80 experiments in 2003.

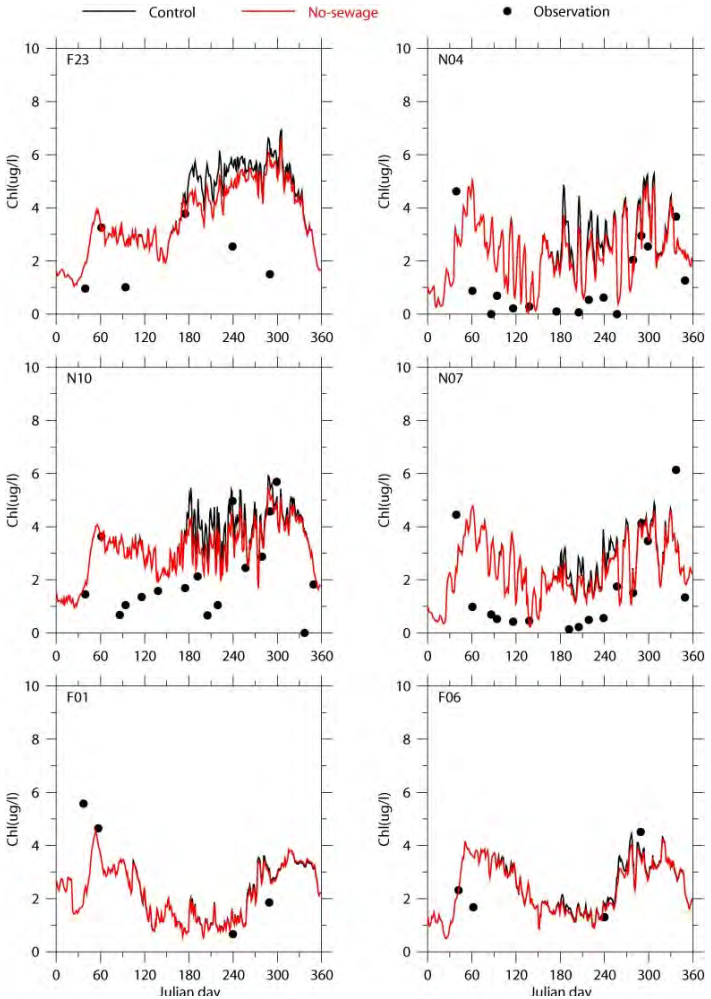

Figure 4.11. Comparison of surface chlorophyll concentrations in MB between the CONTROL and No-sewage experiments in 2001.

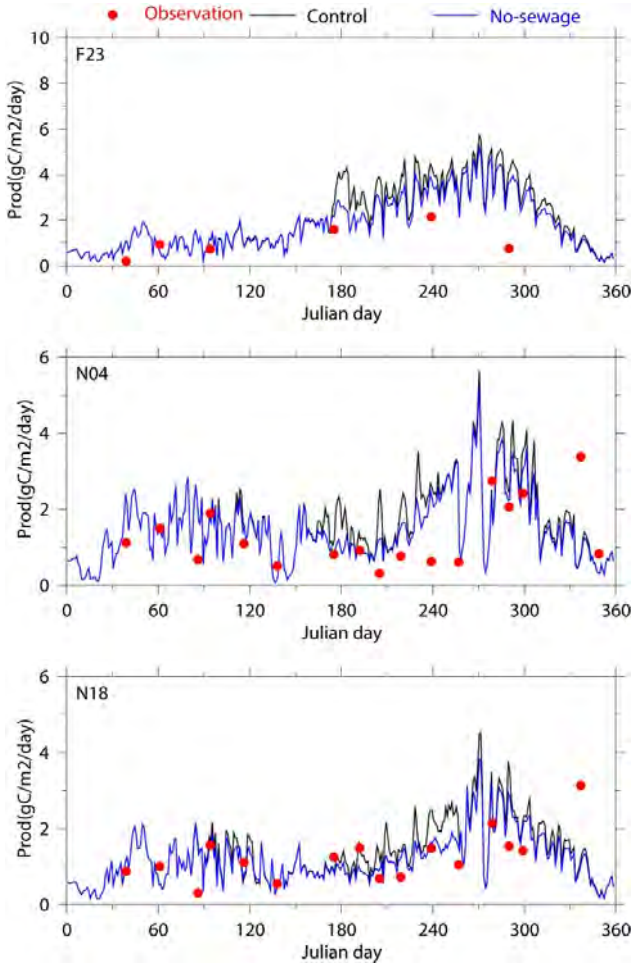

Figure 4.12. Comparison of primary production between the CONTROL and No-sewage experiments in 2001.

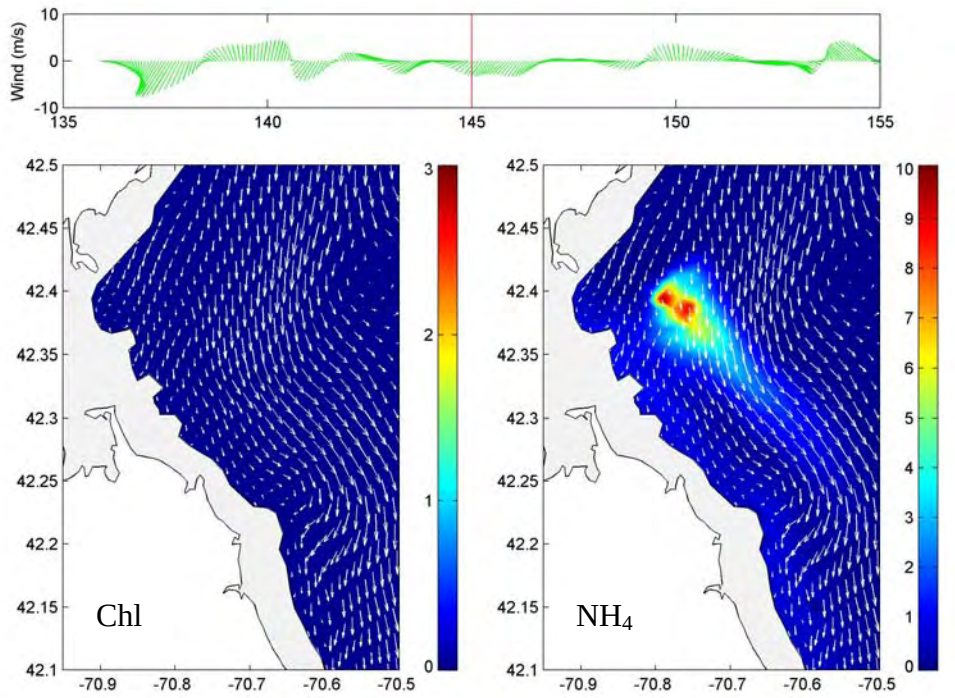

Figure 4.13. Currents and differences of chlorophyll and NH4 concentrations (15m) between the CONTROL and No-sewage experiments in 2001 (day 145).

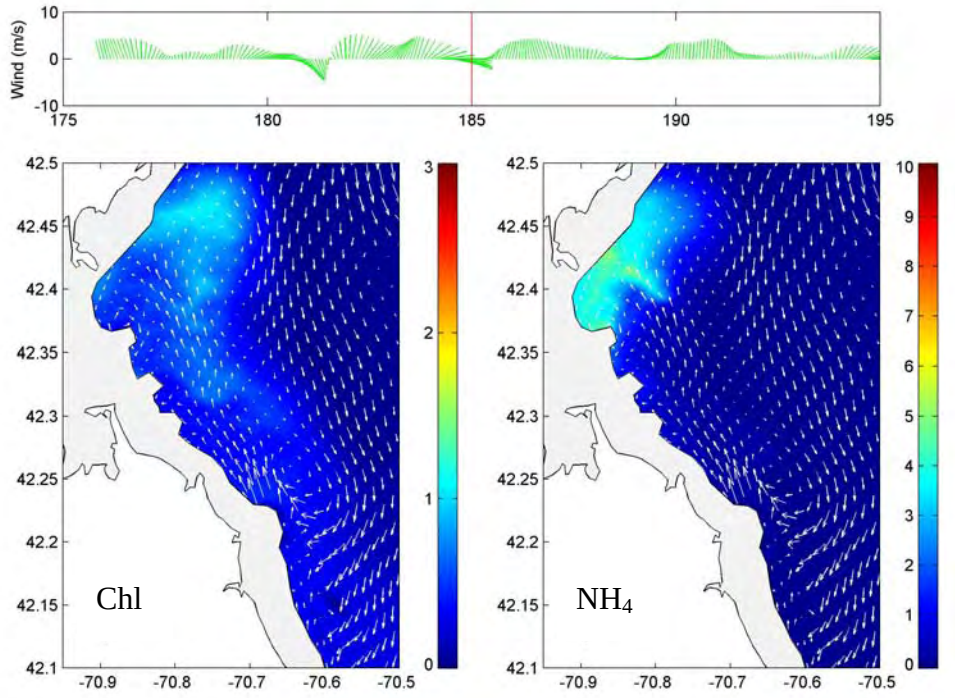

Figure 4.14. Currents and differences of chlorophyll and NH4 concentrations (15m) between the CONTROL and No-sewage experiments in 2001 (day 185).

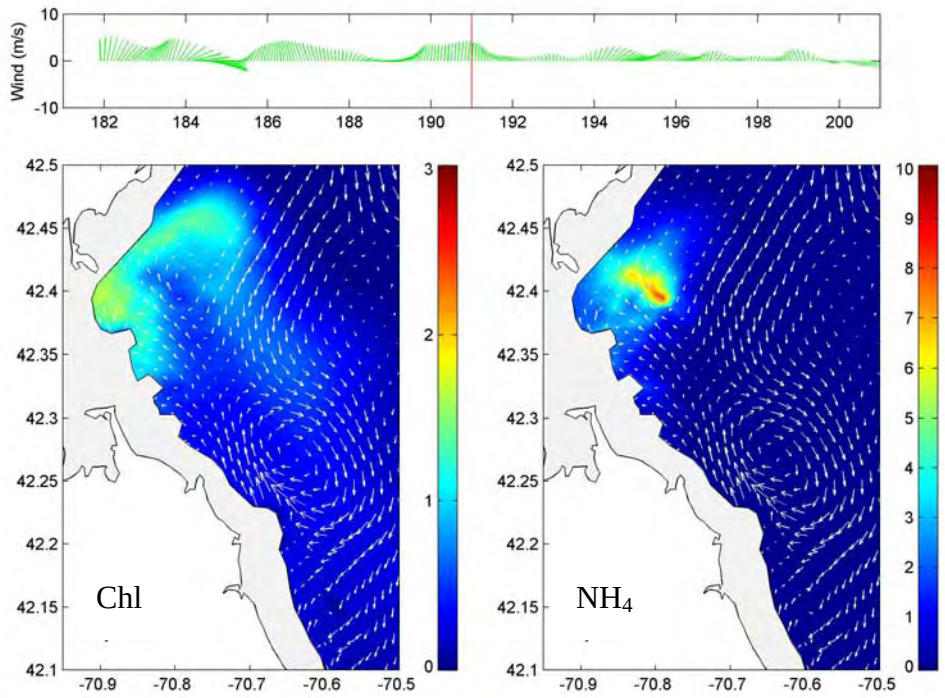

Figure 4.15. Currents and differences of chlorophyll and NH4 concentrations (15m) between the CONTROL and No-sewage experiments in 2001 (day 191).

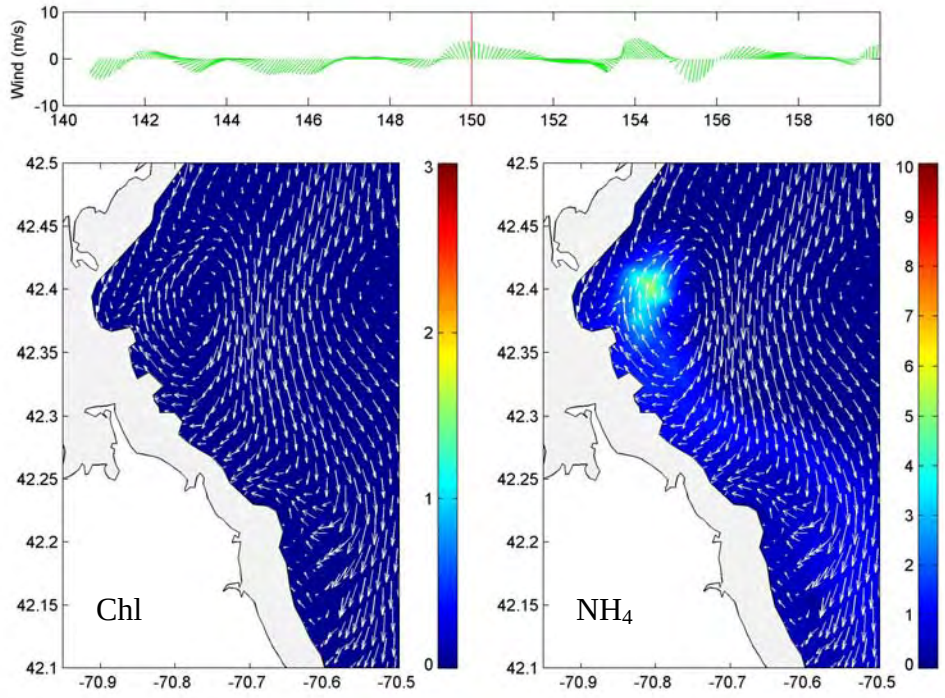

Figure 4.16. Currents and differences of chlorophyll and NH4 concentrations (15m) between the CONTROL and No-sewage experiments in 2001 (day 150).

5. SUMMARY AND RECOMMENDATIONS

5.1 Summary

This study concludes that the modeled water quality variables and processes from the 2002-2004 BEM simulation are well compared to observed ones with the same qualities as previous 1998-2001 simulations. The results also well represent physical, biological and chemical environment and processes in the water column and sediment in the MBS. For example, the model reproduced not only the seasonal cycles of phytoplankton biomass, nutrient concentrations, DO concentrations, and primary production in the MBS, but also the inter-annual variability such as the chlorophyll concentrations during the strong spring bloom and very weak fall bloom in 2004.

The model certainly has limitations. It did not reproduce the early bloom in February 2002; the model over-estimated chlorophyll and bottom PON concentrations; the model over-estimated PP in BH in late summer and early fall; and the model did not reproduce high surface DO values associated with short-term events in summer. The causes for these mismatches between model and observed results are complicated by the natural complexity of an ecosystem, empirical formulation and limitation of model schemes and resolution. All of these need to be further investigated.

Improving the BEM will first require improving the hydrodynamic model. For example, over-smoothed vertical distribution of chlorophyll may be caused by over-estimated vertical mixing. In summer during upwelling events, the hydrodynamic model tends to predict warmer temperature in western MB than the observed, which may lead to over-estimation of phytoplankton biomass (and chlorophyll). A higher horizontal resolution in both hydrodynamic and BEM models may improve horizontal gradients of temperature, salinity, currents and mixing from the hydrodynamic model and gradients of nutrients, production and biomass in the BEM model.

Two sensitivity experiments conducted suggest that results from the BEM are sensitive to empirical formulas of air-sea O_2 exchange and phytoplankton growth. Better empirical formulas for these biogeochemical processes require better understandings of these processes first, which have to be done by observations.

The experiment with and without effluent nutrients indicates the possible impacts of the MWRA effluent on the chlorophyll and PP near the outfall site. When the coastal current is southward corresponding to the GOM current intrusion and northerly or northeasterly winds, the effluent is quickly transported southward out of the outfall site and dispersed. When the coastal current is northward corresponding to southerly or southeasterly winds, the effluent can be entrapped in mesoscale eddies near the outfall site and its vicinity, which can significantly enhance the local PP and chlorophyll concentrations.

The analysis of observed and modeled results in 2002-2004 indicates that there are (1) significant short-term blooms, (2) significant long term variability in algal blooms associated with the interannual variability of temperature, salinity, and circulation in MB, and (3) episodic events such as *Phaeocystis* blooms. The BEM has captured most of these variability and events. As scientists are trying to refine the model and improve the predictability and quality of the model, the current model results have sufficient accuracies and reliability that can be used by managers and other scientists in their studies, monitoring and management.

5.2 Recommendations

Based on this and previous simulations, we recommend 4 future studies:

1. Mesoscale physical-biogeochemical processes. Mesoscale processes such as eddies, filaments and coastal jets frequently take place in the MBS due to complex interactions between winds, the GOM intruding currents, freshwater plumes and topography. For example, two anticyclonic eddies, one between the outfall site and the north shore, and another between the outfall site and Hingham, were found in the modeled results during southerly or southwesterly winds. These eddies can significantly alter the transport and retention of effluent and its impacts on the local water quality and ecosystem. Because these eddies have a horizontal scale of 5-20 km and last for 2-7 days associated with certain winds and GOM water intrusion events, they cannot be resolved by regular monthly surveys with a survey distance of 10-20 km between 2 stations. Studies on these mesoscale physical-biogeochemical processes will not only improve the

predictive capability of the BEM, but also strengthen the entire monitoring program.

2. Retrospective studies. With more than 10 year monitoring and numerical modeling, retrospective studies can bring insight into the mechanisms leading the occurrences of specific events such as the *Phaeocystis* bloom in 2004, the missing blooms in spring 1998 and fall 2004 and the most recent red-tide event in late spring 2005. With better understandings of these events, the models can be then improved and possibly predict the occurrences of these events.

3. Improving the boundary conditions. The monitoring for biogeochemical processes near the open boundary should be prioritized and enhanced so that the construction of open boundary conditions can be automated, and modeling errors can be reduced. A mooring station (GoMOOS A) as part of the Gulf of Maine Ocean Observing System (GoMOOS) has been deployed in the North Passage since August 2001, which monitors temperature (3 depths), salinity (3 depths), currents (profiles) and DO (50m) fields. Since October 2005, a fluorometer was deployed at 3m depth to measure the surface chlorophyll. Heavy reliance on empirical assumptions are unavoidable for the model assimilation of these single station and few-depth observations, especially the DO and chlorophyll measurements. We recommend increasing horizontal and vertical coverage for biogeochemical parameters along the boundary for effectively improving model open boundary conditions.

4. The effects of zooplankton grazing. As indicated in previous report (Jiang and Zhou, 2004c), zooplankton grazing can significantly affect phytoplankton production. The over-estimated late summer and fall phytoplankton production in the BEM may be due to under-estimated zooplankton grazing. A quantitative study based on zooplankton population models should be made to evaluate the effect of zooplankton grazing on the seasonal variation of phytoplankton groups.

6. REFERENCES

Adams, E. E., J. W. Hansen, R. L. Lago, P. Clayton, and X. Zhang (1992), A simple box model of the nitrogen cycle in Boston Harbor and the Massachusetts Bays, *Civil Engr. Pract., fall 1992,* 91-103.

Banks, R. B. and F. F. Herrera. 1977. Effect of wind and rain on surface reaeration. J. Envir. Engr. Div., ASCE. **103:** 489-504.

Becker, S. (1992), The seasonal distribution of nutrients in Massachusetts and Cape Cod Bays, MS thesis, University of New Hampshire, 127pp.

Bienfang, P.K., P.J. Harrison and L. M. Quarmby (1982), Sinking rate response to depletion of nitrate, phosphate and silicate in four marine diatoms, *Marine Biology, 67*, 295-302.

Bigelow, H.B. 1927, Physical oceanography of the Gulf of Maine (Part II). Bulletin of the Bureau of Fisheries, 40: 511-1027.

Butman, B., 1976. Hydrography and low frequency currents associated with the spring runoff in Massachusetts Bay Memoires. Societe Royale des Sciences de Liege, 6: 247-275.

Butman, B., Bothner, M.H. Lightsom, F.L. Gutierrez, B.T., Alexander, P.S., Martini, M.A., and Strahle, W.S., 2002, Long-term Oceanographic Observations in Western Massachusetts Bay offshore of Boston, Massachusetts: Data Repor for 1989-2000, U.S. Geological Survey Digital Data Series 74.

Culver, M.E., and W.O. Smith, Jr. (1989), Effects of environmental variables on sinking rates of marine phytoplankton, *J. Phycol., 25*, 262-270.

Di Toro, D. M. 2001, *Sediment Flux Modeling*, Wiley-Interscience, New York, 624 pp.

Evans, G.T. and V. Garçon, (1997), One-Dimensional Models of Water Column Biogeochemistry. JGOFS Report No. 23, Scientific Committee Oceanic Research, 89pp.

Geyer, W. R., Gardner, G. B., Brown, W. S., Irish, J., Butman, B., Loder, T., and Signell, R. P. 1992, Physical oceanographic investigation of Massachusetts and Cape Cod Bays. Massachusetts Bay Program. MBP-92-03, 497pp.

Hendry, R., and I. He (1996), *Technical report on objective analysis (OA) project*,

Bedford Institute of Oceanography, Dartmouth, Nova Scotia, 105pp.

HydroQual, Inc. 2000, Bays Eutrophication Model (BEM): modeling analysis for the period 1992-1994. Boston, Massachusetts Water Resources Authority. ENQUAD 2000-02, 158pp.

HydroQual, Inc. 2001, Boundary sensitivity for the Bays Eutrophication Model (BEM). Boston: Massachusetts Water Resources Authority. Report ENQUAD 2001-14. 90pp.

HydroQual, Inc. 2003, Bays Eutrophication Model (BEM): modeling analysis for the period 1998-1999. Boston, Massachusetts Water Resources Authority. ENQUAD 2003-03, 318pp.

HydroQual, Inc. and Normandeau Associates, Inc. 1995, A water quality model for Massachusetts and Cape Cod Bays: Calibration of the Bay Eutrophication Model (BEM). Boston, Massachusetts WAter Resource Authority. ENQUAD 1995-08, 402pp.

HydroQual, Inc. and Signell, R.P. 2001, Calibration of the Massachusetts and Cape Cod Bays Hydrodynamic Model: 1998-1999. Boston, Massachusetts Water Resources Authority. ENQUAD 2001-12, 170pp.

Hyer, P.V., C. S. Fang, E. P. Ruzeck, and W. J. Hargis (1971), Hydrography and hydrodynamics of Virginia estuaries, studies of the distribution of salinity and dissolved oxygen in the upper York system, Virginia Institute of Marine Science.

Jiang, M.S. and Zhou, M. 2003, Massachusetts Bay Hydrodynamic Model and Water Quality Model results in 1998-99: Comparison Report between HydroQual and University of Massachusetts Boston Runs. Boston, Massachusetts Water Resources Authority. ENQUAD 2003-10, 42pp.

Jiang, M.S. and Zhou, M. 2004a, The summer Ekman pumping and its implications to the deep water renewal in Massachusetts and Cape Cod Bays. Proceedings of the 8th Estuarine Coatal Modelling. San Francisco. 11-3-0003. p929-948.

Jiang, M.S. and Zhou, M. 2004b. Calibration of the Massachusetts and Cape Cod Bays hydrodynamic model: 2000-2001. Boston, Massachusetts Water Resources Authority. Draft Report. ENQUAD 2004-08. 71pp.

Jiang, M.S., G.T. Wallace, M. Zhou, S. Libby and C.D. Hunt, 2006a, Summer formation of a high nutrient low oxygen pool in Cape Cod Bay. *JGR-Oceans* (in review).

Jiang, M.S., M. Zhou, S. Libby and C.D. Hunt, 2006b, Influences of Gulf of Maine intrusion on the Massachusetts Bay spring bloom, *JGR-Oceans* (in review).

Kropp, R. K., Diaz, R., Dahlen, D., Boyle, J. D., and Hunt, C. D. 2002, 2001 Harbor Benthic Monitoring Report. Boston, Massachusetts Water Resources Authority. ENQUAD 2002-19, 74pp.

Kropp, R. K., Diaz, R., Hecker, B., Dahlen, D., Boyle, J. D., Abramson, S. L., and Emsbo-Mattingly, S. 2001, 2000 Outfall Benthic Monitoring Report. Boston, Massachusetts Water Resources Authority. ENQUAD 2001-14, 148pp.

Laws, E. A., and M. S. Chalup (1990), A microalgal growth model, *Limnol. Oceanogr*., *35*, 597-608.

Libby, P. S., Hunt, C. D, Geyer, W. R., Keller, A. A., Oviatt, C. A., and Turner, J. T. 2000, 1999 Annual Water Column Monitoring Report. Boston, Massachusetts Water Resources Authority. ENQUAD 2000-09, 180pp.

Libby, P. S., Hunt, C. D, McLeod, L. A., Geyer, W. R., Keller, A. A., Borkman, D., Oviatt, C. A., and Turner, J. T. 2001, 2000 Annual Water Column Monitoring Report. Boston, Massachusetts Water Resources Authority. ENQUAD 2001-17, 196pp.

Libby P.S., Geyer W.R., Keller A.A., Turner J.T., Borkman D., Mickelson M.J., Hunt C.D., Oviatt C.A. 2002**.** 2001 Annual Water Column Monitoring Report. Boston: Massachusetts Water Resources Authority. Report ENQUAD 2002-22. 100pp.

Libby P.S., Geyer W.R., Keller A.A., Turner J.T., Borkman D.G., Oviatt C.A. and Hunt C.D. 2003. 2002 Annual Water Column Monitoring Report. Boston: Massachusetts Water Resources Authority. Report 2003-09. 105 pp.

Libby P.S., Geyer W.R., Keller A.A., Turner J.T., Borkman D.G. and Oviatt C.A. 2004. 2003 Annual Water Column Monitoring Report. Boston: Massachusetts Water Resources Authority. Report 2004-07. 154 p.

Libby P.S., Mansfield A.D., Keller A.A., Turner J.T., Borkman D.G., Oviatt C.A. and Mongin C.J. 2005. Semiannual water column monitoring report: February-June 2004. Boston: Massachusetts Water Resources Authority. Report 2004-12. 294 pp.

Lynch, D.R., Naimie, C.E. and Werner, F.E., 1996. Comprehensive coastal circulation model with appliction to the Gulf of Maine. Cont. Shelf Res., 12: 37-64.

Maciolek, N. J., Diaz, R. J., Dahlen, D., Hecker, B., Gallagher, E. D., Blake, J. A., Williams, I. P., Emsbo-Mattingly, S., Hunt, C., and Keay, K. E. 2003, 2002 Outfall Benthic Monitoring Report. Boston, Massachusetts Water Resources Authority. ENQUAD 2003-13, 166pp.

Menzie-Cura & Associates, 1991, Sources and Loadings of Pollutants to Massachusetts Bay. Prepared for the Massachusetts Bay Program, Massachusetts Coastal Zone Management, US. EPA. Technical Report NO. MBP-91-01.

Platt, T., et al., Photoinhibition of photosynthesis in natural assemblages of marine phytoplankton, *J. Mar. Res.*, **38**, 687-701, 1980.

Signell, R.P., Jenter, H.L., and Blumberg, A.F., 1996. Circulation and effluent dilution modeling in Massachusetts Bay: model implementation, verification and results. USGS Open File Report 96-015, U.S. Geological Survey, Woods Hole.

Smolarkiewicz, P. K., 1984, A fully multidimensional positive definite advection transport algorithm with implicit diffusion. *J. Comput. Phys.*, **54**, 325-362.

Taylor D. 2001, Trends in water quality in Boston Harbor during the 8 years before offshore transfer of Deer Island flowsBoston, Massachusetts Water Resources Authority. ENQUAD 2001-05, 54pp.

Taylor D.I. 2004. Harbor-Bay eutrophication-related water chemistry changes after 'offshore transfer'. Boston: Massachusetts Water Resources Authority. Report 2004-06. 83 p.

Tucker, J., Giblin, A. E., Hopkinson, C. S., and Vasiliou, D. 2001, Benthic Nutrient Cycling in Boston Harbor and Massachusetts Bay: 2000 Annual Report. Boston, Massachusetts Water Resources Authority. ENQUAD 2001-07, 48pp. 2001.

Tucker, J., Kelsey, J., Giblin, A., and Hopkinson, C. S. 2002, Benthic Metabolism and Nutrient Cycling in Boston Harbor and Massachusetts Bay: Summary of Baseline Data and Observations after One Year of Harbor-to-Bay Diversion of Sewage Effluent. Boston, Massachusetts Water Resources Authority. ENQUAD 2002-13, 83pp.

Tucker J, Kelsey S, Giblin A.E. and C. S. Hopkinson, 2003. 2002 annual benthic nutrient flux monitoring report. Boston: Massachusetts Water Resources Authority. Report 2003-08. 52 p.

Tucker J, Kelsey S, Giblin A.E. and C. S. Hopkinson, 2004. 2003 annual benthic nutrient flux monitoring report. Boston: Massachusetts Water Resources Authority. Report 2004-05. 68 p.

Turner, J.T., 1994, Planktonic Copepods of Boston Harbor, Massachusetts Bay and Cape-Cod Bay, 1992. *Hydrobiologia*. 293: 405-413.

Wanninkhof , R. (1992), Relationship between wind speed and gas exchange over the ocean, *J. Geophys. Res*., *97*, 7373-7378.

Werme, C and Hunt, C. D. 2002, 2001 outfall monitoring overview. Boston: Massachusetts Water Resources Authority. ENQUAD 2002-18, 84pp.

Werme, C. and Hunt, C. D. 2000, 1999 Outfall monitoring overview. Boston, Massachusetts Water Resources Authority. ENQUAD 2000-14, 72pp.

Werme, C. and Hunt, C. D. 2003, 2002 Outfall monitoring overview. Boston, Massachusetts Water Resources Authority. ENQUAD 2003-12, 80pp.

Appendix A. Model kinetic equations for nitrogen

Here we outline the biogeochemical processes simulated in the BEM. Notations and descriptions of model parameters are listed in Table 2.2 and will not be described below.

1) Phytoplankton (P_c) growth is determined by net growth (μ), sinking loss (k_{sp}) and grazing loss (k_{grz}),

$$G_p = \left(\mu - k_{sp}(T) - k_{grz}(T)\right)P_C \tag{A1}$$

where T denotes the ambient water temperature.

The specific net growth rate μ of phytoplankton is defined as,

$$\mu = \left(\mu_{\max} G_T(T) - k_{RB}\right)G_N(N) \tag{A2}$$

where $\mu_{\max}$ is nutrient-saturated growth rate, $G_T(T)$ is temperature correction factor, and $G_N(N)$ is nutrient limitation factor.

Temperature dependence of phytoplankton growth is determined by,

$$G_T(T) = \begin{cases} \exp\left(-\beta_1\left(T - T_{OPT}\right)^2\right) & T \le T_{OPT} \\ \exp\left(-\beta_2\left(T_{OPT} - T\right)^2\right) & T \ge T_{OPT} \end{cases} \tag{A3}$$

Nutrient uptake follows Liebig's law with the limitation of individual nutrient determined by Michaelis-Menten kinetics,

$$G_N(N) = \min\left(\frac{DIN}{k_N + DIN}, \frac{DIP}{k_P + DIP}, \frac{Si}{k_{Si} + Si}\right) \tag{A4}$$

where *DIN* is total dissolved inorganic nitrogen, *DIP* is total dissolved inorganic phosphorus and Si is dissolved silicic acid (silicate).

Nutrient saturated growth rate ($\mu_{\max}$) is based on the balance growth model developed by Laws and Chalup (1990),

$$\mu_{\max} = \frac{G_{pre}(1-k_{RG})(1-f_{SC})I)}{G_{pre}/G_{pr0} + I(1+G_{pre}/(I_S G_{pr0}))} \quad \text{(A5)}$$

where $I(z,t)$ is solar radiation.

Chlorophyll to carbon ratio is also following the formulation by Laws and Chalup (1990),

$$a_{ChlC} = \frac{1-(1-QF)(1-\mu/\mu_{\max}) - f_{SC} - (\mu + k_{RB})(1-k_{RG})G_{pre}}{W_{CChl}} \quad \text{(A6)}$$

and phytoplankton endogenous respiration is determined by,

$$k_{PR} = \frac{k_{RB} + k_{RG}\mu}{1-k_{RG}} \quad \text{(A7)}$$

The total primary productivity is determined by,

$$GPP = (\mu + k_{PR})P_c \quad \text{(A8)}$$

and total respiration and grazing is,

$$Loss = (k_{PR} + k_{grz}(T))P_c \quad \text{(A9)}$$

2) Light

Light attenuation accounts for background attenuation and phytoplankton self-shading,

$$k_{ext} = k_{base} + k_c a_{ChlC} P_{tot} \quad \text{(A10)}$$

where P_{tot} is total phytoplankton biomass of the three phytoplankton groups. Thus the solar radiation at depth z (upward positive with origin at sea surface) is,

$$I(z,t) = I_{surf}(t)\exp\left(\int_0^z k_{ext}\,dz\right) \quad \text{(A11)}$$

where $I_{surf}(t)$ is surface solar radiation that can be calculated from daily mean solar radiation (I_{tot}),

$$I_{surf}(t) = \frac{I_{tot}}{0.635 f} \sin\left(\frac{\pi\left(t - t_{sunrise}\right)}{f} \right) \quad \text{(A12)}$$

The saturation solar radiation is determined by the average light level for the previous three days,

$$I_s = \left(I_{tot_{n-3}} + I_{tot_{n-2}} + I_{tot_{n-1}}\right)/3 \quad \text{(A13)}$$

3) Algal settling (Bienfang et al., 1982; Culver and Smith, 1989),

$$k_{sp}(T) = \left(V_b + V_N\left(1 - G_N(N)\right)\right)\theta_{sp}^{(T-20)} / H \quad \text{(A14)}$$

4) Zooplankton grazing

$$k_{grz}(T) = k_{grz0}\theta_{grz}^{(T-20)} \quad \text{(A15)}$$

5) Hydrolysis of particulate organic matter to dissolved organic nitrogen

$$R_{LPON} = k_{LPON}\theta_{LPON}^{T-20} \frac{P_{tot}}{K_{mp} + P_{tot}} LPON \quad \text{(A16a)}$$

$$R_{RPON} = k_{RPON}\theta_{RPON}^{T-20} \frac{P_{tot}}{K_{mp} + P_{tot}} RPON \quad \text{(A16b)}$$

6) Mineralization of dissolved organic nitrogen to ammonia

$$R_{LDON} = k_{LDON}\theta_{LDON}^{T-20} \frac{P_{tot}}{K_{mp} + P_{tot}} LDON \quad \text{(A17a)}$$

$$R_{RDON} = k_{RDON}\theta_{RDON}^{T-20} \frac{P_{tot}}{K_{mp} + P_{tot}} RDON \quad \text{(A17b)}$$

7) Nitrification

$$R_{Nit} = k_{Nit}\theta_{Nit}^{T-20} \frac{DO}{k_{Nit\_DO} + DO} NH_3 \quad \text{(A18)}$$

8) Denitrification

$$R_{Denit} = k_{Denit}\theta_{Denit}^{T-20}\frac{k_{Denit\_DO}}{k_{Denit\_DO}+DO}NO_3 \quad \text{(A19)}$$

9) Exudation of total primary productivity (*GPP*) into dissolved organic carbon

$$R_{exud} = a_{NC} f_{ExDOC} GPP \quad \text{(A20)}$$

10) Nitrogen to carbon ratio

$$a_{NC} = \frac{QF + (1-QF)\,\mu/\mu_{\max}}{W_{CN}} \quad \text{(A21)}$$

11) Settling of particulate organic nitrogen

$$k_{PON}(T) = \frac{V_{PON}}{H}\theta_{PON}^{T-20} \quad \text{(A22)}$$

Massachusetts Water Resources Authority
Charlestown Navy Yard
100 First Avenue
Boston, MA 02129
(617) 242-6000
http://www.mwra.state.ma.us